DEFORMATION AND RECOVERY OF IRON POLYCRYSTALS

DEFORMATION AND RECOVERY OF IRON POLYCRYSTALS

By

MICHAEL HENRY SCHANKULA, B.A. Sc., M.A.Sc.

A Thesis

Submitted to the School of Graduate Studies

in Partial Fulfilment of the Requirements

for the Degree

Doctor of Philosophy

McMaster University

June 1970

DOCTOR OF PHILOSOPHY (1970) McMASTER UNIVERSITY
(Metallurgy and Materials Science) Hamilton, Ontario.

TITLE: Deformation and Recovery of Iron Polycrystals

AUTHOR: Michael Henry Schankula, B.A.Sc. (University of Waterloo)
M.A.Sc.

SUPERVISOR: Professor J.D. Embury

NUMBER OF PAGES: (x); 148

SCOPE AND CONTENTS:

The effect of grain size on the work hardening behavior of polycrystalline iron, copper, and 70/30 alpha brass has been studied using stress relaxation techniques. The stress relaxation technique has been used to monitor the variation of internal stress during work hardening as a function of grain size in these materials. It is shown that, for certain conditions dependent on the temperature and the nature of slip, the work hardening behavior of a metal polycrystal is grain size dependent and can be expressed in terms of a modified Hall-Petch equation with a slope dependent on the degree of plastic strain. A simple dimensional argument is developed to show that under conditions of planar slip, where the slip distance is equivalent to the grain diameter, the grain size dependent work hardening is related to the accumulation of geometrically necessary dislocations required for the compatible deformation of the polycrystal.

Recovery experiments have been used to study the thermal stability of the work hardened structure formed at different deformation temperatures in iron polycrystals.

ACKNOWLEDGMENTS

The author is greatly indebted to Professor J. D. Embury for his advice and guidance throughout the course of the work.

Special thanks are also due to the members of the mechanical metallurgy research group, especially Dr. D. J. Lloyd, for their advice and criticism.

The author appreciates the work done on the drawings by Mr. Martin van Oosten and also the assistance in many ways of Mr. Rick Jarachowicz.

And also, thanks to Mrs. Anita Miltimore for the accurate typing of this thesis in such a short time.

Financial support for the research by the National Research Council of Canada and financial support for the author in the form of a Steel Company of Canada, Limited Graduate Research Fellowship is also gratefully acknowledged.

TABLE OF CONTENTS

		Page
CHAPTER 1	INTRODUCTION	1
CHAPTER II	LITERATURE REVIEW	3
	2.1 Plastic Deformation and Strain Hardening of Metal Polycrystals	3
	2.1.1 Introduction	3
	2.1.2 Classical Theories of Polycrystal Deformation	4
	(i) Continuity of Material	6
	(ii) Continuity of Stress	6
	2.1.3 Effect of Grain Size on Polycrystal Deformation	10
	(a) Dislocation Pile Up Model	10
	(b) Grain Boundary Source Model	15
	(c) Work Hardening Model	16
	(d) Dislocation Storage Model	18
	2.1.4 Components of Flow Stress and Nature of Internal Stress in Deformed Polycrystals	22
	2.1.5 Experimental Determinations of the Components of the Flow Stress	26
	(a) Indirect Techniques	27
	(b) Direct Techniques	29

		Page
	2.2 Recovery of Internal Stress in Deformed Polycrystals	31
CHAPTER III	EXPERIMENTAL PROCEDURES	33
	3.1 Introduction	33
	3.2 Materials and Specimen Preparation	34
	3.3 Measurement of Mechanical Response	37
	3.3.1 Stress-Strain Measurements	37
	3.3.2 Stress Relaxation Tests	41
	3.4 Observations of X-ray Asterism	45
	3.4.1 Description of Back Reflection X-ray Camera	45
	3.4.2 Information Obtainable from X-ray Asterism	48
CHAPTER IV	EXPERIMENTAL RESULTS	52
	4.1 Introduction	52
	4.2 Measurment of Internal Stress and Effective Stress	52
	(a) Iron at 298°K	53
	(b) Iron at 195°K	56
	(c) Alpha Brass at 195°K	57
	(d) Copper at 298°K	60
	4.3 Work Hardening Behavior	63
	(a) Iron at 298°K	63
	(b) Iron at 195°K	63
	(c) Alpha Brass at 195°K	66
	(d) Copper at 298°K	66

		Page
	4.4 Grain Size Dependence of Internal Stress	68
	4.4.1 Analysis of Internal Stress-Grain Size Results	73
	4.5 Observations of X-ray Asterism	77
CHAPTER V	THERMAL RECOVERY OF INTERNAL STRESS IN DECARBURIZED IRON	92
	5.2 Experimental Procedure	92
	5.2.1 Materials and Apparatus	92
	5.2.2 Method of Evaluating Recovery	93
	5.2.3 Electron Microscope Study	95
	5.3 Experimental Results	96
	5.3.1 Recovery of Internal Stress	96
	5.3.2 Electron Microscopy Results	101
	(a) Effect of Deformation Temperature on the Dislocation Distribution	101
	(b) Effect of Recovery on the Dislocation Distribution	110
	5.4 Discussion of Results	110
	5.4.1 Effect of Temperature on Work Hardening	110
	5.4.2 Recovery of Internal Stress	112
CHAPTER VI	DISCUSSION OF RESULTS	119
	6.1 Introduction	119
	6.2 Effect of Grain Size on Internal Stress	120

Page

6.2.1 Dislocation Storage Model for the Internal Stress-Grain Size Relation 122

6.3 Summary and Conclusions 138

APPENDIX A STRESS RELAXATION IN THE INSTRON 140

REFERENCES 144

LIST OF FIGURES

FIGURE		PAGE
3.1	Specimen grips and alignment block	38
3.2	Stainless steel tensile testing fixture	39
3.3	Schematic diagram of load weighing system and X-Y chart drive system	42
3.4	Stress relaxation of a plastically deformed tensile specimen	43
3.5	Assembled X-ray micro-beam diffraction camera	46
3.6	Exploded view of collimator assembly	47
3.7	Schematic diagram showing effect of lattice curvature on intensity of Laue spot	50
4.1	Stress relaxation of decarburized iron strained 12% at 298°K	54
4.2	Determination of m* in decarburized iron from stress relaxation at 298°K	55
4.3	Stress relaxation of decarburized iron. Prestrained 12% at 298°K, restrained 0.5% at 195°K	58
4.4	Determination of m* in decarburized iron from stress relaxation at 195°K	59
4.5	Stress relaxation of 70/30 alpha brass strained 2.5% at 195°K	61
4.6	Determination of m* in 70/30 alpha brass from stress relaxation at 195°K	62

FIGURE		PAGE
4.7	Internal stress and effective stress as a function of strain for decarburized iron (a) at 298°K and (b) at 195°K	64
4.8	Internal stress and effective stress as a function of strain for (a) 70/30 alpha brass at 195°K and (b) copper at 298°K	65
4.9	Effective stress as a function of strain for a number of selected grain sizes in 70/30 alpha brass	67
4.10	Internal stress as a function of strain for decarburized iron at 298°K	69
4.11	Internal stress as a function of strain for decarburized iron at 195°K	70
4.12	Internal stress as a function of strain for 70/30 alpha brass at 195°K	71
4.13	Internal stress as a function of strain for copper at 298°K	72
4.14	Internal stress as a function of $D^{-1/2}$ for decarburized iron	74
4.15	Internal stress as a function of $D^{-1/2}$ for 70/30 alpha brass and copper	75
4.16	Hall-Petch slope as a function of strain for all the materials tested	76
4.17	Back reflection Laue patterns from a coarse-grained iron polycrystal (above) and a fine-grained iron polycrystal (below)	79
4.18	Back reflection Laue patterns from center and grain boundary regions of an iron polycrystal	80

FIGURE		PAGE
4.19	Back reflection Laue patterns from a coarse-grained brass polycrystal (above) and a fine-grained brass polycrystal (below)	81
5.1	Schematic diagram showing the effect of recovery on $_{int}$ and the method used to evaluate the degree of recovery	94
5.2	Effect of recovery treatment on stress relaxation	97
5.3	Effect of recovery treatment on stress relaxation	98
5.4	Progress of recovery in decarburized iron prestrained at 298°K and 195°K	99
5.5	Progress of recovery in decarburized iron	100
5.6	Dislocation structure in iron strained 5% by rolling at 298°K	102
5.7	Dislocation structure in iron strained 5% by rolling at 298°K	103
5.8	Dislocation structure in iron strained 5% by rolling at 195°K	104
5.9	Dislocation structure in iron strained 5% by rolling at 195°K	105
5.10	Dislocation structure of fully recovered iron prestrained 5% at 298°K	106
5.11	Dislocation structure of fully recovered iron prestrained 5% at 298°K	107
5.12	Dislocation structure of fully recovered iron prestrained 5% at 195°K	108

FIGURE		PAGE
5.13	Dislocation structure of fully recovered iron prestrained 5% at 195 °K	109
5.14	Temperature dependence of the time required for various amounts of recovery	115
5.15	Dependence of activation energy for recovery on the fraction of recovery	116
6.1	Schematic diagram of a polycrystal strained in uniaxial tension	124
6.2	Schematic diagram showing lattice rotation in a deformed grain	125
6.3	Burgers circuit construction used to calculate ρ_{geom}.	125
6.4	Grain size dependent portion of internal stress as a function of strain for decarburized iron at 298°K	129
6.5	Grain size dependendent portion of internal stress as a function of strain for 70/30 alpha brass at 195°K	130
6.6	Increment of internal stress due to grain size for 70/30 alpha brass at 195°K	131
6.7	Increment of internal stress due to grain size for decarburized iron at 298°K	132
6.8	Variation of Hall-Petch slope with strain	136
A-I	Schematic of tensile testing machine	143

CHAPTER I

INTRODUCTION

The great usefulness of metals as structural materials depends primarily on the combination of their high strength and ductility. The useful strength of a metal may be greatly improved by the process of work hardening. In terms of modern concepts of deformation, which primarily involve the generation and motion of dislocations, the increase in strength due to work hardening may be defined as the increase in stress required for dislocation motion. This is a good definition because it permits us to discuss strengthening mechanisms in terms of the generation and movement of dislocations through a matrix (under an applied stress) and the impedance of this movement by the interaction of dislocations with potential barriers.

One of the important methods employed in metallurgical practise to improve the strength of metals is the refinement of the grain size. The basic idea is that grain boundaries act as barriers to dislocation movement and that a decrease in the grain size will result in an increase in strength.

The influence of grain size on the flow stress σ_f of polycrystals of average grain diameter D has been expressed in terms of the Hall-Petch equation (Hall, 1951; Petch 1953),

$$\sigma_f = \sigma_o + k_f D^{-1/2} \qquad 1.1$$

where σ_o and k_f can be best described as experimental parameters. Equations of this type have been used to describe both the initial yield stress

and the subsequent flow stress developed during work hardening.

The overall objective of the present work has been to study the effect of grain size on the flow stress developed in a metal polycrystal during work hardening. In order to examine in detail the grain size dependence of the flow stress during work hardening cognisance must be taken of the factors controlling the accumulation of dislocations in polycrystals during plastic deformation. Observation of the flow stress is an indirect method of studying the accumulation of dislocations in the sense that the total flow stress is usually considered to be the sum of both a thermal and an athermal component. In general, the athermal component or internal stress can be related directly to the density of dislocations in the specimen. In this work the internal stress developed during work hardening has been monitored with the aid of stress relaxation experiments. If stress relaxation experiments are performed after various amounts of plastic strain in specimens of different grain sizes, the process of dislocation accumulation in polycrystals can be studied. This type of observation has been used in the present study to establish the effect of grain size on the rate of dislocation accumulation in polycrystalline iron, copper and 70/30 alpha brass.

Since recovery at elevated temperatures is a process whereby the density of dislocations accumulated during plastic deformation is gradually reduced, it has been used to examine the stability of the work hardened state in iron after deformation at room temperature and $-78^{\circ}C$. It is shown that the thermal stability of the work hardened structure is directly related to the arrangement of accumulated dislocations.

CHAPTER II

LITERATURE REVIEW

2.1 Plastic Deformation and Strain Hardening of Metal Polycrystals

2.1.1 Introduction

A comprehensive theory of plastic flow and the phenomenon of strain hardening should account for both the behavior of single crystals and polycrystals containing large numbers of crystals separated by high angle boundaries. The plastic deformation of individual single crystals is in itself extremely complex and has been studied thoroughly by many competent researchers. No attempt is made here to review this subject as a number of excellent reviews have appeared in the past few years. The emphasis in this review is aimed at the analysis of stress and strain in an aggregate of crystals (normally called a polycrystal) when the whole aggregate is strained plastically. A great deal of attention has been concentrated on deriving the flow stress of a polycrystal from the properties of individual single crystals. The basic premise in these theories is that the plastic behavior of a polycrystal must be explained in terms of the plastic behavior of a single crystal subject to the boundary conditions on forces and displacements which the surrounding crystals impose. Many attractive theories to describe the mechanism of plastic deformation of polycrystals have been formulated on this basis.

The above theories however lack the ability to deal with the effect of grain size on the plastic deformation of a metal polycrystal. This arises from the basic assumption made in all of the above theories that the work of deformation is entirely accounted for by simultaneous glide on several of the available slip systems in each grain. The operation of many slip

systems satisfies the macroscopic compatibility conditions but does not satisfy the discontinuities which may arise on a microscopic scale in the vicinity of the grain boundaries. Any extra work which may be needed to satisfy these microscopic discontinuities is assumed not to contribute substantially to the energy of deformation. It is well documented in the literature however that many metals show an increase in the flow stress with a decrease in grain size. Various models have been proposed to account for the influence of grain size and these will be reviewed.

For a clear understanding of the deformation behavior of a polycrystal it is essential to define the nature of the flow stress. The stress applied to a specimen during straining may be resolved into two components, a thermal and an athermal component. A distinction between these two components is necessary in order to formulate a theory of the temperature and strain rate dependence of the flow stress. Seeger's theory of the flow stress is reviewed and its relevance in distinguishing between the two components of the flow stress is discussed.

Progress towards an understanding of polycrystal deformation can hardly be made without the aid of careful experimental observation. Numerous experimental attempts have been made to observe the stress-strain relation in polycrystals, and although they have contributed enormously to our knowledge, some of the observations are confusing and contradictory. Recently experimental attempts have been made to measure separately the relative magnitudes of the components of the flow stress. This separation is important in the study of both work hardening and other aspects of crystal plasticity, such as solid solution strengthening. The experimental techniques will be critically reviewed with special emphasis given to those employed in this thesis.

2.1.2 Classical Theories of Polycrystal Deformation

Considerable attention has been given to the problem of polycrystal

deformation originating with the work of Sachs (1928). The first real success came with the classical theory of Taylor (1938). Taylor's calculation has been generalized by Bishop and Hill (1951) and by Kocks (1958). Excellent reviews on this work have appeared in books by Cottrell (1953) and Tegart (1966) and much of the present review is based on these texts.

Most early workers concentrated their attention on calculating the tensile flow stress of a polycrystalline aggregate from the critical shear stress of a single crystal of the same material. The tensile flow stress, σ, of a single crystal is related to the critical shear stress τ by the relation $\sigma = m\tau$. 'm' is the orientation factor $(\cos\phi \cos\lambda)^{-1}$ where ϕ is the angle between the normal to the slip plane and the axis of tension and λ is the angle between the direction of slip and the axis of tension. (E. Schmid, 1924). The value of m differs for differently oriented crystals and the problem in predicting the behavior of a random polycrystal is to find the appropriate value. Suppose that in an aggregate the number of crystals with orientations in the range m to m + dm is N(m) dm. Then in theory a mean orientation factor

$$\bar{m} = \frac{\int m\, N(m)\, dm}{\int N(m)\, dm} \qquad 2.1$$

can be obtained by integrating over all grains. A value of $\bar{m} = 2.238$ has been obtained by Sachs (1928) for randomly oriented single crystal grains of a face-centered cubic metal. On the assumption that each grain deforms independently of its neighbours, Sachs proposed that this value be used to calulate the tensile flow stress of a polycrystal, assuming that $\sigma = \bar{m}\tau$.

The problem was next considered by Taylor (1938, 1955), who compared the stress-strain curves of polycrystals and single crystals of aluminum. He found good agreement when the value $\bar{m} \simeq 3.1$ is used, but not when $\bar{m} \simeq 2.2$. Taylor discussed the cause of this discrepancy and

found the above method of averaging unsatisfactory for two very good reasons.

(i) Continuity of Material. If each crystal deformed on only a single slip system, gaps would be created at the grain boundaries, because different crystals would deform in different directions. For ductile materials this is known not to happen and the continuity of material is everywhere preserved during plastic deformation. This means that each grain is deformed into a shape that is defined by the deformation of its neighbours, and not merely into one of the restricted class of shapes that can be generated by slip on a single system. It was known by Von Mises (1928) that an unrestricted change of shape (without change in volume) requires slip to take place on at least five different systems, i.e. on five different orientations of slip plane and direction. Some of these systems cannot be favorably oriented with respect to the axis of loading and must therefore have large values of m. Thus the effective mean orientation factor $\overline{m}$ must be greater than the value obtained by assuming that only the most favorably oriented system in each grain is active.

(ii) Continuity of Stress. Because of the continuity of the material the stress in any grain cannot be independent of the stresses in other grains. The stress distribution must be such that the forces exerted through any grain boundary, or any other surface in the body, are in static equilibrium. This does not mean that the stress is necessarily continuous in all its components; it is sufficient if the components that contribute through a surface are continuous through that surface. Nevertheless, the continuity condition places a restriction on the stress distribution that is not allowed for in the averaging theory of Sachs.

Taylor attempted to satisfy these continuity conditions by assuming that each grain undergoes the same homogeneous strain as the bulk material. However, this assumption overlooks the differences in orientation which do

not allow some grains to support as much load, without yielding, as others and violates the second continuity condition.

To produce this homogeneous strain at least five differently oriented slip systems have to operate in each grain. The choice of sets of slip systems actually depends on two conditions, one geometrical and one physical. The geometrical condition exists because some slip systems are not independent of one another. Taylor concludes that, for a face-centered cubic metal which has available 12 slip systems, there are only 96 irreducible and geometrically satisfactory combinations of five slip systems out of a possible 792 selections.

To choose a physically possible set of slip systems from the geometrically possible sets, Taylor postulates that this will be a set on which the work of deformation is least. During an increment of plastic strain, $d\varepsilon$, the work of deformation on the slip planes is $\sum_{i=1}^{n} \tau_i \, d\gamma_i$ where τ_i and $d\gamma_i$ are the shear stress and increment of shear strain on the ith slip plane, and where the sum is taken over all slip planes. In terms of macroscopic stress and strain the work of deformation is $\sigma d\varepsilon$ (if a system of combined stresses is applied, $\sigma d\varepsilon$ means $\sigma_{xx} \, d\varepsilon_{xx} + \ldots + \sigma_{xy} \, d\varepsilon_{xy} + \ldots$ etc.). According to the principle of virtual work this must equal the work done on the slip planes,

$$\sigma \, d\varepsilon = \sum_{i=1}^{n} \tau_i \, d\gamma_i \qquad 2.2$$

so that Taylor's postulate selects a set of shears with which the strain $d\varepsilon$ can be accomplished by the smallest applied stress σ. Taylor ignores the energy stored during deformation. This is a reasonable assumption in single crystals where the fraction of the work of deformation which is stored is about 1/20. The actual shear stress τ_i is assumed by Taylor to have the same value in every slip system operating in the crystal at

every stage of deformation. Then the product $\tau_i \, d\gamma_i$ can be replaced by $\tau_s \left| d\gamma_i \right|$ where $\left| d\gamma_i \right|$ denotes the absolute magnitude of $d\gamma_i$. In the restricted case where τ_s is the same on all slip systems, Eq. (2.2) can be written as

$$\sigma \, d\varepsilon = \tau_s \sum_{i=1}^{n} d\gamma_i \qquad 2.3$$

which shows that Taylor's postulate means that the set of slip systems actually used is one for which $\sum_{i=1}^{n} \left| d\gamma_i \right|$ is a minimum. The validity of this postulate has been proved by a theorem due to Bishop and Hill (1951).

Taylor applied his theory to the tensile deformation of a face-centered cubic metal. The problem is to find, for each orientation of a single crystal grain, the set of slip systems for which $\sum_{i=1}^{n} \left| d\gamma_i \right|$ is a minimum and yet gives the required external strain. Taylor calculated the value of the ratio $\overline{m} = \sum_{i=1}^{n} \left| d\gamma_i \right| / d\varepsilon$ for each of 44 orientations of the tensile axis with respect to the crystal orientation. Averaging these values results in an orientation factor of $\overline{m}$ - 3.1 which is considerably bigger than the value of 2.24 of the theories which do not take the first continuity condition into account.

As a test of his theory, Taylor compared the stress-strain curve of polycrystalline aluminum with a curve calculated from that of a single crystal with an orientation in the center of the stereographic triangle. The agreement was not very good for reasons which will be discussed later.

Bishop and Hill (1951) have devised a very elegant mathematical method for the determination of $\overline{m}$ using the equation $\sigma = \overline{m} \, \tau$ and the general properties of the yield behavior of metal single crystals. They have pointed out that the assumption of a homogeneous deformation is not necessary and can be substituted by much more general postulates which take account of the stress-continuity conditions. Their general argument is based on the principal of maximum plastic work for a deformed single

crystal which states that if a crystal undergoes an increment of plastic strain $d\gamma$, the work done by the actual stress τ is not less than that done by any other stress τ' which does not exceed the critical shear stress, i.e. $(\tau - \tau')\, d\gamma \geq 0$.

Bishop and Hill apply this principal to show that the actual work done in a polycrystal is the same as would be done if all the grains underwent the same macroscopic strain. Bishop and Hill, with the aid of their more general argument, were able to determine $\bar{m}$ for a variety of test types from simple tension to simple shear deformation, thereby getting the complete yield surface for a quasi-isotropic, quasi-homogeneous face-centered cubic polycrystal. Their value for the tensile test coincides with that of Taylor.

Kocks (1958) discussed the poor agreement found between Taylor's calculated curve and the stress-strain curve of polycrystalline aluminum. He proposed that the mechanism of the plastic deformation of a polycrystal is similar to that of a free single crystal stressed such as to activate the simultaneous glide of dislocations in many slip systems. He termed this process "polyslip". Assuming polyslip to be the relevant process Kocks derived Taylor's formula for the calculation of the polycrystalline stress-strain curve from the shear-hardening curve of a free single crystal in a general way, partly following Bishop and Hill, but with emphasis on the physical assumptions involved.

An improved experimental check of Taylor's formula is presented by Kocks with the approach that since the concept of the whole theory is polyslip, it is appropriate to choose as the basic single crystal curves, those of exact corner orientation where many slip systems are operating simultaneously. A polycrystal curve calculated from the curve for a $\langle 111 \rangle$ orientation in a single crystal of aluminum is in good agreement with the experimentally observed curves for aluminum polycrystals. He also applied the above method to data available in the literature, Lucke and

Lange (1952), Karpop and Sachs (1927) and found good agreement with the Taylor formula.

2.1.3 Effect of Grain Size on Polycrystal Deformation

None of the theories discussed in the previous section take the grain size into account, apart from assuming that the grain size is fine enough to insure reasonably homogeneous deformation. It is well documented that at low and intermediate temperatures (where mass transport cannot be accomplished by diffusion or grain boundary sliding) the presence of grain boundaries strengthens both pure and alloy polycrystalline materials. Part of this strengthening naturally results from polyslip being enforced in the various grains, however the observed increase in strength with decrease in grain size cannot be explained solely by this theory (Boas and Hargreaves, 1948; Nabarro, 1950). There is an additional strengthening which results from the presence of grain boundaries and several attempts have been made to clarify the nature of this additional strengthening term. A review of this work is the subject of the following sections.

(a) Dislocation Pile Up Model: A dislocation pile up model to account for the effect of grain size on the flow stress of polycrystalline aggregate has been put forward by Armstrong et al (1962). Their theory is based on an extension of the pile up model for yielding to the post yield region of the stress-strain curve of a polycrystal. This derivation is prompted by the experimental observation that for many metal polycrystals the flow σ_f bears an inverse square root relationship to the grain size,

$$\sigma_f = \sigma_o + k_f D^{-1/2} \qquad 2.4$$

where σ_o and k_f are constants and D is the mean grain diameter.

In the original pile up model for yielding the dislocations in a slip

band are blocked at the grain boundaries. Since slip cannot propagate freely across a boundary in a polycrystal, a stress concentration is produced where the slip band is blocked. Eshelby, Frank and Nabarro (1951) gave exact solutions for the length of a pile up and the stress concentration at its head. Their solution for a single-layer, single-ended pile up of discrete edge or screw dislocations in an isotropic medium of shear modulus μ and Poisson's ratio ν gives for the length "ℓ" of the pile up

$$\ell = 2n\,A/\tau \qquad 2.5$$

where n is the number of dislocations in the pile up assumed to be large, τ is the applied stress resolved along the plane of the pile up and A equals $ub/2\pi$ for screw dislocations and $ub/2\pi(1-\nu)$ for edge dislocations. It also gives for the stress concentration τ_{tip} at the tip of the pile up

$$\tau_{tip} = n\tau \qquad 2.6$$

In his original derivation Petch (1953) used these results to derive the yield stress-grain size relation by assuming that there must be produced a critical stress of magnitude $\tau_c = \tau_{tip}$ at the grain boundary in order to propagate plastic slip and that the length of the pile up "ℓ" is the same as the grain size D. By substituting $n = \tau_c/\tau$ into Eq. (2.5) and solving for τ, the Hall-Petch relation is obtained as

$$\tau = \tau_o + \sqrt{2\,A\tau_c}\;D^{-1/2} \qquad 2.7$$

where τ_o is included as a possible friction stress within the grain and the Hall-Petch slope is identified as $k = \sqrt{2\,A\tau_c}$.

Armstrong et al (1962) extended the pile up model of yield to the flow stress at some constant strain after yielding by focusing their attention on the microscopic rather than the macroscopic discontinuities which can occur in the vicinity of the grain boundaries. It is known that the deformation within a grain is not uniform but is concentrated into slip bands, so there is an intense local continuity problem where these bands reach a grain boundary. This problem is not removed by the process of polyslip, so it is not considered in the classical theories of Taylor and Bishop and Hill. According to Armstrong et al. this local continuity problem gives rise to the resistance to the formation of a slip band and this resistance will increase with strain in the band. The arguments used originally for yielding indicate that once this resistance reaches a limiting value because of the production of plastic deformation around the end of the slip band, the shear stress in the operating band is given by

$$\tau = \tau_o + k_s D^{-1/2} \qquad 2.8$$

where $k_s D^{-1/2}$ is the limiting grain boundary resistance in terms of shear stresses and τ_o approximates to the critical shear stress of a free single crystal, although it may be somewhat modified by the polyslip required for deformation within a polycrystal. It should be noted that the most important assumption in this model is that the shear stress, τ, represents the criterion for the continued production of new slip bands from the ends of old ones at the grain boundaries.

In their paper the authors depart slightly from the original model for yielding proposed by Petch and give for the tensile flow stress of a polycrystal,

$$\sigma_f = \sigma_o + k_f D^{-1/2} \qquad 2.9$$

where $\sigma_o = m\tau_o$ and $k_f = \bar{m} k_s$. The authors derive their model from the similarity between a slip band and a crack with respect to the relaxation of shear stress at the tip of a crack. Their derivation yields a slightly different value for the Hall-Petch slope

$$k_s = \tau_{max} r^{1/2} \qquad 2.10$$

where τ_{max} is the stress needed to initiate slip at a distance r from the slip band. There is an orientation problem in the operation of this source similar to the orientation problem encountered in determining the critical shear stress within the various grains of a polycrystal. Thus the average value of τ_{max} required to operate a slip source in its slip plane can be described in terms of the mean orientation factor $\bar{m}$ so that,

$$\tau_{max} = \bar{m}\tau_d \qquad 2.11$$

Thus the value of the Hall-Petch slope in the flow stress-grain size relation (Eq. 2.9) is now given by,

$$k_f = \bar{m}^2 \tau_d r^{1/2} \qquad 2.12$$

The authors have used the above relations to explain the sensitivity of the flow stress to grain size by emphasizing that the principle factors of importance are the number of slip systems, the shear modulus and dislocation locking. They attribute the low grain size sensitivity observed in f.c.c. metals to the large number of slip systems, small $\bar{m}$ and the absence of dislocation locking, small τ_d. If alloying elements are added to increase locking effects as in alpha-brass then τ_d is increased leading to increased k, and the grain size dependence remains to higher strains.

The grain size sensitivity of the flow stress in b.c.c. metals is

attributed to the locking effects of interstitials which leads to a large τ_d and hence large k_f. The authors assume that even after yield, locking is still important in continuing the propagation of slip bands.

The reduced number of slip systems in h. c. p. metals results in a large orientation factor $\bar{m}$ and is assumed to be responsible for the increased sensitivity to flow stress observed in these metals.

A serious handicap in the above theory is that there is no direct quantitative relationship between the grain boundary resistance term $k_f D^{-1/2}$ and strain ε . The effects of strain can only be inferred indirectly, through changes in k_f.

Petch (1969) has recently examined the flow stress-grain size relationship in Cu-Zn solid solutions. He found that as the stacking fault energy and the testing temperature of the material is lowered the Hall-Petch slope increases with plastic strain. Petch suggests that the observed increases in k_f really represents a σ_o effect masquerading as a k_f effect. Thus the observations indicate the existance of a grain size dependent work hardening term that contributes to k_f. This is essentially a work hardening model although in Petch's theory it is not ascribed a physical basis. This type of model will be discussed more fully in a subsequent section.

Li and Chou (1970) have offered some general criticisms of the pile up model. They cite the lack of direct observation of pile ups in pure metals although pile ups are seen in alloys of low stacking fault energy and long range order. Yet the Hall-Petch relation is found valid in both pure metals and alloys. They also cite some evidence that in Fe-3% Si, dislocations are emitted from grain boundaries at stresses much below the yield stress without the help of pile ups and that these stresses do not seem to depend on grain size, (Worthington and Smith, 1964). Thus the function of the pile up is lost and the validity of the model is questionable.

(b) Grain Boundary Source Model: The grain boundary source theory attempts to explain the sensitivity of flow stress to grain size without invoking the use of pile ups. The theory in its original form was first proposed by Li (1963). A similar version was proposed by Crussard (1963a, b).

In this model Li assumes that grain boundaries act as sources of dislocations. Their capacity to emit dislocations may change with the structure and composition of the grain boundary but is independent of grain size. Let 'm' be the length of dislocations emitted per unit area of grain boundary at the time of yielding. Then the density of dislocations at the time of yielding is, for a spherical grain of diameter D.

$$\rho = 1/2 \quad \frac{(\pi D^2 m)}{1/6\, \pi D^3} = \frac{3m}{D} \qquad 2.13$$

where the factor 1/2 arises from the fact that each boundary is shared by two grains. It appears to be an established experimental fact that the stress required to move dislocations in the forest formed by all the dislocations generated from the grain boundaries is (Nabarro, Basinski and Holt, 1964),

$$\tau = \tau_o + \alpha \mu b \sqrt{\rho} \qquad 2.14$$

where α is a constant and b is the magnitude of the Burgers vector. Substituting Eq. (2.13) into Eq. (2.14) gives

$$\tau = \tau_o + \alpha \mu b \sqrt{3m} D^{-1/2} \qquad 2.15$$

which is a Hall-Petch relation with the slope

$$k = \alpha \mu b \sqrt{3m} \qquad 2.16$$

The above discussion is only concerned with the initiation of plastic deformation which is controlled by the generation of dislocations from grain boundaries. However, since the present treatment utilizes the concept of work hardening near the grain boundary a suitable extension is possible to include the effect of higher strains, (Li, 1963). A kinetic equation as proposed by Johnston and Gilman (1959) to include dynamic recovery is used to describe the effect of plastic strain on the Hall-Petch slope. In this equation dynamic recovery is defined as the annihilation of dislocations during deformation. It was found that without recovery, the Hall-Petch slope increases with strain but the intercept τ_o remains unchanged. However, with dynamic recovery, the Hall-Petch slope may decrease with strain and the intercept may increase depending on the relative rates of work hardening and dynamic recovery.

As cited previously the Petch slope is found to increase with strain by Armstrong et al (1962) for zinc and mild steel if the strain is measured after the Luder's region. It is also found to increase with strain by Kuhlmann-Wilsdorf and Wilsdorf (1953) for α-brass and by Keeler (1955) for zirconium. However it is found to decrease with strain for copper and aluminum by Carreker and Hibbard (1953) and for silver by Carreker (1957). Li concludes from these observations the possibility that dynamic recovery is faster in f. c. c. metals than in b. c. c. or h. c. p. metals or in alloys having low stacking-fault energy. Quantitative comparison of Li's model with existing experimental data is very difficult, the critical problem being the inability to measure separately the magnitude of dynamic recovery occurring during straining.

(c) Work Hardening Model: As another alternative to the pile up model for the effect of grain size on flow stress Conrad (1963, a, b) and Meakin and Petch (1963) proposed a model based on the variation of dislocation density with grain size. This theory has been termed the "work hardening theory" and was recently reviewed by Li and Chou (1970).

The effect of grain size on dislocation density is not well understood in this model and a proportionality between dislocation density and the reciprocal of the grain size is derived in the following way. It is assumed as a first approximation that the average distance of slip, $\bar{x}$, is proportional to the grain size D,

$$\bar{x} = \beta D \qquad 2.17$$

where β is simply a proportionality constant. Since the plastic strain is given by (Orowan 1940),

$$\varepsilon = \phi \rho b \bar{x} \qquad 2.18$$

where ε is the tensile strain, ρ is the density of dislocations contributing to the strain and ϕ is an orientation factor. Assuming that ρ represents the total dislocation density in the specimen and substituting Eq. (2.17) into Eq. (2.18) gives,

$$\rho = \varepsilon / b\beta' D \qquad 2.19$$

where $\beta' = \phi\beta$.

The well known linear relation between yield or flow stress and the square root of dislocation density is either assumed or proven experimentally to be, (c.f. Eq. 2.14)

$$\tau = \tau_o + \alpha \mu b \sqrt{\rho} \qquad (2.14)$$

Substituting Eq. (2.19) into Eq. (2.14) gives,

$$\tau = \tau_o + \alpha \mu b \sqrt{\varepsilon / b\beta'} \quad D^{-1/2} \qquad 2.20$$

which is a Hall-Petch relation with the following slope

$$k_f = \alpha \mu b \sqrt{\epsilon / b\beta'} \qquad 2.21$$

A similar version of the model has been proposed by Louat as quoted by Marcinkowski and Fisher (1965).

Conrad, Feuerstein and Rice (1967, 1968) have tested this model in Nb strained in both rolling and tension. Over the range of grain size investigated, they showed that the dislocation density increases in an approximately linear manner with strain in accord with Eq. (2.19). They also showed that the flow stress varies as the square root of the dislocation density and that τ_o and α are independent of grain size as required by Eq. (2.20). They offer this evidence as support for the work hardening model. The model fails to explain the decrease in k with strain as found in copper and aluminum by Carreker and Hibbard (1953) and silver by Carreker (1957).

A major criticism of the model, raised by Li (1968) is the argument used to find the relationship between dislocation density and strain. Knowing the average slip distance only gives you the number of dislocations which have slipped and does not tell you anything about the number of dislocations which may actually accumulate due to that amount of slip.

(d) Dislocation Storage Model: A model to explain the effect of grain size on the flow stress of polycrystalline aggregates has been proposed by Ashby (1970). The model was originally formulated to explain why many two-phase alloys containing rigid particles work harden faster than do pure single crystals, but Ashby has indicated that it is equally applicable to polycrystals.

In order to acquire a clear understanding of this theory, it is essential to define adequately the term work hardening. A simple

definition of work hardening is that during the plastic deformation of a metal polycrystal the flow stress increases. The reason for this is that during straining dislocations are trapped and accumulate in the material. These trapped or stored dislocations impede the motion of glide dislocations and thus increase the flow stress.

Dislocations are stored during straining for two separate reasons: either they are required for the compatible deformation of various parts of the specimen or they accumulate by trapping one another in a random way. A familiar example of the first reason for storage is the plastically bent beam, (Nye, 1953). The uniform plastic bending of a single crystal beam to a curvature K can be accomplished by distributing edge dislocations parallel to the axis of bending, with a density K/b. In this simple case a geometric relationship exists between the deformation (described by K) and the number of dislocations (ρ) needed to accommodate it with minimum internal stress. These dislocations are called geometrically-necessary dislocations (Cottrell, 1964) and the density of such dislocations is indicated in this thesis by $\rho_{geom.}$. The density of these dislocations is directly related to the gradients of plastic deformation with distance and the minimum density of dislocations necessary to produce any arbitrary deformation can be similarly calculated, (Nye, 1953; Bilbyetal, 1958; Kroner 1962).

In two-phase alloys and metal polycrystals gradients of plastic strain are imposed by the microstructure. A polycrystal may be considered to be plastically non-homogeneous because when it is deformed each grain deforms by a different amount, depending upon its orientation and the constraints imposed on it by its neighbors. Accordingly gradients of strain are introduced into each individual grain even when the material is strained in simple tension. Such materials are defined by Ashby to be 'plastically non-homogeneous'. A pure single crystal, correctly oriented and suitably stressed deforms in a fairly uniform way. Such a

crystal is considered to be plastically homogeneous. Of course small deviations from uniform slip do occur, but these deviations are due to the mutual trapping of dislocations and not the microstructure of the crystal.

Ashby considers the pattern of deformation in a plastically non-homogeneous material in the following manner. He imagines the deformation divided into a general, uniform deformation, during which a density $\rho_{stat.}$ of statistically-stored dislocations accumulates due to random trapping, followed by a local non-uniform deformation during which a density $\rho_{geom.}$ of geometrically necessary dislocations accumulate. The first contribution ($\rho_{stat.}$) is the result of chance encounters in the material and their presence causes's the material's characteristic work hardening. There is no simple geometric argument to predict the density of these dislocations. The second contribution ($\rho_{geom.}$) is defined as the dislocation array which provides for compatible deformation of the parts of the plastically non-homogeneous material, and which has stresses associated with it which nowhere exceed the local yield stress (which may be larger than the bulk yield stress). The procedure proposed by Ashby is to calculate the displacements which are required for compatible deformation; to insert an array of dislocations which produces these displacements; and finally to check that the stress field due to these dislocations does not exceed the local yield stress anywhere. This 'local yield stress' is, in fact, the stress required to nucleate some other dislocation array of lower energy; thus it may be the local stress required to nucleate cross slip, or to nucleate slip on some other slip system. This process gives us the array of geometrically-necessary dislocations introduced by the non-uniform flow.

According to this procedure the dislocation density accumulated during straining can be considered made up of two parts. The first $\rho_{stat.}$ is a characteristic of the material; that is of the crystal structure,

shear modulus, stacking fault energy etc. The second $\rho_{geom.}$ is a characteristic of the microstructure, that is, the geometric arrangement of grains and phases; to a first approximation it is independent of the material. The total dislocation density is assumed simply to be the sum ($\rho_{stat.} + \rho_{geom.}$). This is obviously an oversimplification valid at small dislocation densities and in general the two components will interact with one another altering both the rate of dislocation accumulation and the rate of dislocation annihilation. Dislocation annihilation or dynamic recovery is neglected in this theory, but it is well known to play an important role in the work hardening behavior of metal polycrystals.

The above theory can be applied to the deformation of a polycrystal undergoing uniform tensile strain ε. If each grain undergoes uniform strain the result is that overlap of material occurs in some places, and voids appear in others. Ashby concludes that the amount of overlap or void is always proportional to $D\varepsilon/2$. For a complete discussion of this result, see Ashby (1970). The number of geometrically-necessary dislocations forced into each grain during this part of the deformation is roughly $D\varepsilon/4b$. The area of a grain in this two-dimensional analysis is roughly D^2, so that the density of geometrically-necessary dislocations is,

$$\rho_{geom.} = \frac{\varepsilon}{4bD} \qquad 2.22$$

$\rho_{geom.}$ measures the dislocation density over and above that accumulated statistically, and thus (on this model) is the origin of the grain-size dependent part of the work hardening in polycrystals. This expression is similar to that derived by Conrad, Feuerstein and Rice (1967, 1968) by a different argument involving the assumption that the average slip distance for dislocations is proportional to the grain size.

The stored dislocations of both types act as obstacles to

further slip and contribute to the work hardening of the polycrystal. For simplicity it is convenient to describe the array of stored dislocations by its average density, neglecting the type and distribution of the array. In this way it is possible to have a relationship between the flow stress τ, and the total dislocation density ρ_{total}, (Nabarro, Basinski and Holt, 1964) namely,

$$\tau = \tau_o + C\mu b\sqrt{\rho_{total}} \qquad 2.23$$

The total dislocation density, ρ_{total}, is simply $(\rho_{stat.} + \rho_{geom.})$. Under certain conditions depending primarily on the nature of slip, (Ashby, 1970) ρ_{geom} will dominate and the total dislocation density is given by Eq. (2.22). Inserting this value into Eq. (2.23) yields,

$$\tau = \tau_o + C'\mu\sqrt{b\varepsilon/D} \qquad 2.24$$

Thus the model provides an explanation for the way in which the stress-strain curve of a polycrystal is influenced by the grain size. It predicts a parabolic stress-strain curve when the influence of grain size dominates the work hardening behavior.

As mentioned previously the effect of dynamic recovery has been neglected in the derivation of this model. Even at room temperature it can reduce the value of $\rho_{geom.}$ and can lead to a time and temperature dependent stress-strain behavior. An important aspect of the present study is that it attempts to define the factors controlling the relative magnitudes of $\rho_{geom.}$ and $\rho_{stat.}$ in polycrystals.

2.1.4 Components of Flow Stress and Nature of Internal Stress in Deformed Polycrystals

In the previous sections on the deformation of polycrystals the

flow stress was divided into two components, namely a lattice friction component and a grain size component. The idea behind this classification is that the lattice friction term represents the resistance of the lattice to dislocations moving within the grains and the grain size term represents the net stress opposing dislocation motion due to the presence of grain boundaries. Obviously this is an oversimplification and it is worthwhile to examine the flow stress in more detail.

Seeger (1957) was the first to propose that the flow stress may be considered to consist of two components: a thermal component τ_{eff} which is dependent on temperature and strain rate, and an athermal component σ_{int} which is dependent on temperature only through the magnitude of the shear modulus μ. These ideas form the basis of Seeger's theory of the flow stress, which he considers is a prerequisite to the development of a theory of work hardening.

Consider a tensile test in which the rate of straining prescribed by the tensile machine is $\dot{\gamma}$. For glide on one system only, the shear strain is given by the well known Orowan formula

$$\dot{\gamma} = b\rho x \qquad 2.25$$

where b is the magnitude of the Burgers vector, ρ is the total density of dislocations which have moved and x is the average distance of motion of each dislocation. In general the dislocation movement will be resisted by obstacles which can be overcome with the aid of thermal energy and the applied stress. Assuming that the thermal activation can be described by absolute reaction rate theory with an activation energy $U(\tau)$ which depends on the applied shear stress τ, then the strain rate is given by,

$$\dot{\gamma} = b\rho x \, \nu_o \exp\left\{ - \frac{U(\tau)}{kT} \right\} \qquad 2.26$$

where ν_o is a frequency factor which depends on the nature of the obstacle and the way in which it is overcome, and k is Boltzmann's constant. The equation of the flow stress as a function of the absolute temperature T and the strain rate $\dot{\gamma}$ is obtained by solving Eq. (2.26) for τ . In order to accomplish this it is necessary to know the function $U(\tau)$ explicity. Seeger based his calculation of $U(\tau)$ on the following model.

Plastic flow in crystals is reached when a sufficiently large number of dislocations in the glide plane are able to move over distances large compared with the mean separation between dislocations. The applied stress must be large enough to overcome the opposing action of the stress fields of the dislocations surrounding a moving dislocation for simple motion. The main contribution comes from dislocations which are roughly parallel to the moving one and have the same Burgers vector. If these dislocations are distributed in a random way, and if the density per unit area is ρ', this opposing stress is given by

$$\tau_{int} = \alpha b \mu \sqrt{\rho'} \qquad 2.27$$

where μ denotes the shear modulus, and α is a constant of the order 1/5 whose exact value depends on the details of the dislocation arrangement, Poisson's ratio ν , and the character of the dislocations involved. These dislocations represent a fluctuating internal stress with a wavelength of the order of the mean distance between dislocations, i.e. 10^{-4} cm in annealed metal crystals and somewhat smaller in cold worked ones. In all cases of practical interest it is so large that thermal fluctuations do not assist the applied stress in overcoming these opposing stresses. They give rise to a contribution to the flow stress which is temperature independent except for a small indirect dependence due to temperature variation of the

elastic constants. This is the origin of the athermal component and has been indicated by the index int.

According to Seeger the other contribution to the flow stress of pure f. c. c. metals comes from the dislocations that penetrate the glide plane more or less perpendicularly, forest dislocations, and which therefore have little or no elastic interaction with the dislocations moving in the glide plane. The theory of dislocations cutting through the forest dislocations is very complicated and Seeger confines himself to the simplest version of the theory. Essentially the cutting of dislocations results in the formation of jogs with a characteristic thermal activation energy. Impurities in the crystal also contribute to the flow stress both by their direct interaction with dislocations, which is strongly temperature dependent, and indirectly by their influence on dislocation density which would be almost temperature independent. The forest dislocations and impurity atoms of the first type are termed short range obstacles (less than about 10 atomic distances) and are thought to be the origin of the thermal component of the flow stress $\tau_{eff.}$ in f. c. c. metals. In b. c. c. metals a contribution to the thermal component is thought to arise from the Peierls stress.

In order to solve Eq. (2.26) for τ, Seeger assumes that there is just one activation energy (U_o) that is rate determining, and that the apparent activation energy depends linearly on the applied stress. Thus we have

$$U = U_o - v(\tau - \tau_{int}) \qquad 2.28$$

where v is termed an 'activation volume'. The stress effective (τ_{eff}) in lowering the activation energy U_o is the difference between the applied stress τ and the opposing internal stress τ_{int}, since the strain rate is determined by those parts of the mobile dislocation density which are

situated in the adverse regions of the internal stress field. Eq. (2.28) serves as the formal definition of the components of the flow stress in what can be considered as 'plastically homogeneous' materials, (eg. single crystals of a pure metal).

Conrad (1965) has extended the above theory to polycrystals to include the effects of grain size on the flow stress. The flow stress now consists of three components, the thermal component τ_{eff}, the athermal component τ_{int} and a grain size effect which is often found to obey the Hall-Petch relation, hence,

$$\tau = \tau_{eff}(T, \gamma) + \tau_{int} + k_f D^{-1/2} \qquad 2.29$$

If the grain size effect is related to stress concentrations associated with the pile up of dislocations at the grain boundary as originally suggested by Hall and Petch, then variations of k_f with strain and temperature would introduce extreme difficulties into the determination of flow stress by Seeger's method. However, in the non-pile up models of the grain size effect the increase in stress with decrease in grain size simply reflects the increase in density of dislocations required to produce the given strain. Hence the grain size effect can be incorporated directly into τ_{eff} and τ_{int}. On this basis it is possible to study the accumulation of dislocations during the deformation of a polycrystal by measuring the magnitudes of the components τ_{eff} and τ_{int}.

2.1.5 Experimental Determinations of the Components of the Flow Stress

Recently several experimental techniques have been proposed for measuring separately the components of flow stress during the plastic deformation of crystalline solids. These techniques may be grouped into two major categories labelled indirect and direct techniques.

(a) Indirect Techniques. Three indirect experimental techniques which have recently been reviewed by Li (1967) are single and double strain rate cycling and non-linear stress relaxation. All of these methods involve measurement of the change in stress for a known change in strain rate. An analysis of the data by the method of dislocation dynamics leads to a calculation of σ_{eff} and σ_{int}. The method of non-linear stress relaxation is employed in this thesis and will be described in detail.

The imposed strain rate during uniaxial deformation can be divided into elastic and plastic components,

$$\dot{\varepsilon}_t = \dot{\varepsilon}_e + \dot{\varepsilon}_p \qquad 2.30$$

When the test is stopped $\dot{\varepsilon}_t = 0$, and so

$$\dot{\varepsilon}_p = -\dot{\varepsilon}_e = -\frac{1}{E}\frac{d\sigma}{dt} \qquad 2.31$$

where $d\sigma/dt$ is the stress relaxation at any time t and E represents the combined elastic modulus of specimen and machine.

Using the relation proposed by Orowan (1940) between the plastic strain rate $\dot{\varepsilon}_p$, the density of mobile dislocations ρ, and the average velocity v of these dislocations,

$$\dot{\varepsilon}_p = \phi b \rho v \qquad 2.32$$

where b is the Burgers vector and ϕ is a geometric factor, combined with the Gilman-Johnston (1959) power law between the velocity of dislocations and the effective stress,

$$v = B(\sigma - \sigma_{int})^{m^*} \qquad 2.33$$

where B is the mobility and m* is a constant over the normal range of effective stress, an equation for stress relaxation can be obtained as,

$$\dot{\varepsilon}_p = \phi \rho bv = \phi B \rho (\sigma - \sigma_{int})^{m*} \qquad 2.34$$

where σ_{int} is the internal stress and the term $\sigma - \sigma_{int}$ represents the effective stress acting on the dislocation.

Substituting Eq. (2.34 into Eq. (2.31) for $\dot{\varepsilon}_p$ gives

$$\frac{d\sigma}{dt} = - \phi B \rho Eb(\sigma - \sigma_{int})^{m*} \qquad 2.35$$

Assuming a constant mobile dislocation density and a constant internal stress during stress relaxation, Eq. (2.35) can be integrated to give,

$$\sigma - \sigma_{int} = k (t + a)^{-n} \qquad 2.36$$

where $n = 1/(m^* - 1)$, $k = \rho bB \phi E(1-m^*)$ and "a" is a constant of integration.

Differentiating Eq. (2.36) gives

$$\frac{d\sigma}{dt} = - nk (t + a)^{-n-1} \qquad 2.37(a)$$

or $$\log \frac{d\sigma}{dt} = \log (-nk) + (-n-1) \log (t + a) \qquad 2.37(b)$$

If Eq. (2.36) is to describe stress relaxation, a plot of log stress rate (or log strain rate) against log time must be linear at long times, as indicated by Eq. (2.37(b)). The slope of this linear part will be equal to (-n-1) and can be used to calculate values of $m^* = n-1/n$. The

deviation from linearity of the log $d\sigma/dt$ versus log t plot gives a value for "a". Knowing m* and "a", Eq. (2.36) can be used to calculate the long range internal stress, σ_{int}. The difference between the applied stress at t = 0 and σ_{int} gives the initial effective stress. This analysis can only be applied to materials which obey the initial assumptions that,

(i) the mobile dislocation density remainsconstant during stress relaxation,

(ii) the internal stress also remains constant.

These assumptions imply that the rate of relaxation is determined solely by the effective stress and that no work hardening or recovery occur during the relaxation period.

(b) Direct Techniques. The direct experimental techniques involve the use of stress relaxation to directly estimate the magnitudes of the internal and effective stress. The method simply consists in determining the level at which no stress relaxation is observed. At this point the applied stress is assumed to be exactly balanced by the internal stress and thus the plastic strain rate of the specimen is zero. This technique is labelled the zero relaxation rate method and can be achieved either by letting the stress relax with time until the relaxation rate is zero, continuous relaxation method (Rodriguez, 1968) or by incremental unloading and loading of the specimen and observing the stress at which the relaxation rate is zero, incremental unloading or "dip" test. (Gibbs, 1966; Lloyd and Embury, 1970)

The continuous relaxation method can be employed to measure the level of internal stress and effective stress in almost any material provided the time interval to reach the fully relaxed state is not prohibitively long. Long periods of relaxation demand great stability in the measuring devices and temperature control. It is also assumed in this method that the internal stress remain unchanged during the relaxation period. For this reason the continuous relaxation method is not feasible for tests at high

temperature (e. g. creep tests) or for that matter on any material that recovers at room temperature.

The incremental unloading or dip test technique has been suggested in order to overcome the above difficulties. The technique depends on the ability to measure a "negative stress relaxation". The argument being that when the applied stress σ is smaller than σ_{int} the specimen will contract due to the backward motion of dislocations under the stress $\sigma_{int} - \sigma$. This technique has met with some success in measuring the level of internal stress during high temperature creep experiments (Nix and Barrett, 1968; Lloyd and Embury 1970). A distinct advantage is that σ_{int} can be determined in a relatively short time duration, (i. e. before any recovery events become significant). A stringent requirement in this technique is the ability to measure or control specimen extensions of the order 10^{-6} to 10^{-7} inches.

Some investigators have employed this technique at intermediate and low temperatures where the method is subject to some doubt (MacEwan et al, 1969). Specimen contractions may occur in some materials at lower temperatures but it is difficult to separate this out from contraction or expansion in the testing machine itself. Guiu (1969) has been able to verify that a negative stress relaxation also arises from contractions in some parts of his tensometer. He states that these machine contractions are present at almost any stress level, but during the straining of a relatively soft specimen they are not observed until the stress relaxation due to specimen elongation is small.

It is worth mentioning at this point that the theoretical basis of this method is somewhat tenuous. The supposition that negative stress relaxation results from the motion of dislocations under a "back stress", $\sigma_{int} - \sigma$ arises out of the indiscriminate use of the "sinh" function in thermally activated deformation theory (MacEwan et al, 1969). In a theoretical argument Schoek (1965) pointed out that back fluctuations are

generally negligible but may become important depending on the distribution of local obstacles. However, the use of the sinh function to take account of them is not justified in his opinion.

2.2 Recovery of Internal Stress in Deformed Polycrystals

When a metal is deformed, the stress required to continue deformation increases continuously with strain. In the previous sections this was defined as work hardening and originates from the continued increase in dislocation density with strain. It has been shown that if a deformed metal is heated to a temperature below that required for recrystallization, the defect concentration is reduced without the movement of grain boundaries. This is called recovery. The processes occurring in recovery can be divided into two general categories, those involving the movement and annihilation of point defects, and those involving the annihilation and redistribution of dislocations. Only the latter will be discussed in this review.

Several excellent reviews have been published in recent years concerning the process of recovery. For example, Beck (1954), reviewed quite extensively the phenomena of recovery, subgrain growth and recrystallization. The recovery of mechanical properties was reviewed by Perryman (1957). The differences in the effects of single and complex slip were recognized. This is quite important since in the deformation of a polycrystalline metal, deformation will occur on more than one slip system and local regions will be bent and/or twisted relative to one another. This twisting and bending becomes more severe, both near the grain boundaries and with increasing strain in any region. The recovery process in any part of a deformed polycrystal thus involves the rearrangement of a high density of both screw and edge dislocations on several planes. This rearrangement occurs by glide and climb processes and

results in a structure consisting of cells or subgrains which are relatively perfect regions of the lattice separated from one another by low angle boundaries. Li (1966) has reviewed in detail the microscopic mechanisms involved during recovery with emphasis on the processes involving the behavior and interaction of single and groups of dislocations. It is apparent from Li's review that the rate and extent of recovery depends to a large extent on the distribution of dislocations after deformation and the subsequent rearrangement with mutual interaction.

Since a number of investigators have shown that the dislocation density decreases during annealing, it is expected that the magnitude of the flow stress decreases also in view of a possible direct relationship between flow stress and dislocation density. However, such a direct relationship has not been established during recovery. In fact Keh (1962), from his concurrent measurements of both flow stress and dislocation density, indicated the absence of such a relationship. Because of this lack of an established relationship between the flow stress and the microstructure during annealing, the understanding of the recovery of work hardening is difficult.

Nevertheless recovery is a process whereby the density of dislocations accumulated during plastic flow is gradually reduced. Thus a knowledge of the rate and temperature dependence of this process for various prestrain conditions might be useful in formulating a model of the work hardened state.

CHAPTER III

EXPERIMENTAL PROCEDURES

3.1 Introduction

One important aspect of the following work was to study the effect of grain size on the shape of the stress-strain curve in metal polycrystals. Tensile tests were performed on a variety of metals to determine the flow stress as a function of grain size. The methods of obtaining accurate measurements of stress and strain are described in section 3.3.1.

In order to measure separately the magnitudes of the effective stress and internal stress as a function of the degree of plastic strain, stress relaxation tests were performed after various amounts of plastic strain. The stress relaxation techniques which have been employed in this thesis are described in section 3.3.2. With this experimental procedure the internal stress and effective stress as well as the flow stress can be monitored as a function of strain in specimens of different grain size.

Tests were performed on iron, copper and 70/30 alpha brass in order to explore the effects of material variables, particularly the slip mode, on the development of effective and internal stress. In addition to tests at room temperature (298^{o}K) several tests were made at 195^{o}K.

Finally a qualitative study of the development of Laue asterism during deformation is made in an attempt to relate the mechanical measurements to the structure of the specimen. A microbeam back reflection X-ray camera with arrangement for irradiating a pre-selected area is described.

3.2 Materials and Specimen Preparation

In order to explore a range of materials which exhibit differences in slip behavior, experiments were performed on decarburized vacuum melted iron, high purity OFHC copper, and a commercial purity alpha brass. The details of heat treatment and methods of specimen preparation for each of these materials are described below.

Iron: The iron specimens were produced from 1 inch diameter rods of Ferrovac-E obtained through the courtesy of the United States Steel Co. Ltd. The original composition of Carbon, Nitrogen and Oxygen were listed as, Carbon .011 wt%, Nitrogen .003 wt% and Oxygen .008 wt%. The Ferrovac-E rods were reduced from the bulk by cold rolling to a thickness of .080 inches. The extent of each reduction was 50% and was followed by intermediate anneals at 800°C in a vacuum of 10^{-5} torr. for 30 mins. After each anneal the specimens were immediately raised to the cold portion of the furnace and allowed to cool in vacuum. Following this treatment the material was cold rolled by various amounts and given a final anneal to obtain the desired grain size. Determinations of grain size were made by the linear intercept method (Smith and Guttman 1953). The details regarding the grain sizes obtained are given in Table 3.1. In order to remove the large yield drop and Luders elongation, the Ferrovac-E specimens were decarburized in wet hydrogen at 650°C for 7 days, followed by 1 day in dry hydrogen. There was no change in grain size as a result of the decarburizing treatment. The concentrations of carbon, nitrogen and oxygen after decarburization are: Carbon .004 wt%, Nitrogen .003 wt%, and Oxygen .008 wt.%.

Alpha Brass: Commercial purity yellow brass sheet, 1/8 inch thick, was obtained through a local supplier. The brass was manufactured to ASTM B36 standards and the maximum limits on composition are listed as: Copper-64.0-68.5 wt. % , Pb-0.15 wt% max., Fe-0.05 wt.% max., remainder zinc. The as received stock was cut into 6 inch by 1 inch strips

and reduced to a thickness of .080 inches by cold rolling. The extent of each reduction was limited to 50%, followed by intermediate anneals at 700°C in an argon atmosphere for 30 min. After each anneal the specimens were immediately raised to the cold portion of furnace and allowed to cool. Following this treatment the material was cold rolled by various amounts and given a final anneal to obtain the desired grain size. Due to the presence of annealing twins in alpha brass and copper, 3/4 of the twin boundaries were counted in the determination of grain size. The details regarding the grain sizes obtained are given in Table 3.1. Analysis of brass specimens after thermal and mechanical treatment gave the following limits on composition: Copper-70-71 wt. %, Pb-not detected, Fe-0.05 wt. % max., remainder zinc.

Copper: The OFHC copper used in these experiments was of 99.995% nominal purity as determined by the suppliers, M and T Metal Co. Ltd., Hamilton. The copper was reduced from 1 1/2 inch diameter rods by cold rolling. Each reduction was not more than 50% and was followed by intermediate anneals at 800°C in a vacuum of 10^{-5} torr. for 30 mins. The specimens were raised to the cold portion of the furnace after each anneal. A range of grain sizes in copper was obtained in the usual manner and the details are listed in Table 3.1.

All the specimens were flat-sheet tensile specimens with a final cold-rolled thickness of .040" and a gauge length of 1.25 inches.

Prior to testing, the specimens were polished to remove any machining damage. The iron specimens were chemically polished in a solution of 2 parts H_3PO_4 to 1 part H_2O_2. Both alpha brass and copper were electrolytically polished in D-2 electrolyte which has a composition of 250 ml H_3PO_4, 500 ml. distilled water, 250 ml. Ethanol, 2 ml Vogel's

TABLE 3.1

Prestrain % reduction of thickness	Annealing Temperature (^{o}C)		Annealing Time (min.)	Grain Size (mm)
		IRON		
50%	800	annealed in vacuum 10^{-5} Torr	30	.050
	700		30	.038
20%	800		30	.087
	750		15	.074
15%	800		30	.180
	750		15	.130
		ALPHA BRASS		
50%	700	annealed in Argon	15	.091
	650		15	.068
	600		15	.031
	525		30	.025
25%	800		15	.160
	700		15	.075
	625		30	.057
10%	800		15	.190
		COPPER		
50%	700	annealed in vacuum 10^{-5} Torr	5	.018
25%	700		15	.030
10%	700		30	.043
5%	800		30	.055

After each anneal the specimens were raised to the cold portion of the furnace.

Sparbeize, 50 ml Propanol and 59 gm. Urea.

3.3 Measurement of Mechanical Response

One of the main objectives of this thesis is to investigate the effect of grain size on the work hardening behavior of metal polycrystals. The standard method was to record the variation of tensile flow stress as a function of strain for a variety of grain sizes. The flow stress however, is composed of two components, a thermal and athermal component and it is of considerable value to measure the effect of strain and grain size on the relative magnitudes of each component. In order to effect this objective, stress relaxation tests were performed for each material at increasing intervals of strain during the tensile tests.

3.3.1 Stress-Strain Measurements

All the materials tested were deformed in tension in a table model Instron testing machine using a crosshead speed of .05 inches per min. The flat sheet tensile specimens were successfully gripped between smooth plates as shown in Fig. 3.1. This assembly allowed for accurate alignment of the specimens in the grips. All the tests were performed in the stainless steel fixture shown in Fig. 3.2. The top end of the fixture is attached to the moving crosshead through a rigid frame and the bottom end pushes against the lower specimen grip. The upper grip is connected to the load cell through a universal joint and the lower connection is made through a hemispherical ball joint.

The tests at 195^{o}K were achieved by immersing the entire system in a bath of dry ice and methanol. This bath is at constant temperature at 195^{o}K and gave a uniform temperature throughout without stirring. Care was taken to ensure that the entire system was at constant temperature prior to the initiation of the test. To facilitate this, both

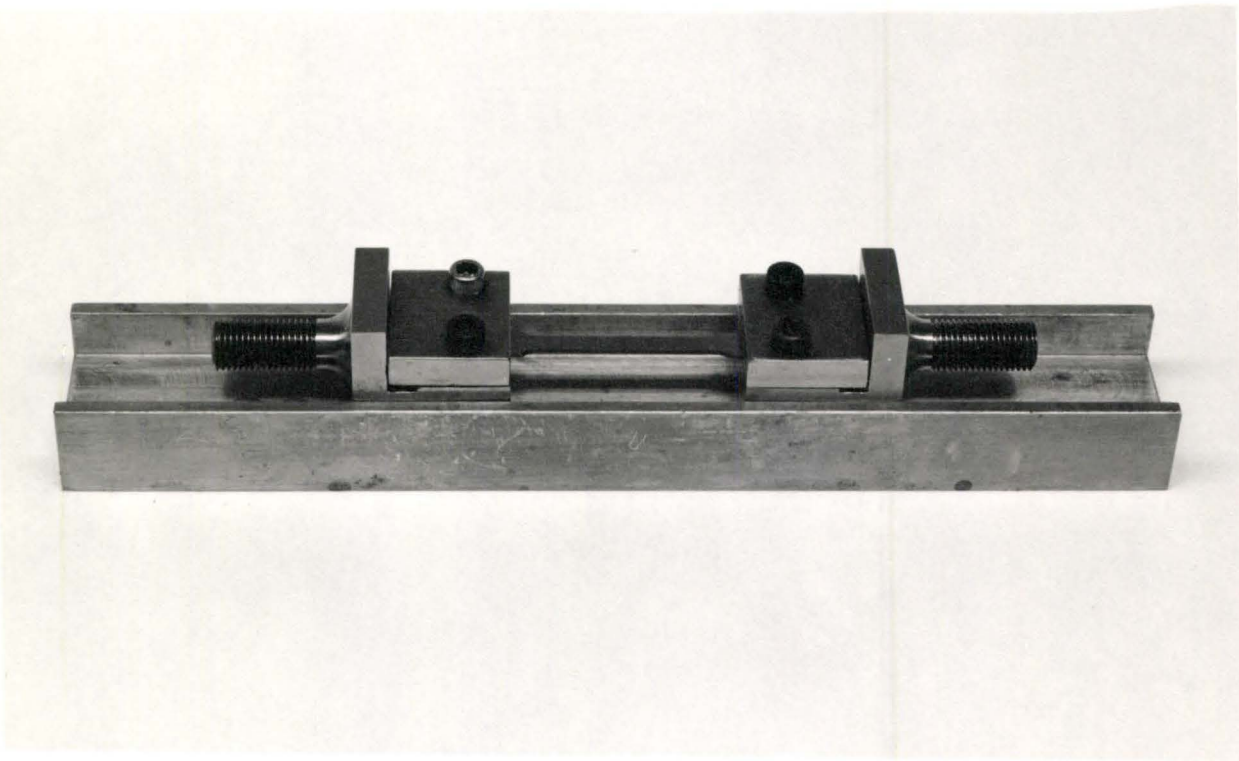

Fig. 3.1 Specimen grips and alignment block.

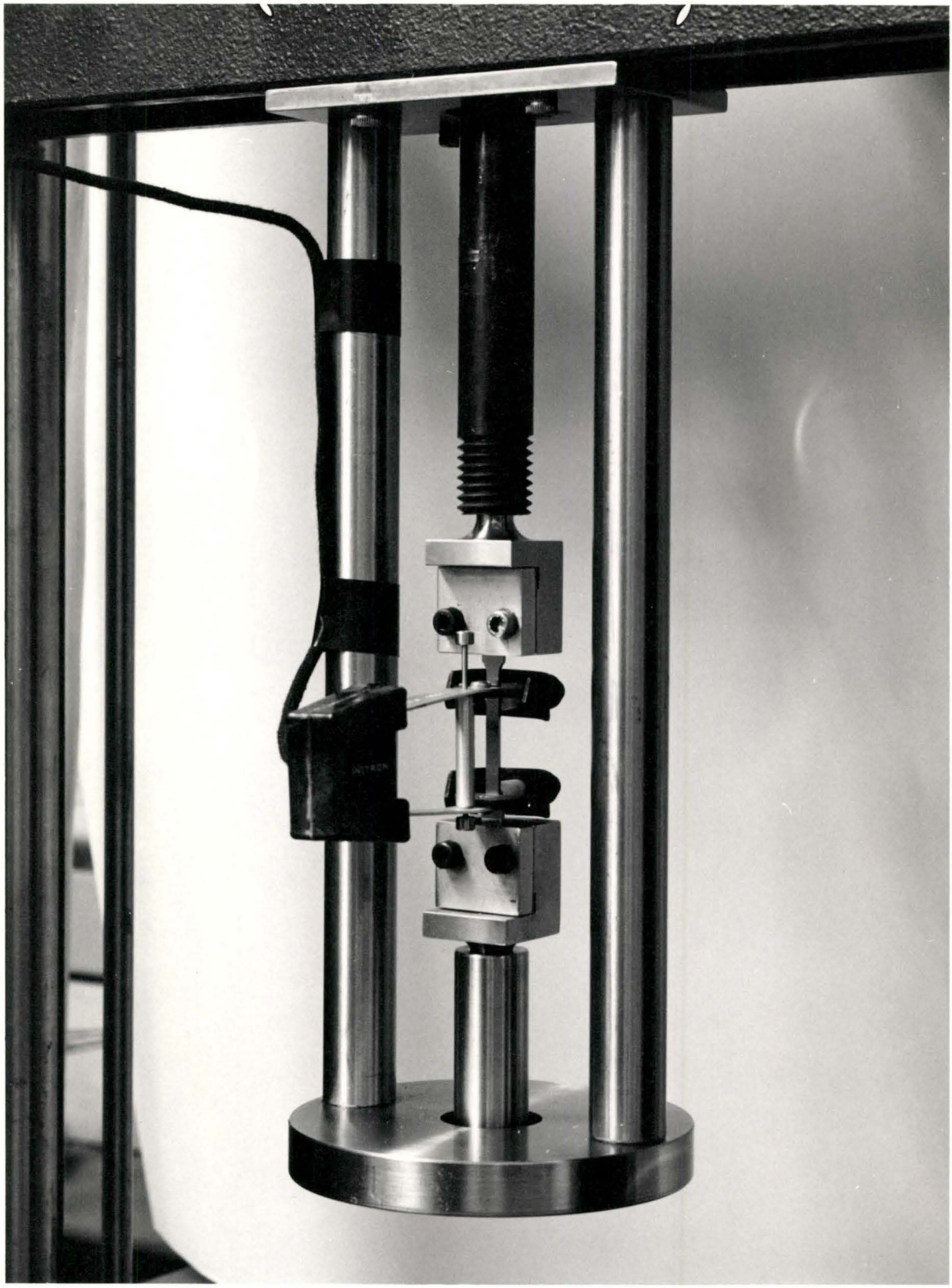

Fig. 3.2 Stainless steel tensile testing fixture.

load and strain were used as sensitive indicators of system equilibration.

The testing machine was equipped with an X-Y servo drive system and the strains were determined using standard Instron extensometers. The extensometers are the clip on type, consisting of four foil type resistance strain gauges bonded to a metallic element to form a four arm Wheatstone bridge circuit. It was connected to the specimen by spring clips, which gave a positive connection, but neither damaged the surface nor bent the specimen. The strain gauges were so constructed that an initial gauge length of one inch was always obtained. The Instron chart was synchronized to the strain gauge movement and a maximum chart travel of 10 inches was available for recording strain. The strain resolving capabilities used in all of the tests were 10^{-3} for strains less than 10% and 2.5×10^{-3} for strains greater than 10%. The strain gauges were calibrated at each test temperature by imposing a fixed movement to a calibration jig and adjusting the chart travel to give the required extension.

Changes in load were monitored by a highly sensitive electronic weighing system with a load cell employing bonded-wire strain gauges. The applied load on the cell causes a proportional change in the resistance of the strain gauges, which are arranged in a bridge circuit and excited by a stabilized oscillator. The resulting signal is amplified, rectified to D. C. and made to operate the pen of a high speed recorder. The load weighing system is easily calibrated by hanging small weights to the upper grip and adjusting the sensitivity. The design of the oscillator and amplifying stages is such that the sensitivity of the system remains constant over long periods of time.

The Instron machine is equipped with a zero load suppression device which is used to record the load on an enlarged scale to minimize errors in load reading. The accuracy of the overall load weighing system is independent of the range in use, and is normally better than $\pm$ 0.5%.

The combination load weighing system and X-Y chart drive system is shown schematically in Fig. 3.3. This type of tensile testing facility provides an accurate measurement of stress and strain for the materials tested.

3.3.2 Stress Relaxation Tests

In order to perform stress relaxation tests during tensile deformation, the crosshead motion of the Instron was arested at the desired strain and the decrease of load or stress were recorded as a function of time. The special characteristics of stress relaxation performed in an Instron testing machine are outlined fully in Appendix A. The load during stress relaxation was recorded on the standard Instron recorder running at a known speed. This was accomplished by switching the recorder from the X-Y servo drive mode to the standard synchronous chart drive mode before arresting the crosshead.

Two distinct stress relaxation methods were employed to determine the magnitudes of the internal stress (σ_{int}) and the effective stress (σ_{eff}). The first, a direct technique, is the continuous stress relaxation method (hereafter denoted as C.S.R.) In the C.S.R. method the crosshead is stopped at point A as shown schematically in Fig. 3.4. The system will then exchange plastic strain in the specimen for elastic strain in the system and the stress on the specimen will be relaxed. This relaxation of stress with time is associated with the motion of dislocations and will continue until either the mobile dislocation density can be reduced to zero or the applied stress is reduced to the value of the internal stress. Thus if the stress relaxation test is performed under conditions in which no complications due to strain ageing, recovery, or work hardening occur, the saturation or zero relaxation rate condition established at point B (Fig. 3.4) can be used to establish the values of σ_{int} and σ_{eff}. A simple check to see if any recovery, work hardening or

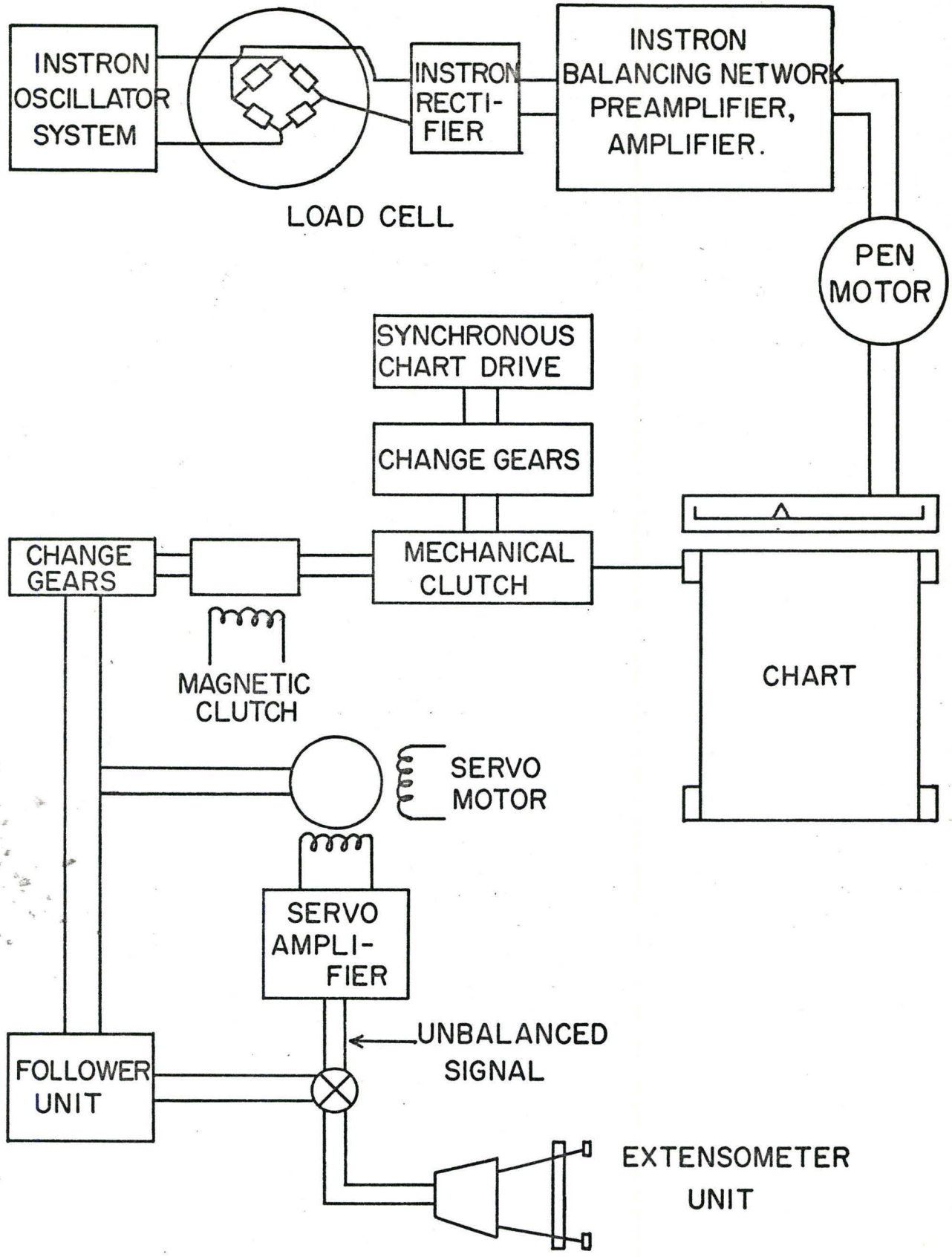

Fig. 3.3 Schematic diagram of load weighing system and X-Y chart drive system.

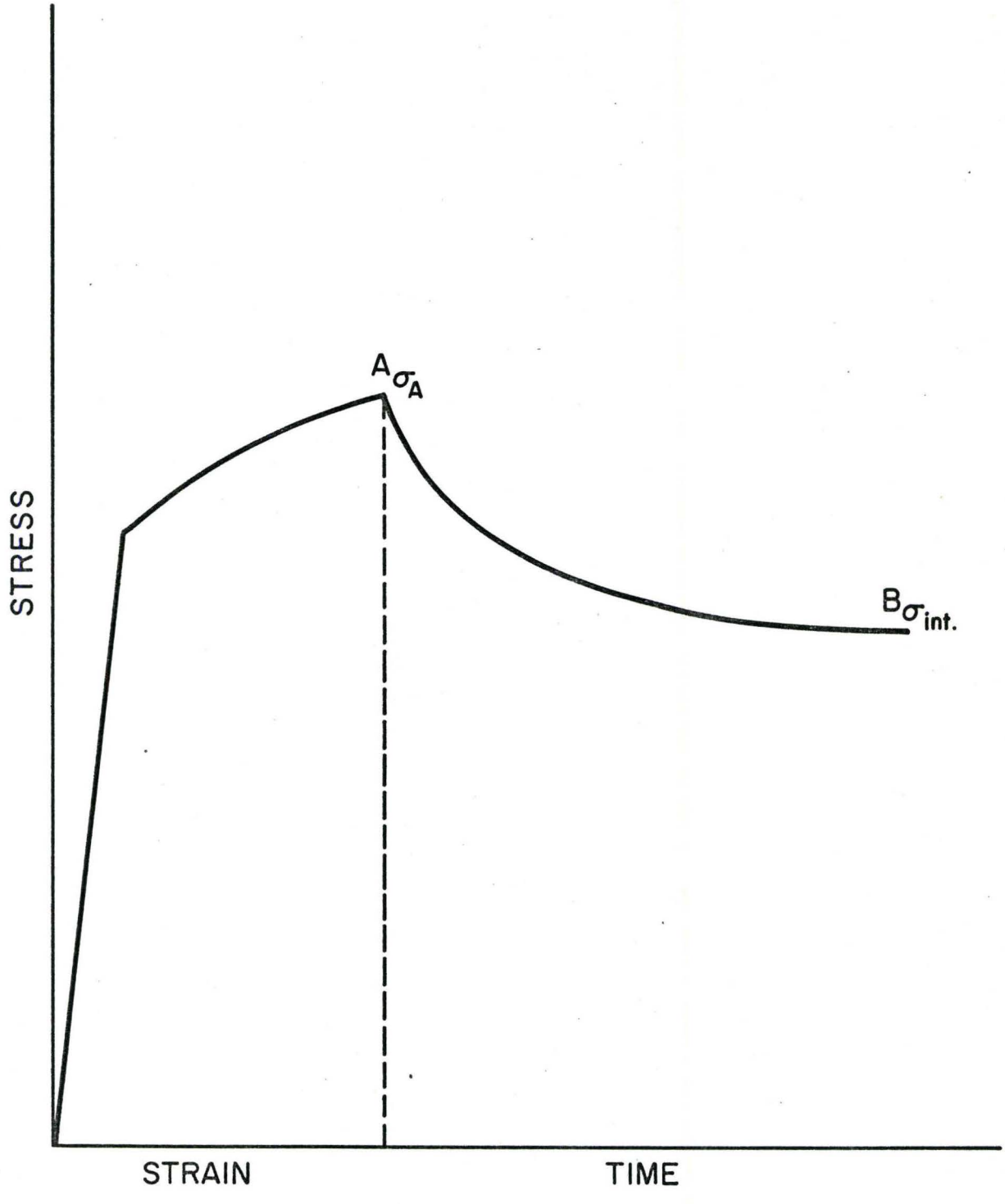

Fig. 3.4 Stress relaxation of a plastically deformed tensile specimen.

strain ageing takes place during stress relaxation is to observe the value of the flow stress upon restraining. Ideally it should be equal to the value at time t = 0 prior to stress relaxation.

Relaxation in the testing system was checked with a rigid specimen keeping all other factors the same. Total machine relaxation was found to be always less than 5% of the total relaxable load and most of it was complete in the first few seconds.

Accurate temperature control is essential during stress relaxation and precaution was taken to ensure that the room temperature never varied by more than $\pm$ 0.5°C. For tests at 195°K, the dry ice-methanol mixture gave a uniform temperature throughout which never varied more than $\pm$ 0.5°C during the relaxation tests.

The second, alternative method of determining the components of flow stress by stress relaxation is due to Li (1967). He has derived expressions relating non-linear stress relaxation behavior to dislocation dynamics. The theory is based on the Gilman-Johnston power law relating dislocation velocity to stress and was reviewed in detail on page 27.

To utilize this method (hereafter denoted as D. D.) the load during stress relaxation is recorded as a continuous function of time. The known speed of the Instron chart paper is used to get the time elapsed from the start of relaxation. The load-time plot is then replotted on load-log time coordinates and the stress relaxation curve is analysed by the method due to Li.

All of the data points reported in this thesis have been obtained by the C. S. R. method. In addition, data for iron at 195°K has also been obtained by the D. D. method. In order to confirm the validity of the C. S. R. technique some measurements of the magnitude of the internal and effective stresses were obtained using both the D. D. and C. S. R. techniques on identical specimens when experimental conditions permitted both methods to be used.

3.4 Observations of X-ray Asterism

3.4.1 Description of Back Reflection X-ray Camera

In order to relate the observations of internal stress to the detailed microstructure of the specimen, the development of Laue asterism during deformation was studied using a Hilger and Watts micro-focus X-ray unit. The back reflection camera used in conjunction with the micro-focus X-ray tube was based on the original design of Otte and Cahn (1959). This design permits rapid and precise setting for irradiating a pre-selected area.

The general arrangement of the apparatus on the Hilger micro-focus X-ray unit is shown in Fig. 3.5. The apparatus consists of three main parts, the collimator assembly, film cassette and specimen stage with X-Y drives. The specimen stage is mounted on a specially designed frame which allows the stage to be positioned accurately at any distance from the film cassette by means of a fine screw drive. The design of the frame ensures that the specimen stage is accurately parallel to the plane of the film and permits the whole assembly to be set perpendicular to the path of the X-ray beam.

The collimator assembly shown in Fig. 3.6 consists of two parts. The main section has a large pinhole of 200u in diameter at the end nearest to focal spot of the X-ray tube. The exit pinhole consists of an electron microscope aperture about 30μ thick with a 50μ pinhole in the center. It is mounted into a separate brass holder which is fitted into the main body of the collimator, permitting apertures of different pinhole sizes to be interchanged if necessary. The whole collimator assembly is accurately fitted into the body of the X-ray tube.

The film cassette is mounted directly onto the frame which is adjusted so that the cassette almost touches the collimator. The central hole in the cassette permits unobstructed passage of the X-ray beam to the specimen. The film to specimen distance is normally set at 1 cm.

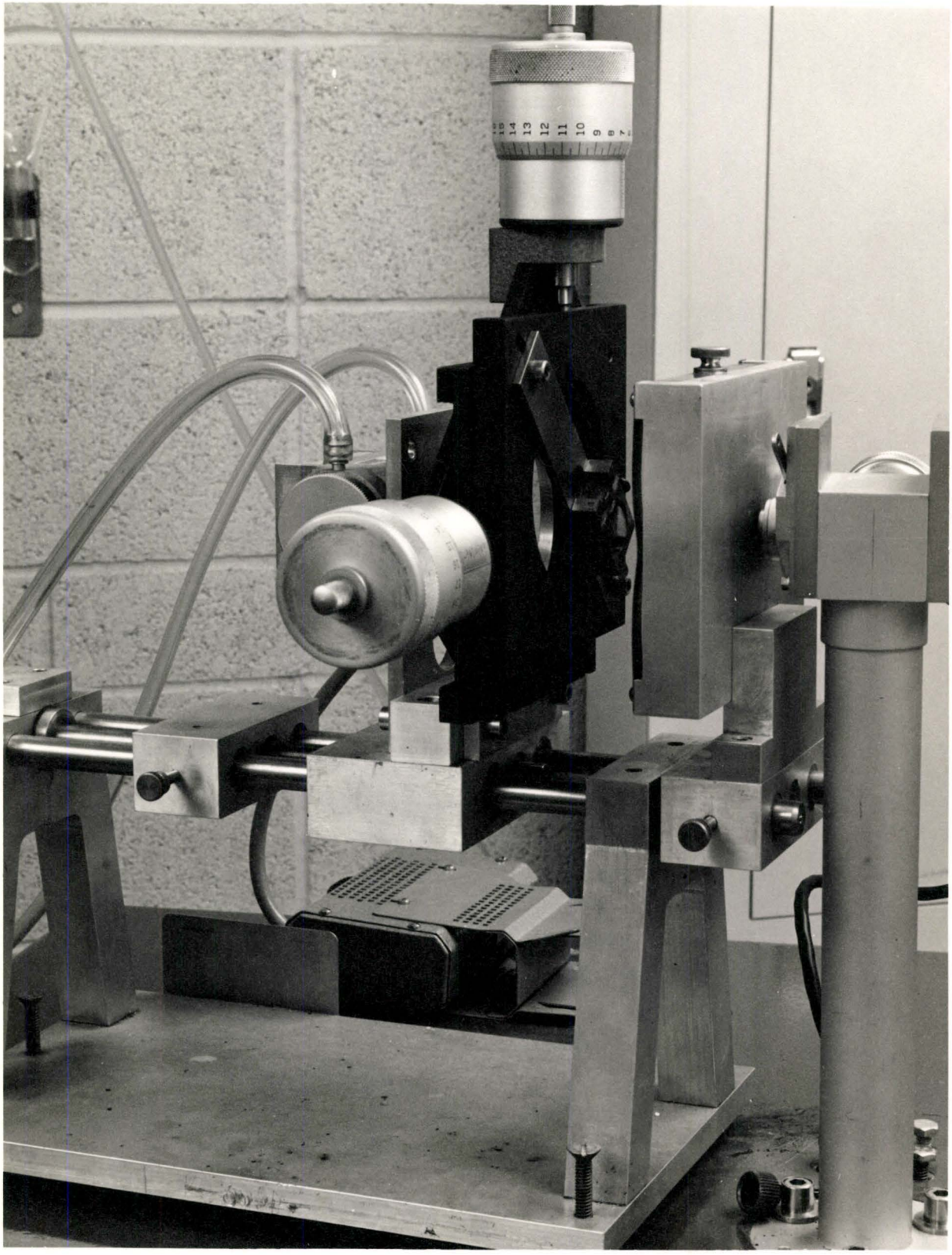

Fig. 3.5 Assembled X-ray micro-beam diffraction camera.

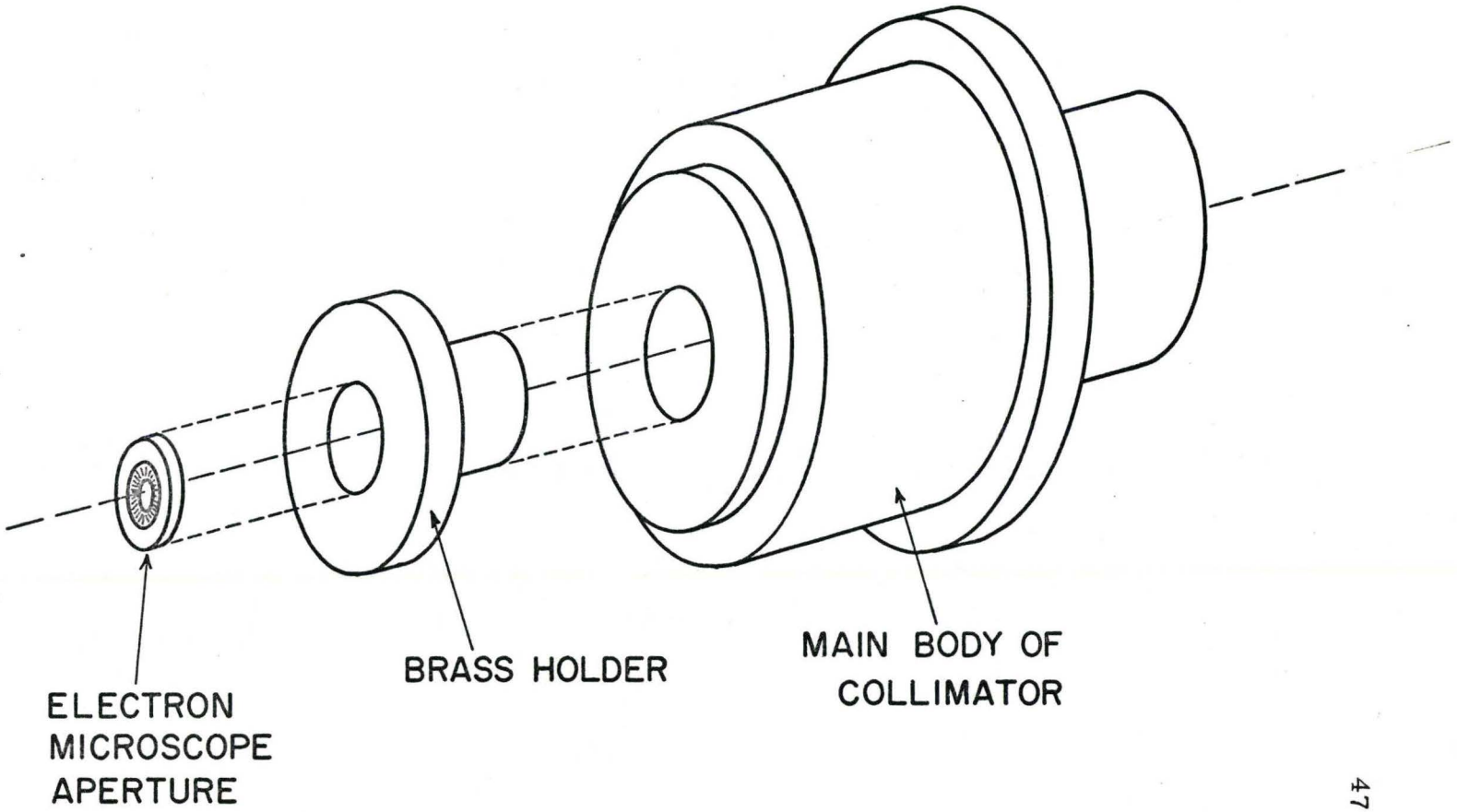

Fig. 3.6 Exploded view of collimator assembly.

The removable specimen stage has two perpendicular micrometer controlled motions, both normal to the X-ray beam and calibrated in units of .0001 inch. The micrometers act against spring loaded platforms on the stage. The stage can be unscrewed from its bracket on the frame and mounted on a bench type microscope for selecting the grain or specimen feature to be examined. The area to be irradiated is selected under the microscope and its distance from a set of crossed tungsten wires (.075 mm. in diameter) adjacent to the sample is measured. The specimen stage is remounted on the X-ray unit and the X-ray beam is then located by means of a proportional counter placed directly behind the specimen stage. The counter is connected to a rate meter in order to observe the reduced beam intensity as the two wires of the crosswire pass in turn through the beam. The intersection of the crosswire is located and the corresponding micrometer readings give the origin of the coordinates for location of the pre-selected area. A displacement by the distance measured on the microscope brings the selected area in front of the beam. The accuracy with which this could be accomplished was better than $\pm$ 15μ as measured on the specimen surface.

3.4.2 Information Obtainable from X-ray Asterism

The plastic deformation of a polycrystal involves a permanent change in shape of the aggregate as a whole. This change in shape is normally accomplished by a uniform lattice deformation (simple shear) plus a non-uniform lattice deformation, defined as the bending and/or twisting of originally flat lattice planes. The non-uniform lattice deformation introduces gradients of plastic strain in the material. In polycrystals the uniform lattice deformation in each grain is usually accompanied by a non-uniform lattice deformation due to the constraints imposed on each grain by its neighbours during deformation. A Laue photograph made on a crystal (or grain) which has been forced to undergo

non-uniform lattice deformation will show elongated spots (asterism). Useful accounts of the origins of X-ray asterism may be found in Barrett and Massalski (1966) and Russell and Ashby (1968).

The Laue spots from a perfect crystal (or grain) should be sharp, their size determined by the size and divergence of the X-ray beam and the crystal to film distance. The effect of non-uniform lattice deformation is shown schematically in Fig. 3.7 in which the intensity profile represents the intensity distribution in the Laue spot. Lattice bending results in an elongation and diffuseness of the Laue spot. The distribution of diffracted intensity across a Laue spot gives a measure of the amount of lattice bending which has occurred. In the simple case of Fig. 3.7(b) the mean lattice curvature K is given by

$$K = \frac{\Delta\phi}{\Delta X} \qquad 3.1$$

where $\Delta\phi$ is the angular rotation of the element of lattice plane ΔX due to lattice bending. In an earlier chapter it was shown that the density of geometrically necessary dislocations ($\rho_{geom.}$) required to accommodate this bending is given by K/b, (Nye, 1953).

In a general deformation the curvature of the lattice is given by (Nye 1953)

$$K_{ij} = \frac{\Delta\phi_i}{\Delta X_j} \qquad 3.2$$

where $\Delta\phi_i$ are the lattice rotations about three orthogonal axes in a Cartesian frame of reference associated with the displacement vector X_j. Nye (1953) has also shown that the dislocation density tensor α_{ij} is related to the curvature tensor K_{ij} by the equation,

$$\alpha_{ij} = K_{ij} - \delta_{ij} K_{kk} \qquad 3.3$$

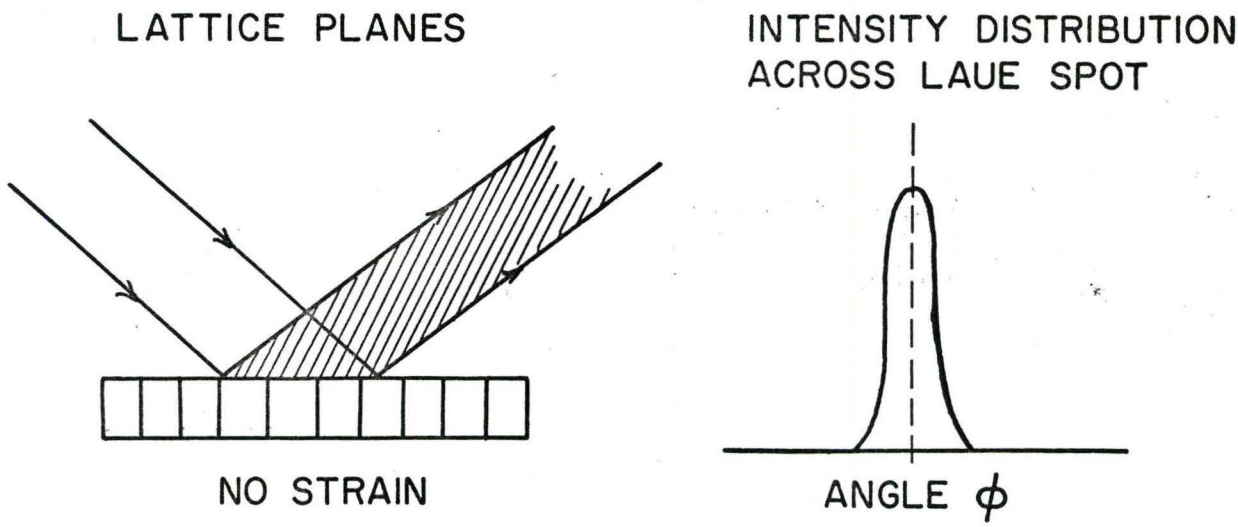

(a)

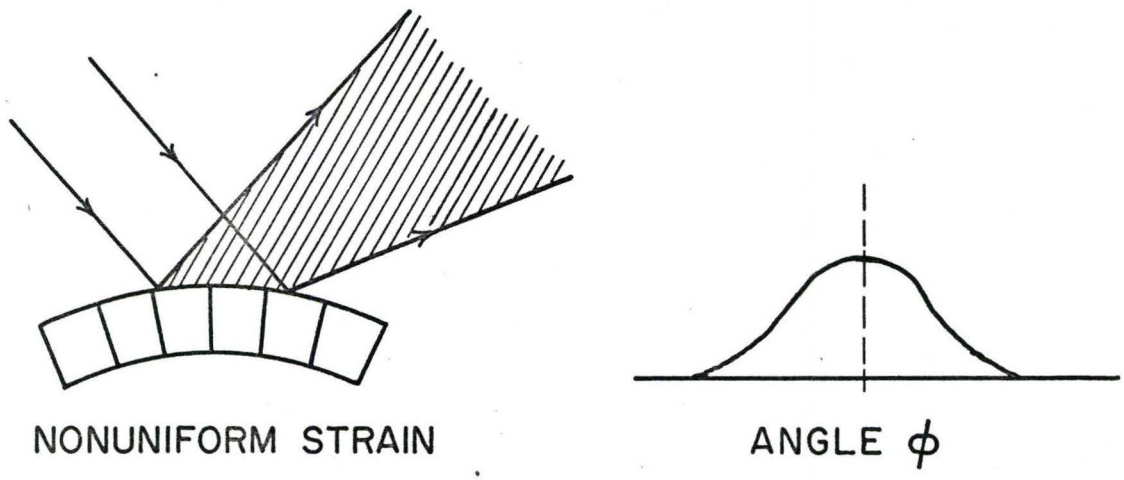

(b)

Fig. 3.7 Schematic diagram showing effect of lattice curvature on intensity of Laue spot.

where i, j, k = 1, 2, 3 and $\delta_{ij} \begin{cases} = 1 & i = j \\ = 0 & i \neq j \end{cases}$.

Thus given the curvatures from measurements of asterism it is theoretically possible to calculate the density of geometrically necessary dislocations required to accommodate them.

It would be highly impractical to attempt to measure the nine components of curvature in a single grain of a deformed polycrystal. In addition, the Laue technique is useless for the quantitative measurement of the angular rotations $\Delta\phi_i$. This is because the wave lengths present in the incident beam do not cover an infinite range and the amount of rotation measured from the spot may be smaller than actually present. (Barrett and Massalski, 1966) For these reasons no quantitative estimate of lattice distortion was attempted from the Laue patterns obtained in this experiment. The method was used only to make qualitative studies of the development of asterism in specimens of different grain sizes as a function of the degree of plastic strain and to compare differences in the degree of asterism developed in the center of the grains and the regions adjacent to the grain boundary.

CHAPTER IV
EXPERIMENTAL RESULTS

4.1 Introduction

The experimental results obtained in the present study concerning the flow stress-grain size relationship are presented in four main sections. The first, section 4.2, reviews the measurements of internal stress and effective stress obtained by the methods of continuous stress relaxation and dislocation dynamics. The applications and limitations of each method are discussed. Section 4.3 describes the work hardening behavior of each of the materials tested. The phenomenon of work hardening is difficult to describe from observations of the flow stress which only reflects the overall response of the material to plastic deformation. In this study the task is facilitated by the measurements of σ_{int} and σ_{eff} as functions of strain. The results on the grain size dependence of internal stress are presented in section 4.4. In order to aid in the interpretation of the data, an analysis of these results is made using a modified Hall-Petch equation. With the aim of correlating the measurements of internal stress with the dislocation structure, observations of X-ray asterism in deformed polycrystals of iron and 70/30 alpha brass are shown in section 4.5.

4.2 Measurement of Internal Stress and Effective Stress

Measurements of internal stress (σ_{int}) and effective stress (σ_{eff}) were obtained as functions of strain and grain size for:

(a) Decarburized iron at 298°K.

(b) Decarburized iron at 195°K.

(c) 70/30 Alpha Brass at 195°K.

(d) Copper at 298°K

All of the results were obtained by the continuous stress relaxation (C. S. R.) method and the data along with estimates of error are shown in Table 4.1 at the end of this chapter. These results were checked wherever possible by the indirect method of dislocation dynamics (D. D.). The interesting features of these determinations are described below.

(a) Iron at 298°K: A determination of σ_{int} and σ_{eff} by the C. S. R. method was made for decarburized iron strained 12% in tension at 298°K. Values of σ_{int} and σ_{eff} were obtained by letting the stress relax until the relaxation rate is observed to be zero, which took less than 30 min. for decarburized iron at 298°K. For this particular specimen the fully relaxed state yields values for σ_{int} and σ_{eff} of 17.7 kg/min^2 and 2.51 kg/min^2 respectively.

To obtain values for σ_{int} and σ_{eff} by the D. D. method the stress relaxation curve is replotted in the form of a load-log time plot shown in Fig. 4.1. The load-log time relation for this iron is non-linear which agrees with the observation of Li (1967). On page 28 the following equation was derived for stress relaxation,

$$\sigma - \sigma_i = k\,(t + a)^{-n} \qquad 4.1$$

This equation is based on a power law relationship between dislocation velocity and stress proposed by Gilman and Johnston. If the above equation is to be obeyed for stress relaxation, a log-log plot of stress (load) rate versus time must be linear at long times. Such a plot is shown in Fig. 4.2. The load rate at any time t during relaxation was obtained by measuring the slopes along the load-log time plot with a derivameter. At long times the log load rate-log time plot is linear as required by Eq. (2.37) on page 28. The slope of the linear portion of this plot is used to calculate the value of the dislocation velocity-stress exponent m*,

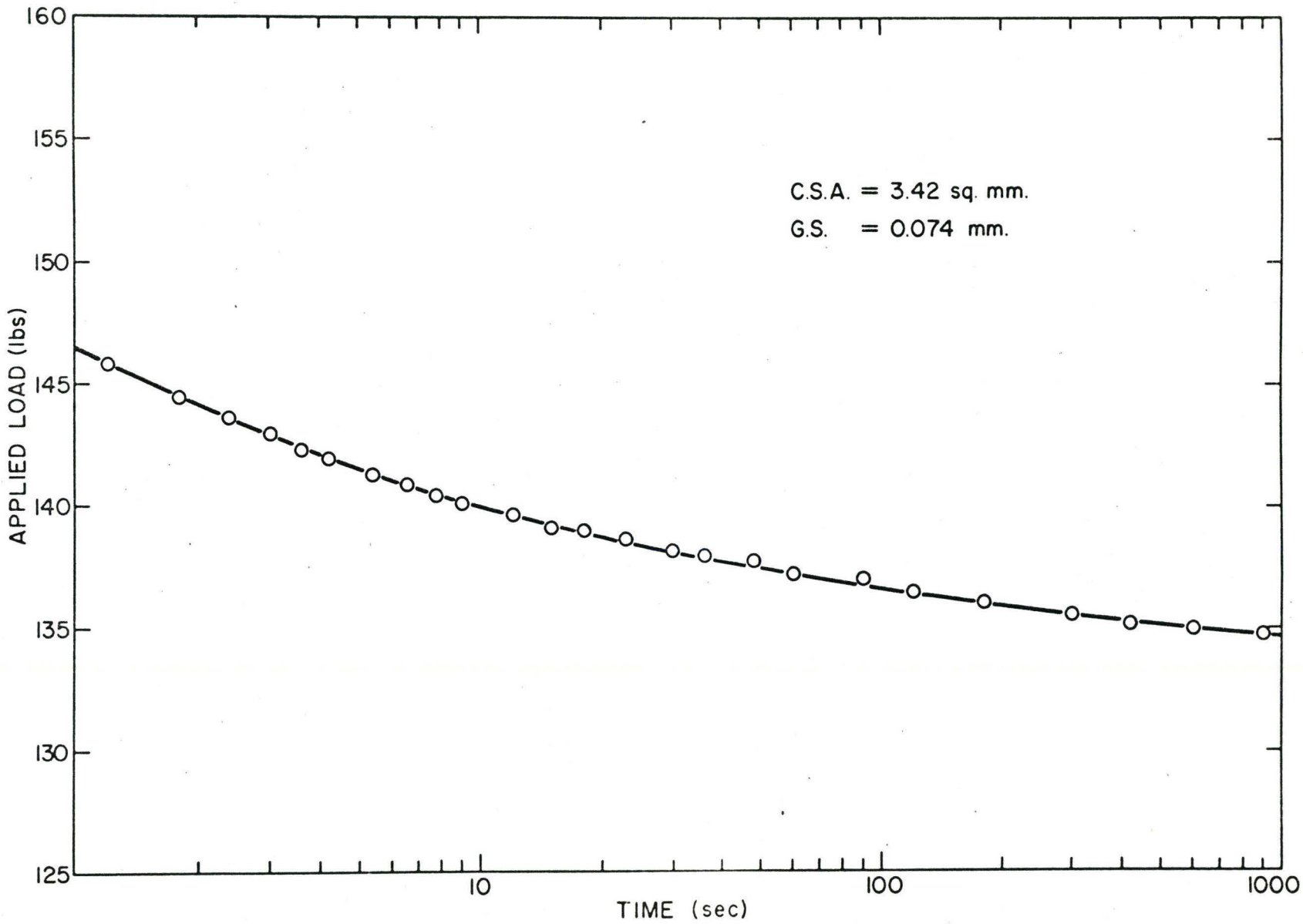

Fig. 4.1 Stress relaxation of decarburized iron strained 12% at 298°K.

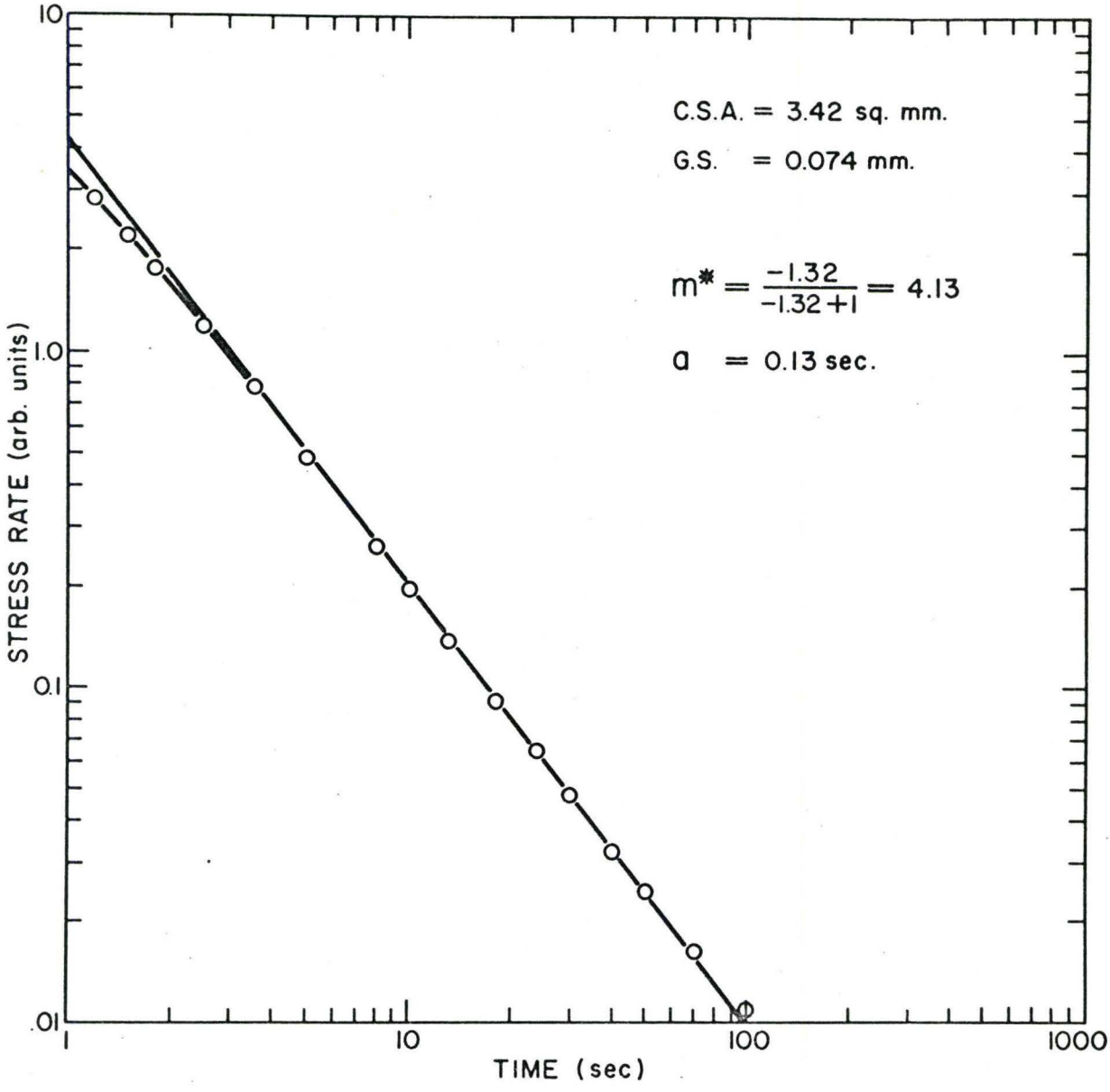

Fig. 4.2 Determination of m* in decarburized iron from stress relaxation at 298 °K.

the deviation from linearity at short times is used to calculate the value of the constant "a" in Eq. (4.1). The respective values of m* and "a" are 4.1 and .13 sec.

By using these values of m* and "a", the internal stress for the relaxation of decarburized iron can be calculated using Eq. (4.1). If σ_1 and σ_2 are the stresses at any two times t_1 and t_2 during stress relaxation, then the average internal stress, σ_{int}, is given by the relation,

$$\frac{\sigma_1 - \sigma_{int}}{\sigma_2 - \sigma_{int}} = \left(\frac{t_1 + a}{t_2 + a}\right)^{-n} \qquad 4.2$$

The value of internal stress calculated by this method for the specimen of decarburized iron strained 12% in tension is 17.6 kg/mm^2. It compares quite well with the value of 17.7 kg/mm^2 obtained by the C.S.R. method. Several other checks were made at different strains and good agreement between the two methods was always observed.

(b) Iron at 195°K: This same specimen was immersed in a low temperature bath at 195°K, strained just beyond yield and the stress allowed to relax in order to compare the value of internal stress at the two temperatures of 298°K and 195°K. It is anticipated that by this method the dislocation structures will be equivalent at both temperatures. Unfortunately a determination of σ_{int} at 195°K is made much more difficult for two reasons. First the technique is highly sensitive to temperature fluctuations and second at low temperatures the time for appreciable relaxation to occur becomes inordinate. For this reason the stress on the specimen was relaxed for an arbitrary period which was normally about 3 hours in the present tests. It should be emphasized that for decarburized iron relaxed at 195°K the C.S.R. method will give an overestimate of the true value of σ_{int}. Allowing for these difficulties

a determination of σ_{int} by the C. S. R. method yields a value of 21.8 $\pm$ 2 kg/mm^2. The effective stress, σ_{eff}, is 15.6 $\pm$ 2 kg/mm^2.

To utilize the D. D. method a load-log time plot was made as shown in Fig. 4.3 and is observed to also be non-linear. An accurate determination of m* at 195^{o}K is very difficult for the two reasons mentioned above. From a log-log plot of load rate versus time which is linear at long times as shown in Fig. 4.4, a best estimate of m* = 10.5 $\pm$ 2 is obtained. By using the value of m* and 'a' obtained from Fig. 4.4, an estimate of σ_{int} = 16.0 $\pm$ 2 kg/mm^2 can be made. This value of σ_{int} obtained by the D. D. method compares favourably with the value of σ_{int} obtained at 298^{o}K. ($\sigma_{int\ (298)}$ = 17.6 kg/mm^2 compared with $\sigma_{int\ (195)}$ = 16.0 $\pm$ 2 kg/mm^2)

Considering the limits of experimental error it can be concluded that the internal stress in decarburized iron is independent of temperature at least for room temperature and below. This conclusion is based on the results obtained from the D. D. method at 195^{o}K.

(c) Alpha Brass at 195^{o}K: Stress relaxation in alpha brass at 298^{o}K is not possible due to the onset of strain ageing during the relaxation period. Consequently alpha brass was strained at 195^{o}K and no strain ageing was observed at this temperature during the relaxation tests. This was checked by reloading the specimen after stress relaxation. In all cases the macroscopic flow stress was the same as at the time t = 0 before relaxation. It has been reported by Balasubramanian et al (1969) that stress relaxation in alpha brass can be analyzed by the method of dislocation dynamics. Thus it is expedient to compare the values of σ_{int} and σ_{eff} obtained in alpha brass by the C. S. R. method with those obtained by the D. D. method.

From continuous stress relaxation curves for alpha brass strained 2.5, 5.0 and 10.0 per cent in tension, values of σ_{int} and σ_{eff}

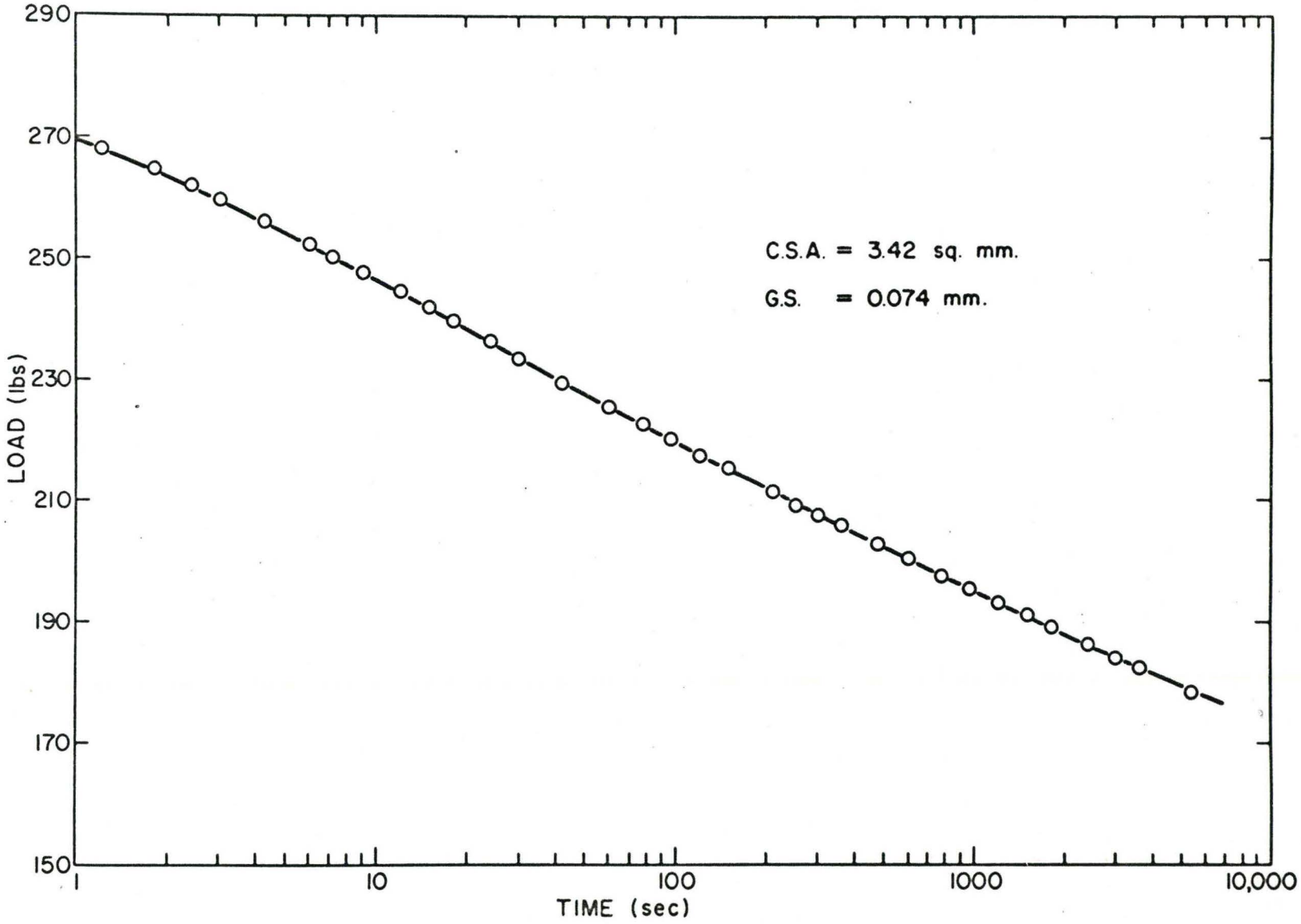

Fig. 4.3 Stress relaxation of decarburized iron. Prestrained 12% at 298°K, restrained 0.5% at 195°K.

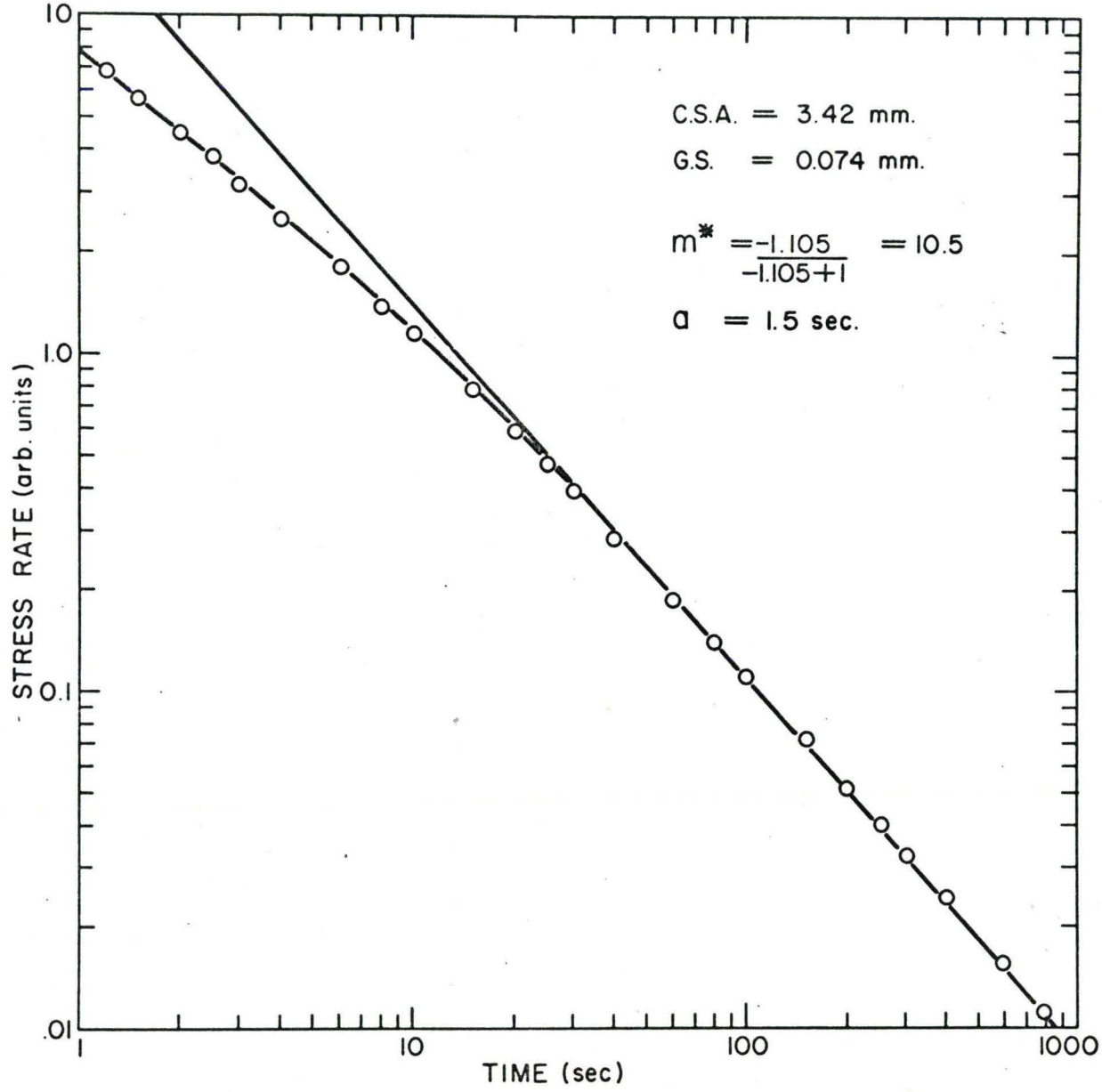

Fig. 4.4 Determination of m* in decarburized iron from stress relaxation at 195°K.

obtained at the fully relaxed state are listed below.

TABLE 4.2

	C. S. R. Method		D. D. Method		
Strain %	σ_{int} (kg/mm^2)	σ_{eff} (kg/mm^2)	σ_{int} (kg/mm^2)	σ_{eff} (kg/mm^2)	m*
2.5	8.7	1.1	8.7	1.1	4.25
5.0	10.1	1.6	10.3	1.4	6.40
10.0	13.3	1.8	-	-	-

For the D. D. method a load-log time plot for 2.5 % strain is shown in Fig. 4.5. The load rate at any time t during relaxation was measured and plotted on log-log coordinates as shown in Fig. 4.6. This plot is linear at long times and the slope of the linear portion is used to calculate a value of m* = 4.25. As before the deviation from linearity at short times gives a value of a = 3 sec. Using these values of m* and 'a' gives σ_{int} = 8.7 kg/mm^2 and σ_{eff} = 1.1 kg/mm^2 which compare favorably with those obtained by the C. S. R. method. Fortunately the relaxation time in alpha brass strained at 195^{o}K is not excessively long and more accurate determinations of σ_{int} and σ_{eff} could be made than was possible for iron deformed at 195^{o}K.

Values of σ_{int} and σ_{eff} were also obtained at 5.0% strain by the D. D. method and good agreement was obtained as shown in Table 4.2. The two methods compare favorably for strains less than 10%. However for strains larger than 10% the stress relaxation behavior of alpha brass is nearly linear with log time making a determination of m* impracticable and a comparison of the two methods is not possible at large strains.

(d) Copper at 298^{o}K: The stress relaxation behavior of copper at 298^{o}K is linear with log time for all values of strain. This type of stress relaxation in copper has been reported previously by Feltham (1961) and

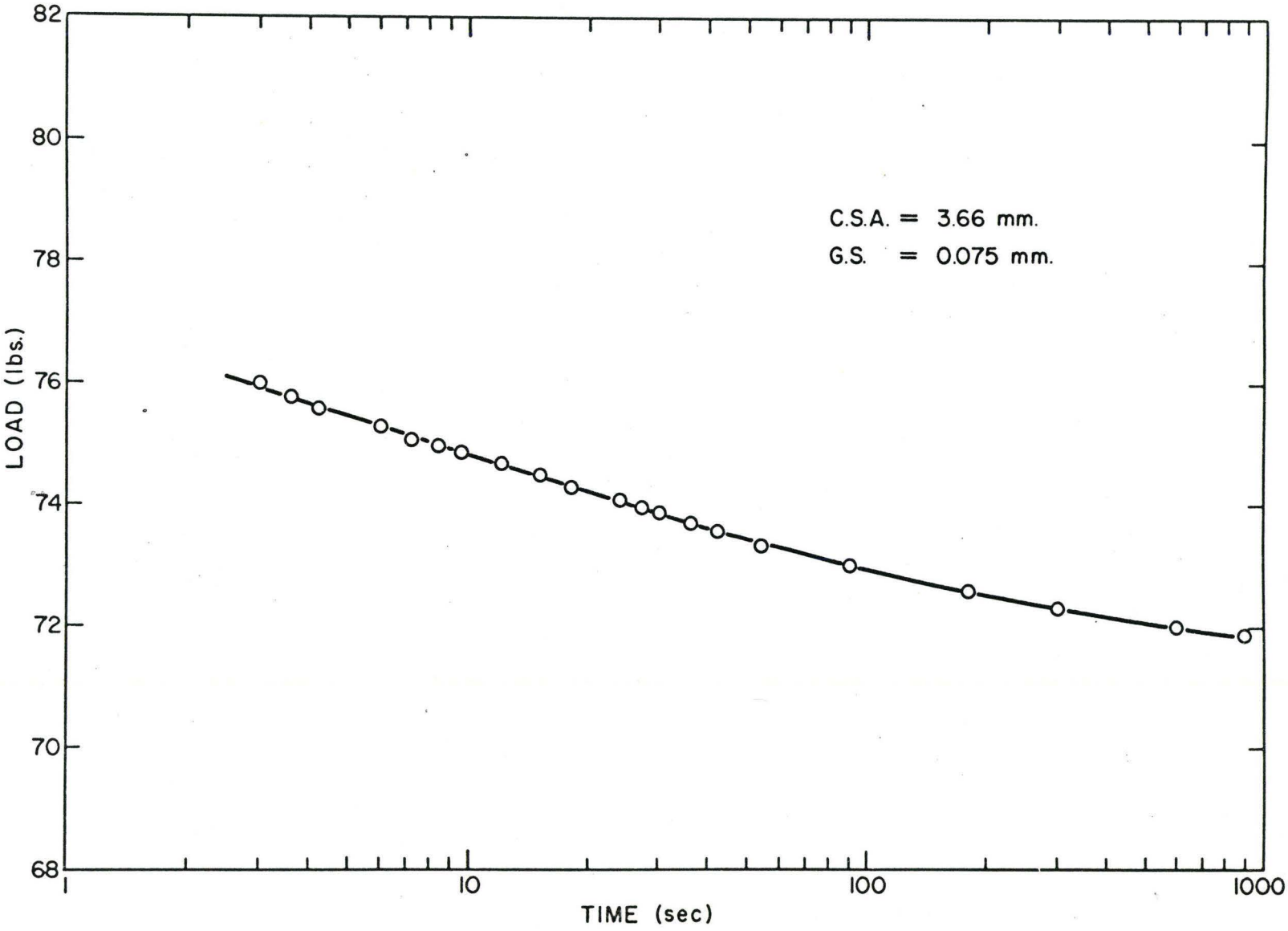

Fig. 4.5 Stress relaxation of 70/30 alpha brass strained 2.5% at 195°K.

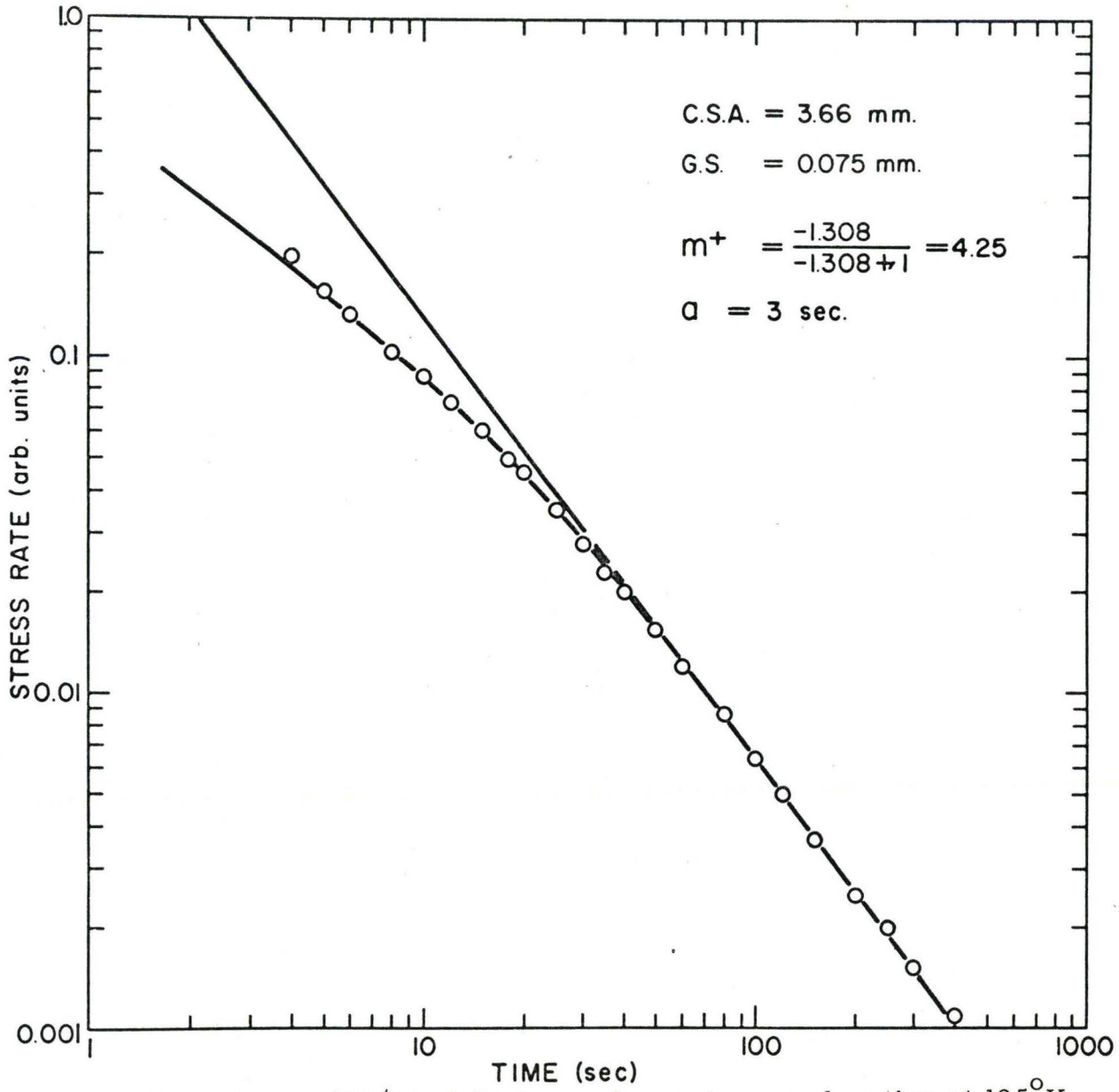

Fig. 4.6 Determination of m* in 70/30 alpha brass from stress relaxation at 195°K.

is attributed to an exhaustion process equivalent to logarithmic creep. Under these conditions it is not possible to use the dislocation dynamics method to determine values of σ_{int} and σ_{eff} and thus a comparison of the two methods cannot be made.

It should be emphasized that value of internal stress established from the C. S. R. method will only be approximate in materials such as copper or alpha brass at large strains where the relaxation process can be considered as an exhaustion process equivalent to logarithmic creep. This is due mainly to the excessively long times needed to reach the fully relaxed state. Although the recovery of internal stress in copper during stress relaxation is a possibility, it must be very slight since the flow stresses immediately before and after relaxation were almost identical.

4.3 Work Hardening Behavior

The internal stress and effective stress during plastic deformation of the various materials have been measured by the C. S. R. method for a range of grain sizes. The values of these stresses together with the applied stress are shown in Fig. 4.7 and Fig. 4.8 for one grain size only in the materials tested. These graphs together with other experimental observations give a good indication of the work hardening behavior exhibited by the various materials and the important results are described below.

(a) Iron at 298°K: For decarburized iron strained at 298°K the effective stress remains almost constant with strain and the entire work hardening results from an increasing internal stress as seen in Fig. 4.7(a). The constant effective stress with strain is independent of grain size and the results are summarized in Table 4.1.

(b) Iron at 195°K: Fig. 4.7(b) shows the internal stress, effective stress and applied stress for decarburized polycrystalline iron at 195°K obtained

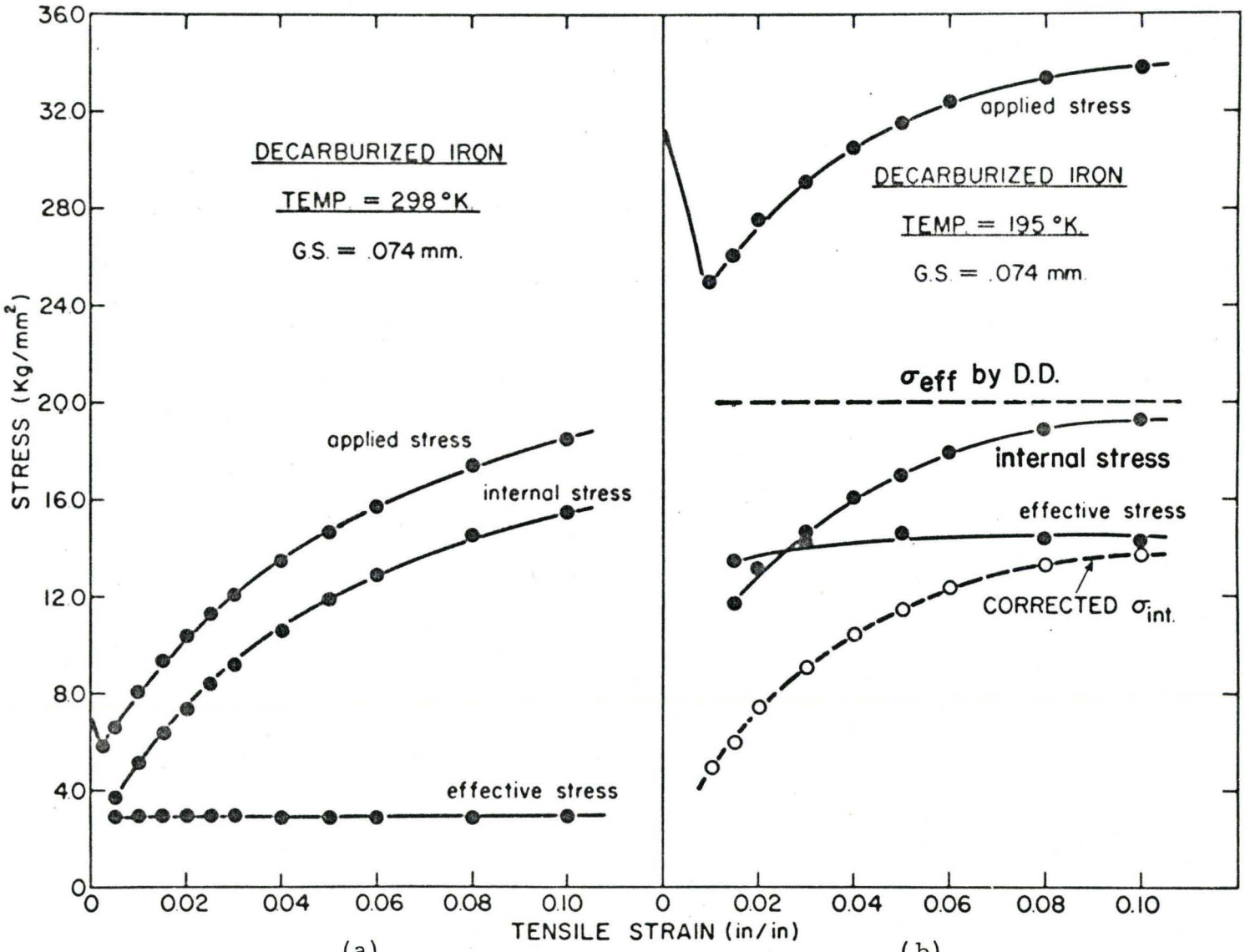

Fig. 4.7 Internal Stress and effective stress as a function of strain for decarburized iron (a) at 298°K and (b) at 195°K.

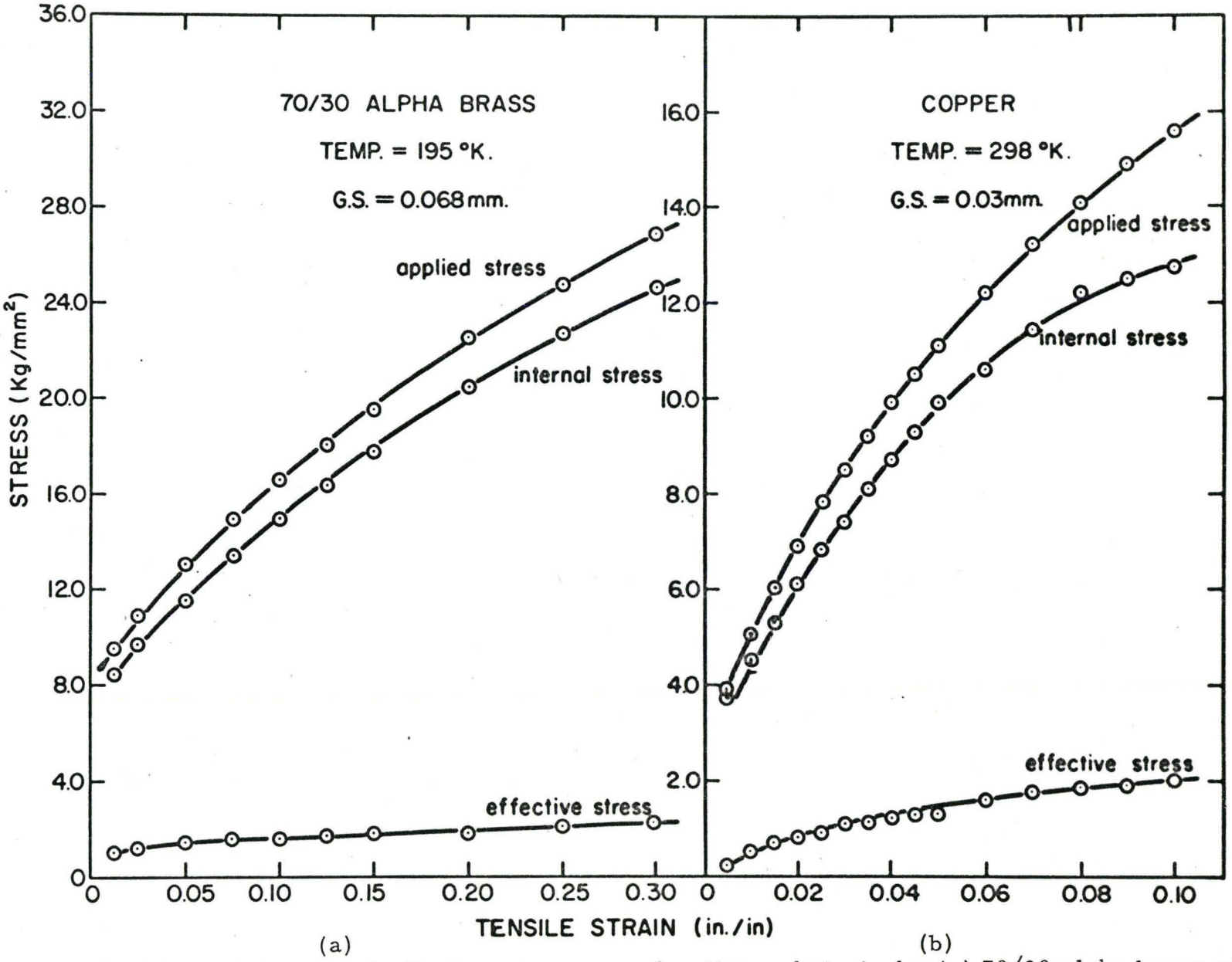

Fig. 4.8 Internal stress and effective stress as a function of strain for (a) 70/30 alpha brass at 195°K and (b) copper at 298°K.

by C. S. R. experiments. The internal stress developed at 195°K is in fair agreement with the internal stress developed in a specimen of similar grain size at 298°K. Although the internal stress at 195°K is somewhat larger, this discrepancy can be attributed mainly to the fact that the C. S. R. method gives an over-estimate of the true value of internal stress. For this reason Fig. 4.7(b) includes a plot of corrected values of internal stress. These corrected values were obtained by determining a value of σ_{eff} at 195°K on a similar specimen by the D. D. method. This value of σ_{eff} was subtracted from the applied stress for various strains to obtain σ_{int} as a function of strain. This is a fairly reliable method since the value of σ_{eff} does not change with strain (Gupta and Li, 1970). On the basis of the corrected plot the internal stress developed at 195°K drops below that developed at 298°K as strain increases. Thus the work hardening rate at 195°K is lower than at 298°K. It is also clear from this plot that the entire increase in flow stress from 298°K to 195°K is due to an increase in the effective stress.

At 195°K the effective stress increases slightly with strain at small strains and then becomes almost constant with strain as shown in Fig. 4.7(b).

(c) Alpha Brass at 195°K: For the case of alpha brass shown in Fig. 4.8(a), although most of the work hardening (90-95%) results from an increase in the internal stress, a small part of it is contributed by the effective stress which increases with strain. The variation of effective stress with strain depends on the grain size as shown in Fig. 4.9. In the coarse-grained specimen (G. D. = .16 mm) the effective stress is almost constant with strain, increasing slightly at large strains. Further refinement of grain size to .025 mm causes a noticeable increase in effective stress for all values of strain.

(d) Copper at 298°K: Fig. 4.8(b) shows the internal stress, effective stress and applied stress for polycrystalline copper at 298°K obtained

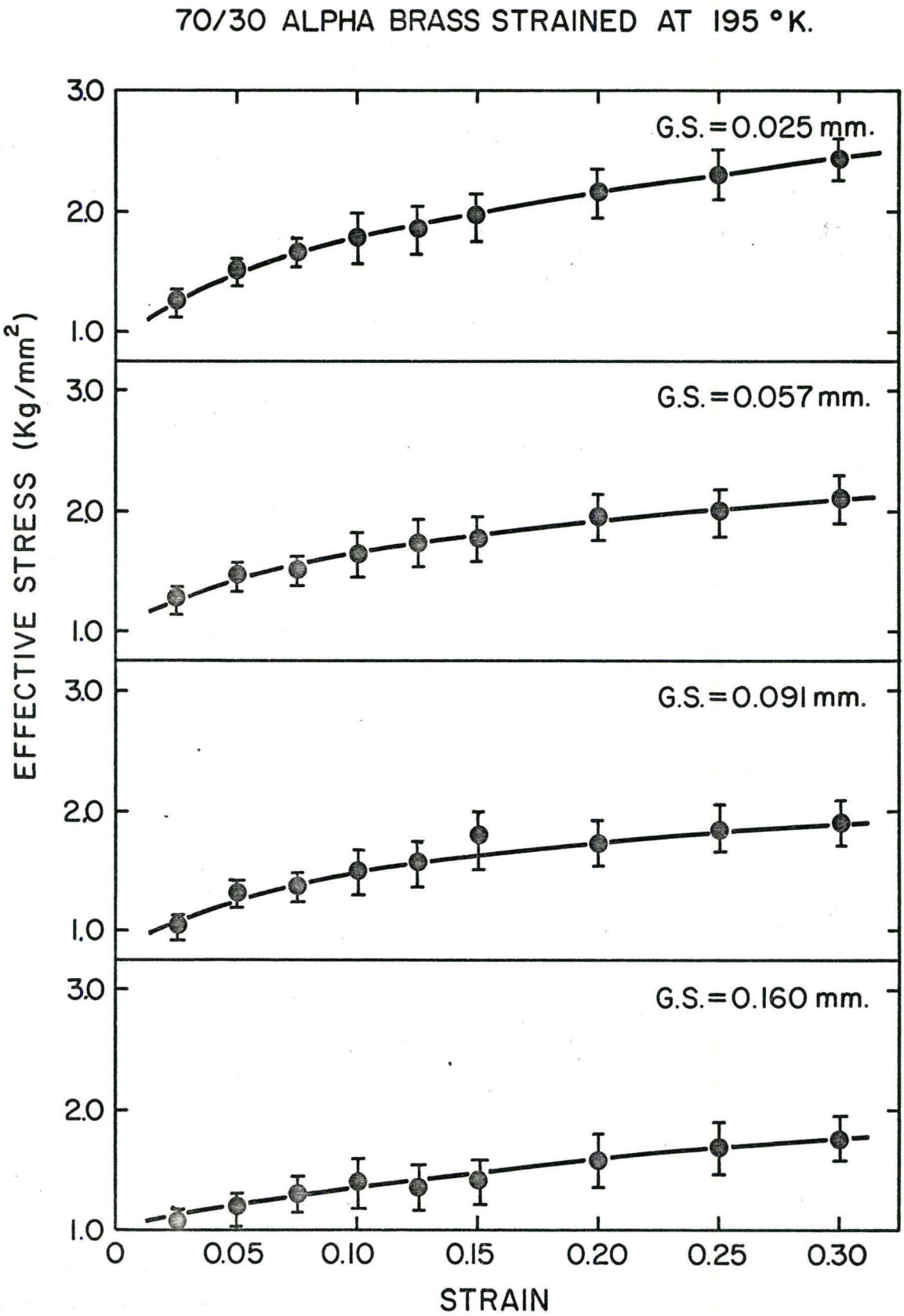

Fig. 4.9 Effective stress as a function of strain for a number of selected grain sizes in 70/30 alpha brass.

by C.S.R. experiments. Most of the work hardening results from an increase in the internal stress, although a part of it is contributed by the effective stress which increases with strain. The variation of effective stress with strain is almost independent of grain size except for very small strains, $< 1\%$ (see Table 4.1).

4.4 Grain Size Dependence of Internal Stress

It is apparent from the above results, that most of the work hardening is due to increases in internal stress. Thus in order to elucidate the effect of grain size on the work hardening behavior of polycrystals, the variation of internal stress with strain for a number of grain sizes is plotted in Figs. 4.10 to 4.13. The salient feature of this data is that the effect of grain size on work hardening is markedly dependent on the material and the temperature of test.

For decarburized iron tested at $298^{\circ}K$ (Fig. 4.10) it is observed that the internal stress produced by a given amount of plastic strain increases with decreasing grain size. The data for iron at $195^{\circ}K$ (Fig. 4.11) shows little grain size dependence of the work hardening rate however. This plot shows both the internal stress determined by C.S.R. experiments and corrected values of internal stress. An average value of $\sigma_{eff} = 20 \pm 2$ kg/mm^2 was determined by the D.D. method and this value was subtracted from the flow stress to obtain the corrected values of σ_{int} as a function of strain for a number of selected grain sizes. Fig. 4.12 shows the data for alpha brass strained at $195^{\circ}K$. It can be seen from this data that the increase of internal stress as a function of strain is markedly grain size dependent. In contrast, for copper at $298^{\circ}K$ (Fig. 4.13), the grain size dependence is small and disappears after some 10% strain.

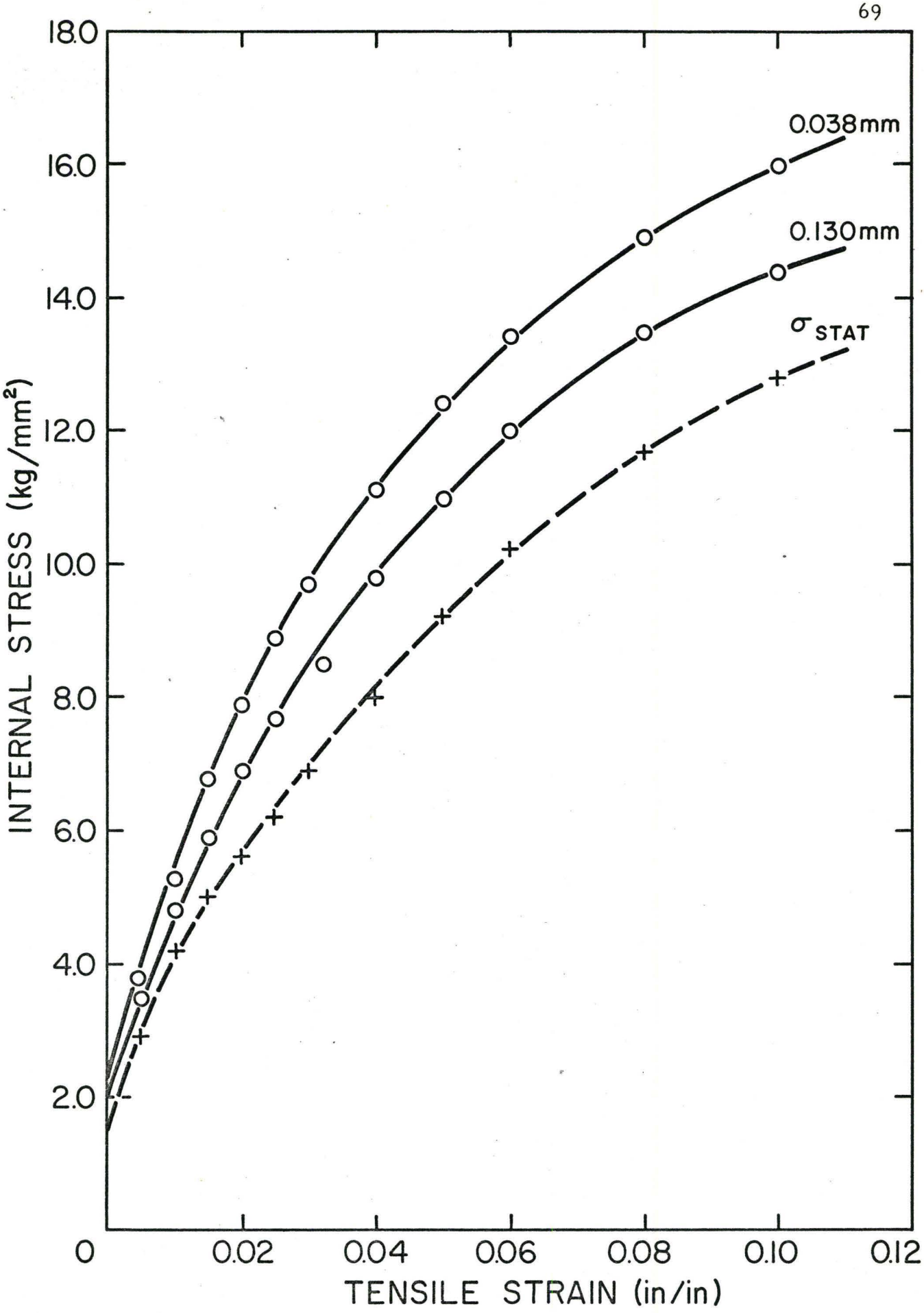

Fig. 4.10 Internal stress as a function of strain for decarburized iron at 298°K.

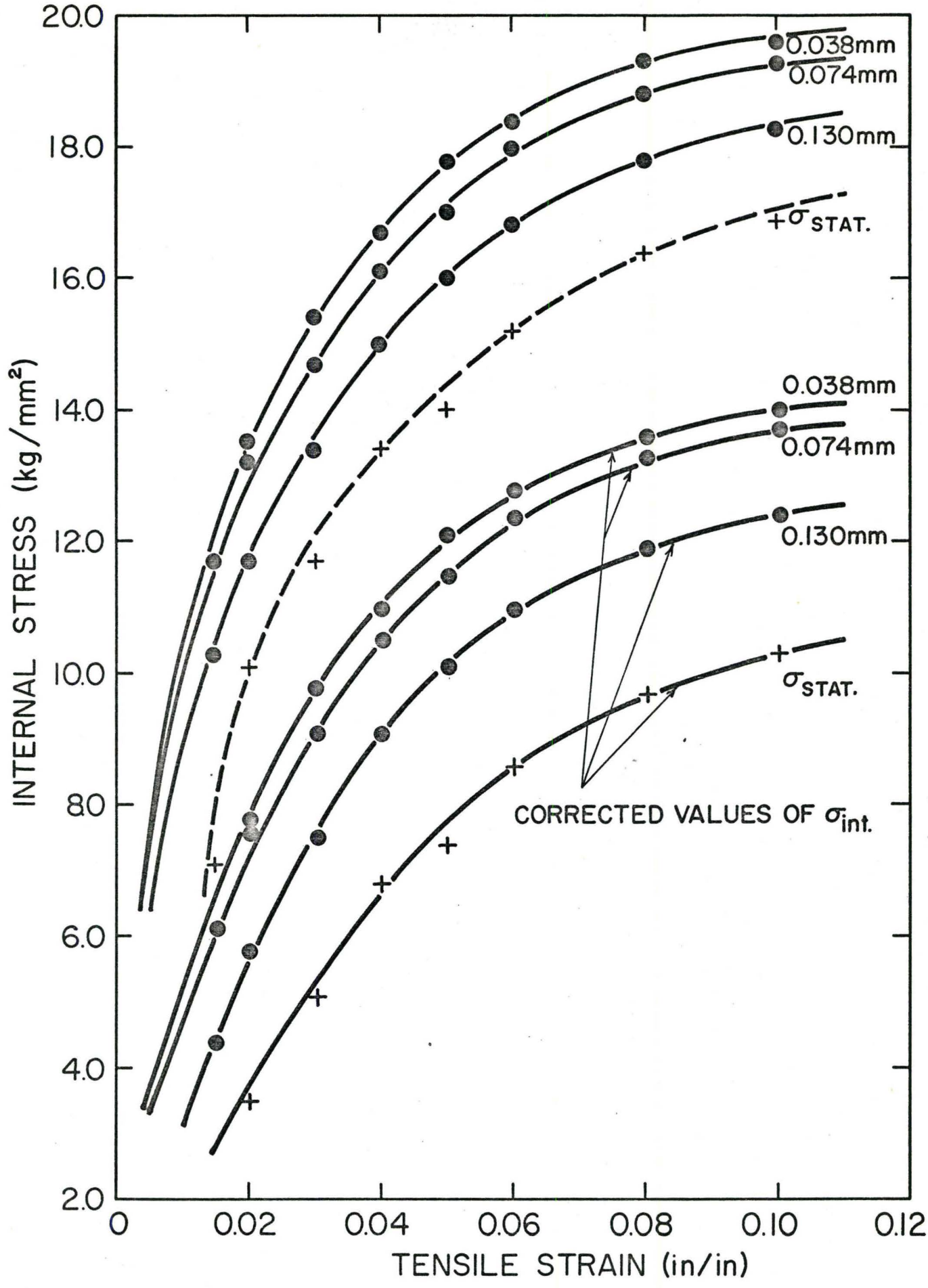

Fig. 4.11 Internal stress as a function of strain for decarburized iron at 195°K.

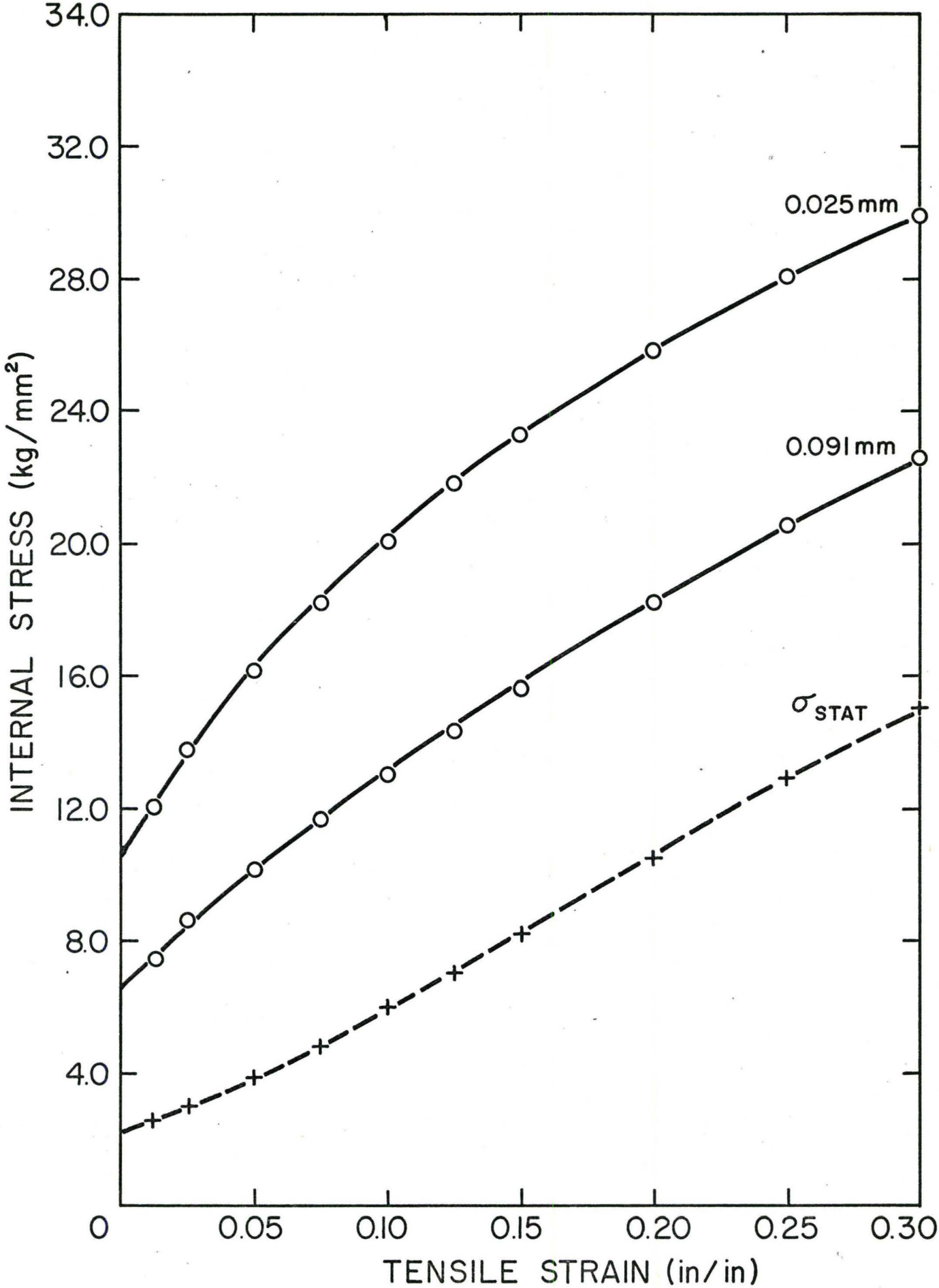

Fig. 4.12 Internal stress as a function of strain for 70/30 alpha brass at

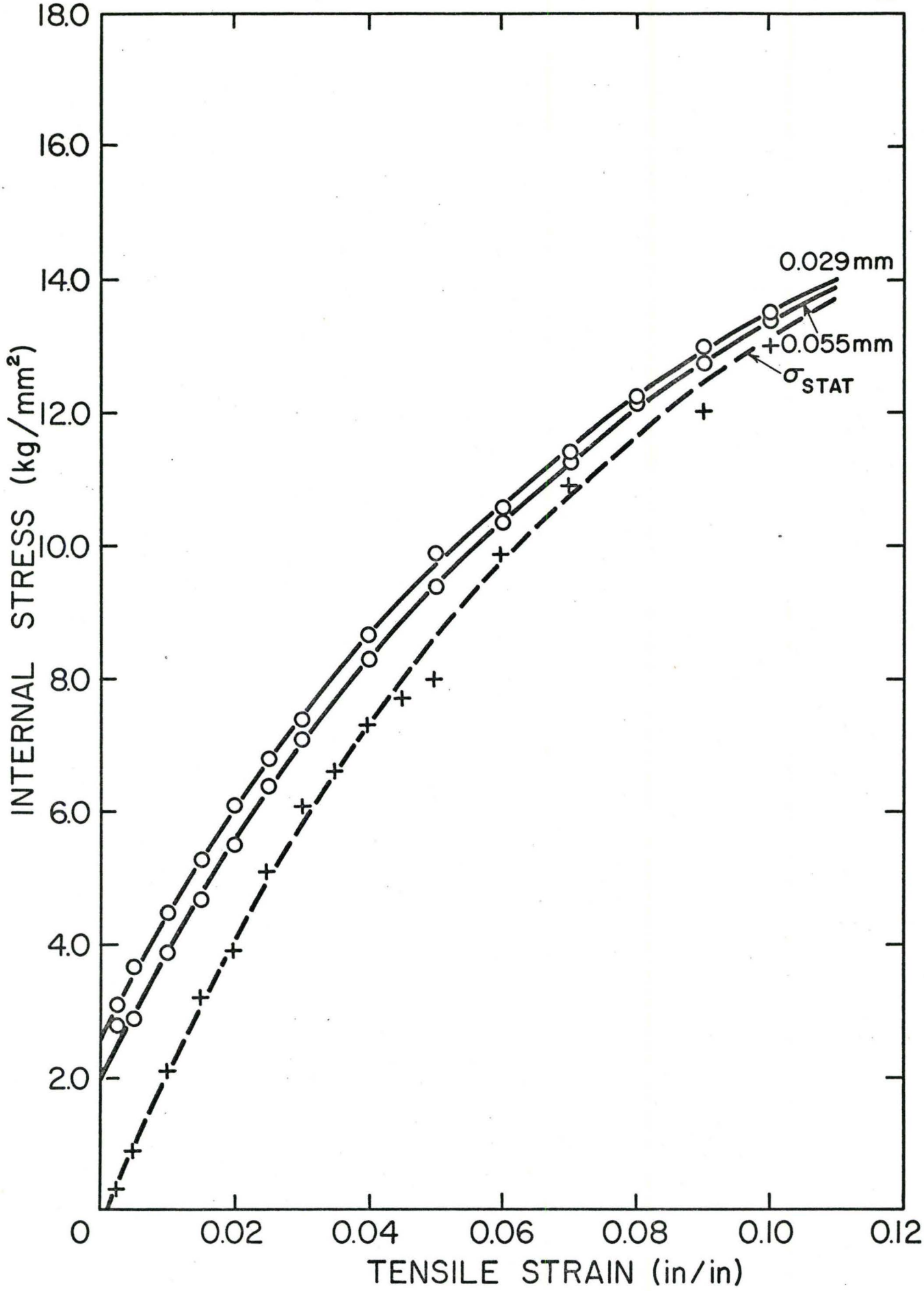

Fig. 4.13 Internal stress as a function of strain for copper at 298°K.

4.4.1 Analysis of Internal Stress-Grain Size Results

From these primary observations it can be concluded that in considering the overall increase in flow stress of metal polycrystals the most important feature is the internal stress or athermal component. Also it is apparent that cognisance must be taken of both the grain size dependent and grain size independent contributions to the internal stress. Thus a further analysis of the data is required to first, delineate the grain size dependent and grain size independent contributions and second to provide a means for rationalizing the experimental data in terms of fundamental dislocation mechanisms.

An appropriate method of analysis is to express the data in terms of a modified Hall-Petch equation in which it is assumed that the grain size dependent contribution can be superimposed on the grain size independent contribution. With this assumption the total internal stress σ_{int} can be considered as the sum of three components,

$$\sigma_{int} = \sigma_{stat} + k_y D^{-1/2} + k_\varepsilon D^{-1/2} \qquad 4.3$$

σ_{stat} is the grain size independent component of internal stress. It can be considered the same as that of an equivalent single crystal and is due to the accumulation of statistically stored dislocations, (Ashby, 1970). $k_y D^{-1/2}$ is the grain size dependent internal stress present at the initial yield event and can only be evaluated by extrapolation to zero plastic strain. The term $k_\varepsilon D^{-1/2}$ represents an additional grain size dependent internal stress which varies with strain.

The total internal stress σ_{int} at a number of selected strains is shown plotted against $D^{-1/2}$ for all the materials tested in Fig. 4.14 and 4.15. It can be seen that this data is described quite well by the modified Hall-Petch equation 4.3. Of particular interest in these plots is the slope $k_f = (k_y + k_\varepsilon)$ and the intercept $\sigma_{stat.}$ on the internal stress axis at $D^{-1/2} = 0$. The values of the slopes and intercepts were obtained by a

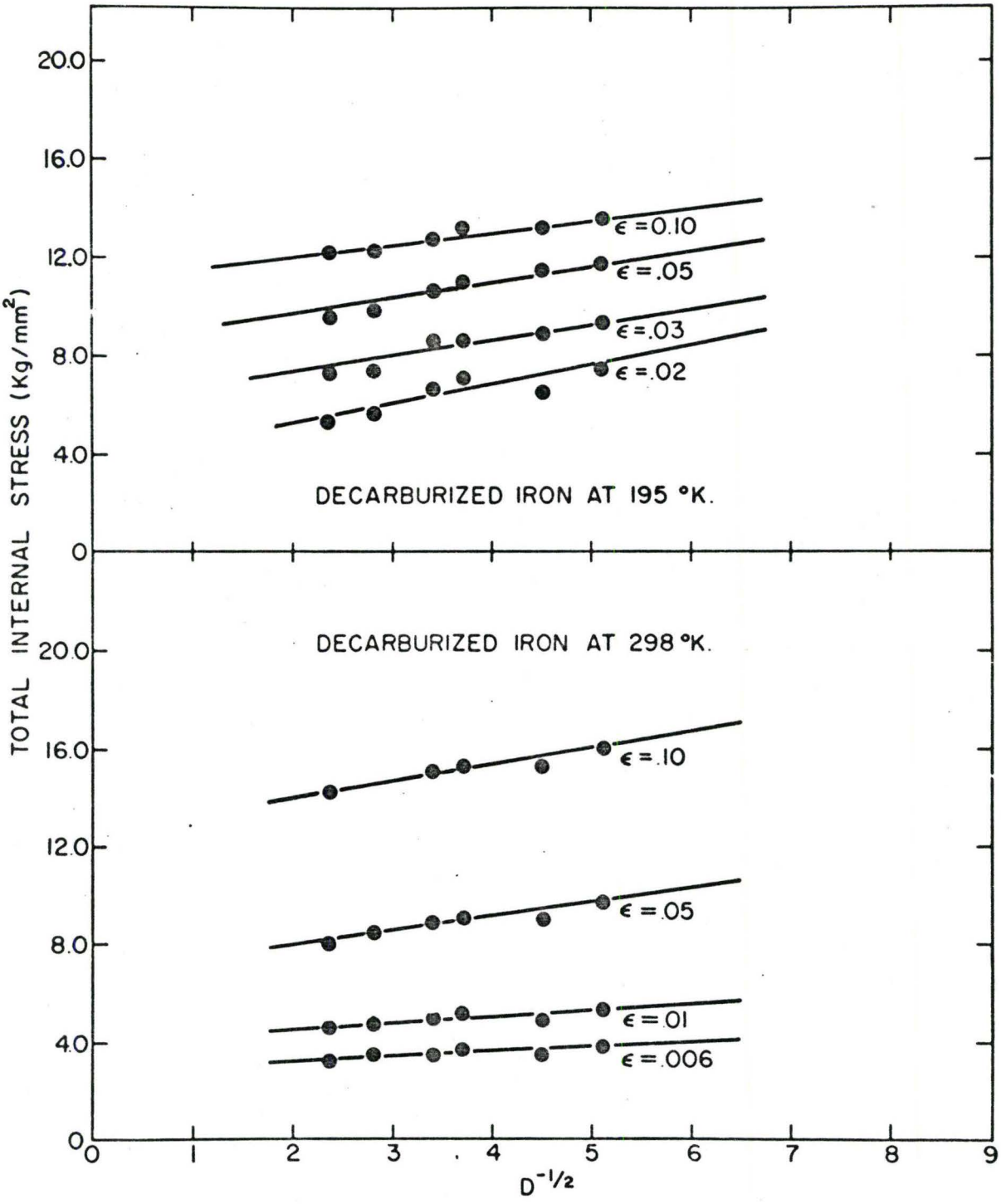

Fig. 4.14 Internal stress as a function of $D^{-1/2}$ for decarburized iron.

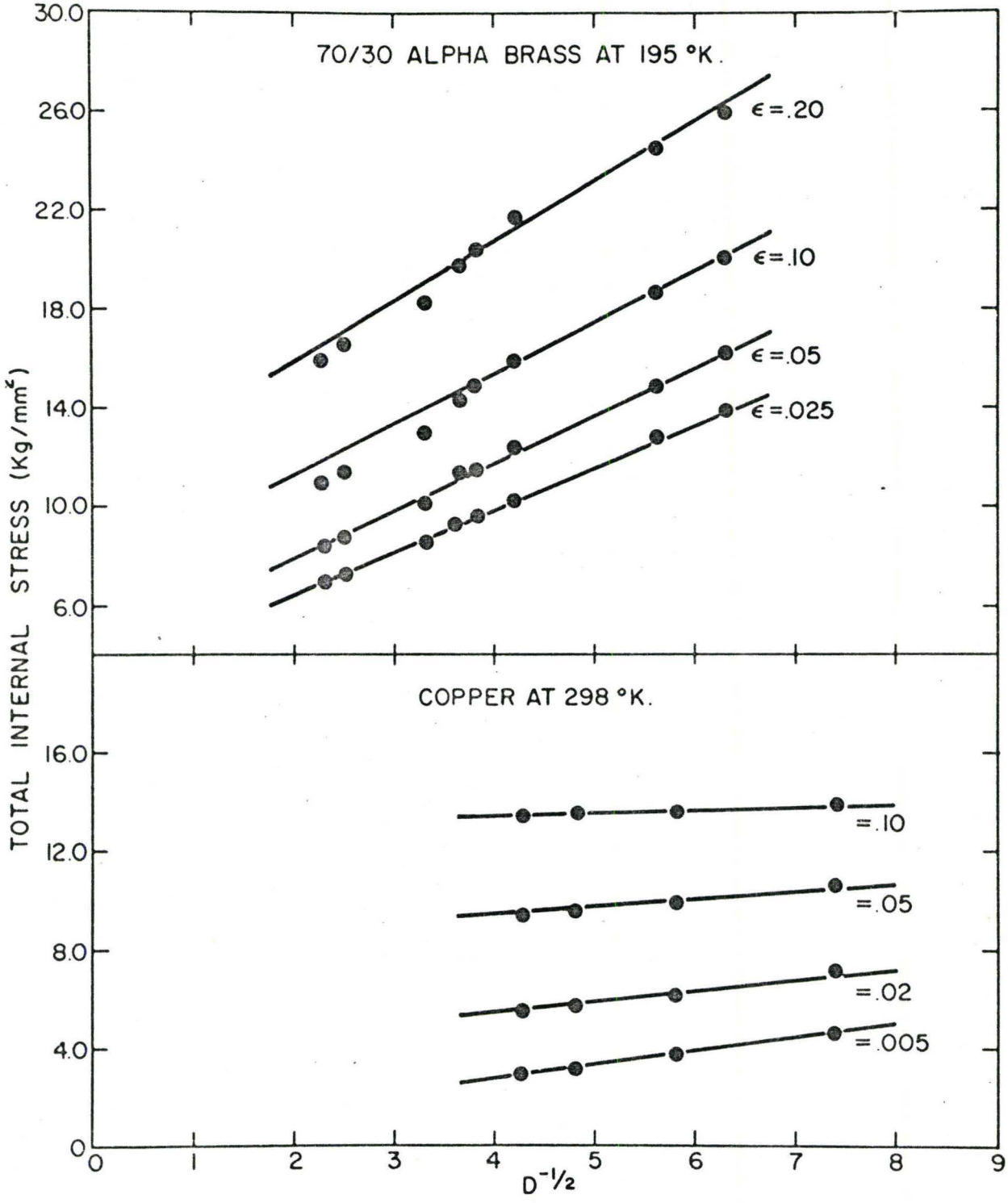

Fig. 4.15 Internal stress as a function of $D^{-1/2}$ for 70/30 alpha brass and copper.

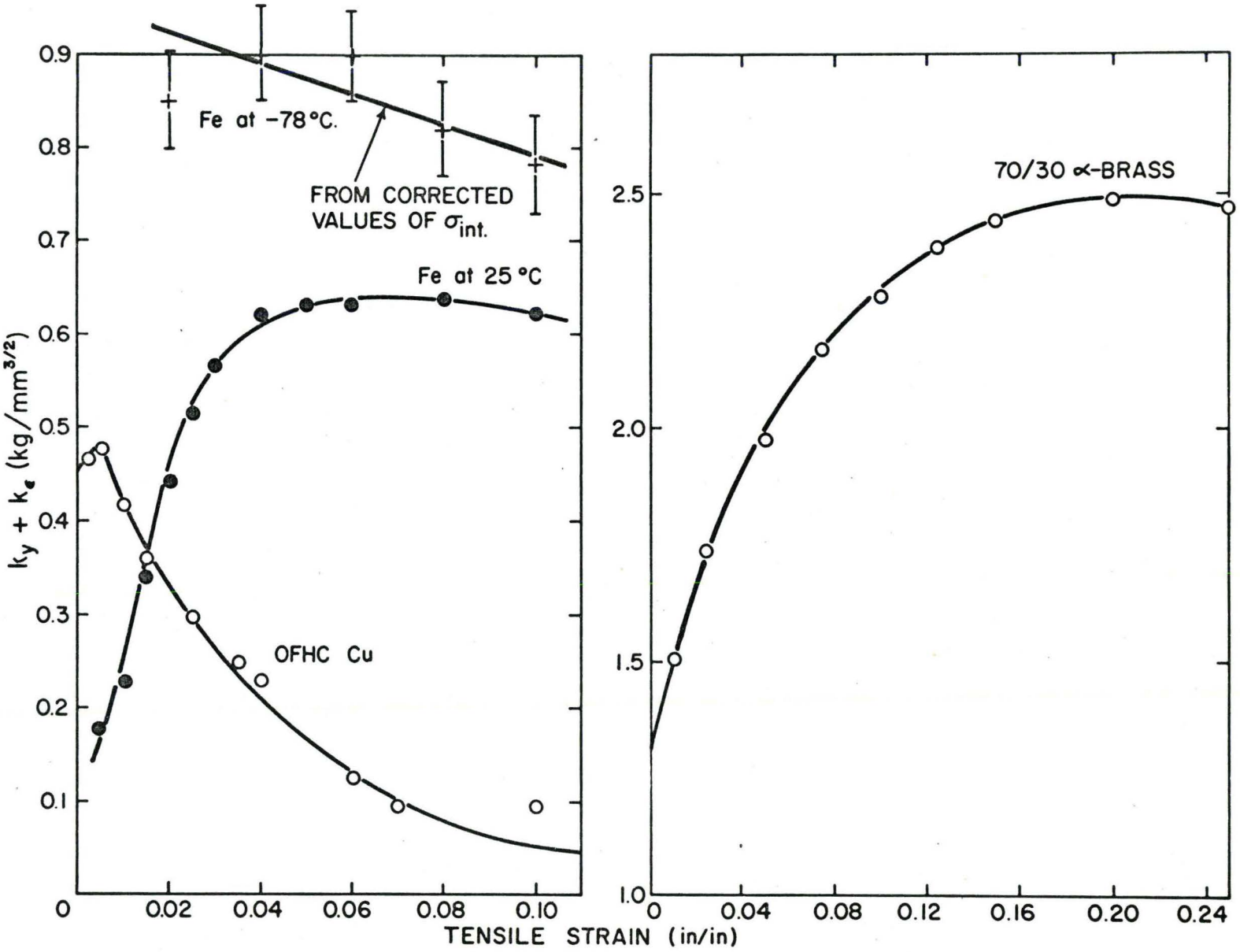

Fig. 4.16 Hall-Petch slope as a function of strain for all the materials tested.

linear regression analysis.

The slope of Eq. 4.3 is plotted as a function of strain in Fig. 4.16 for all the materials tested. It is found to increase with strain for decarburized iron strained at 298°K and for 70/30 alpha brass strained at 195°K indicating that the work hardening rate is grain size dependent. For iron at 195°K and copper at 298°K however the value of the slope decreases with strain indicating no dependence of work hardening rate on grain size. An interesting feature of this result is that the slope for iron strained at 195°K is initially greater than at 298°K, but then decreases with strain to a value approximately equal to the slope at 298°K.

The variation of σ_{stat} with strain is plotted in Figs. 4.10 to 4.13 along with σ_{int} for a number of selected grain sizes. The most striking feature of these graphs is that the grain size dependent contribution to internal stress dominates the work hardening in 70/30 alpha brass whereas for copper, σ_{stat} dominates, and the grain size contributes almost nothing to the work hardening. The results for iron indicate a small contribution to work hardening due to grain size at 298°K but at 195°K the grain size exerts little influence on the work hardening.

4.5 Observations of X-ray Asterism

Coarse and fine-grained specimens of decarburized iron and 70/30 alpha brass were strained in increments of 2.0% and examined by taking Laue patterns between increments. All the results shown in this section were obtained with a beam diameter of the order of 50μ. This size was selected as a compromise between the accuracy of positioning the beam and the length of exposure time.

Fig. 4.17 shows the results of back reflection Laue photographs obtained for decarburized iron strained at 298°K. The Laue spots were sharp before deformation but developed asterism as the strain increased. From the group of patterns shown in Fig. 4.17 there appears to be little

effect of grain size on the extent of asterism developed at each strain. Attempts to photograph asterism at strains higher than 4% in iron were not too successful since the spots became so diffuse that excessively long exposure times are needed. The absence of a grain size effect on asterism in iron is not too surprising since the amount of additional internal stress contributed by grain size is small in iron. It would appear that most of the asterism observed in iron is due to the small lattice rotations associated with tangles of dislocations formed within the grains. Fig. 4.18 shows the development of asterism at the center and grain boundary region of an individual grain in an iron specimen strained to 4%. The diffuseness of the spots is increased near the grain boundary indicating a greater amount of lattice bending and twisting as the boundary is approached. A fine structure is visible in two of the spots in Fig. 4.18 indicating the development of a cell structure near the grain boundary.

The results of Laue back reflection photographs of deformed 70/30 alpha brass polycrystals clearly show an effect of grain size on the extent of asterism as shown in the group of patterns in Fig. 4.19. In the coarse-grained sample very little asterism is present even after large strains. The apparent lack of asterism in the coarse-grained sample suggests that very little tangling occurs within the grains. However, the spots are quite elongated in the fine-grained specimen and increase in size with increasing strain. This observation suggests that the strain gradients are more severe in the fine-grained brass specimen resulting in an increase in the amount of asterism. It appears then that in 70/30 alpha brass the grain boundaries are the primary obstacles to slip resulting in a strong dependence of asterism on grain size. This result agrees with the measurements of internal stress which clearly show that the additional internal stress due to grain size dominates the work hardening in fine-grained brass specimens.

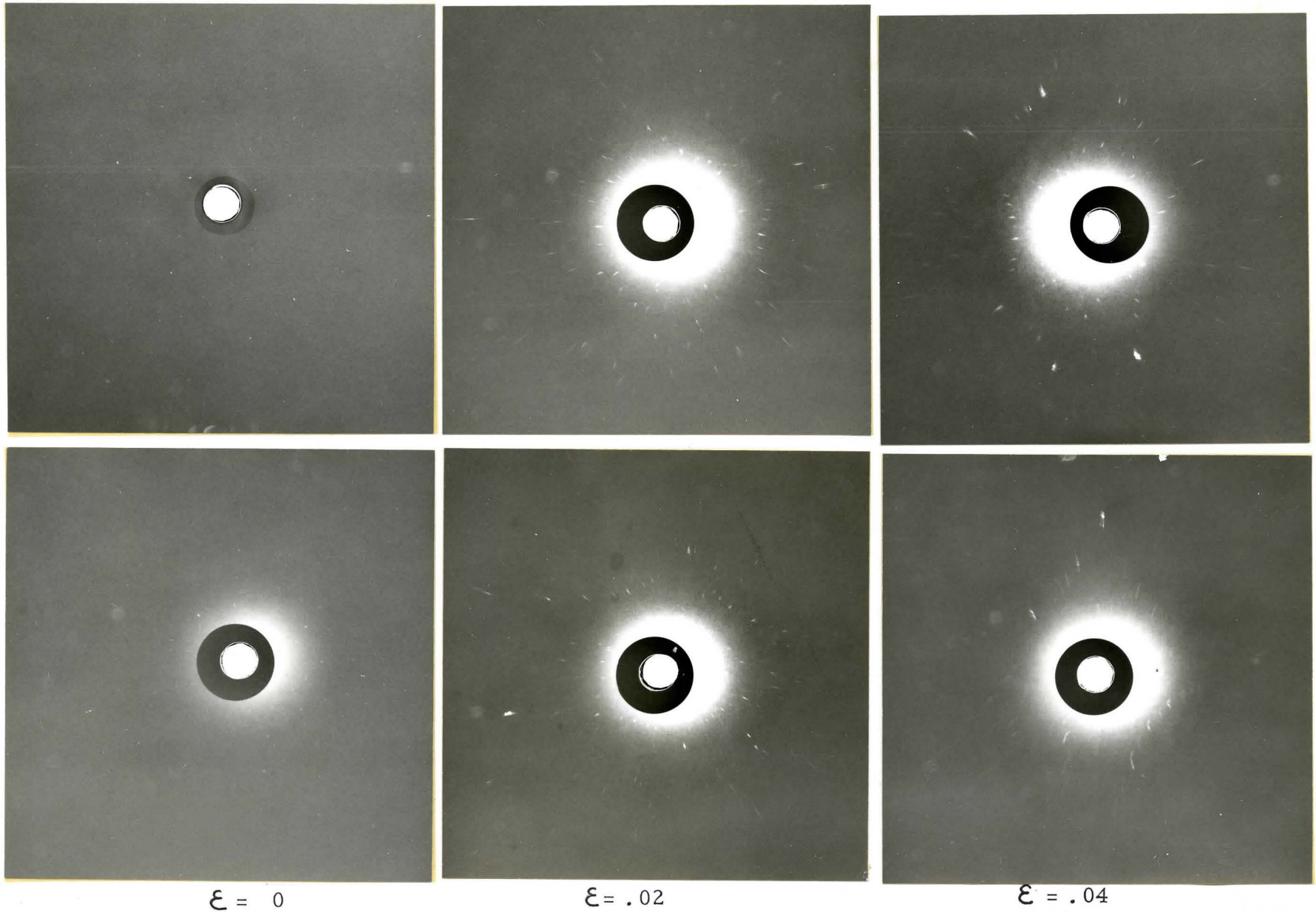

Fig. 4.17 Back reflection Laue patterns from a coarse-grained (G. D. = .18 mm) iron polycrystal (above) and a fine-grained (G. D. = .05 mm) iron polycrystal (below).

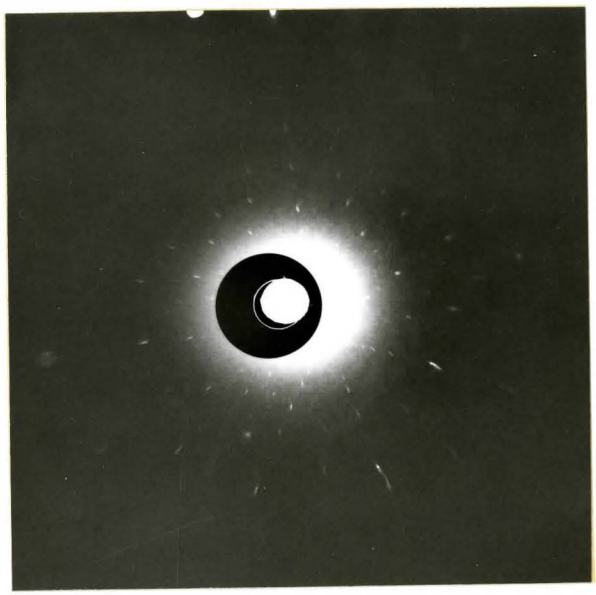

Grain Center

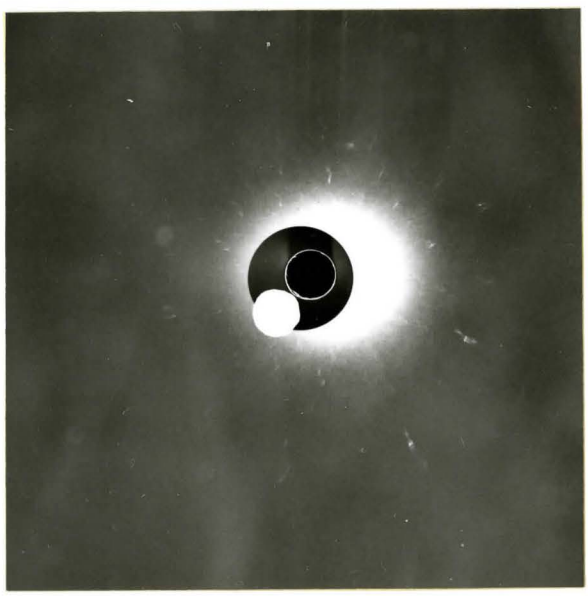

Region Near Grain Boundary

Fig. 4.18 Back reflection Laue patterns from center and grain boundary regions of an iron polycrystal strained 4% at 298°K. (G. D. = .18 mm)

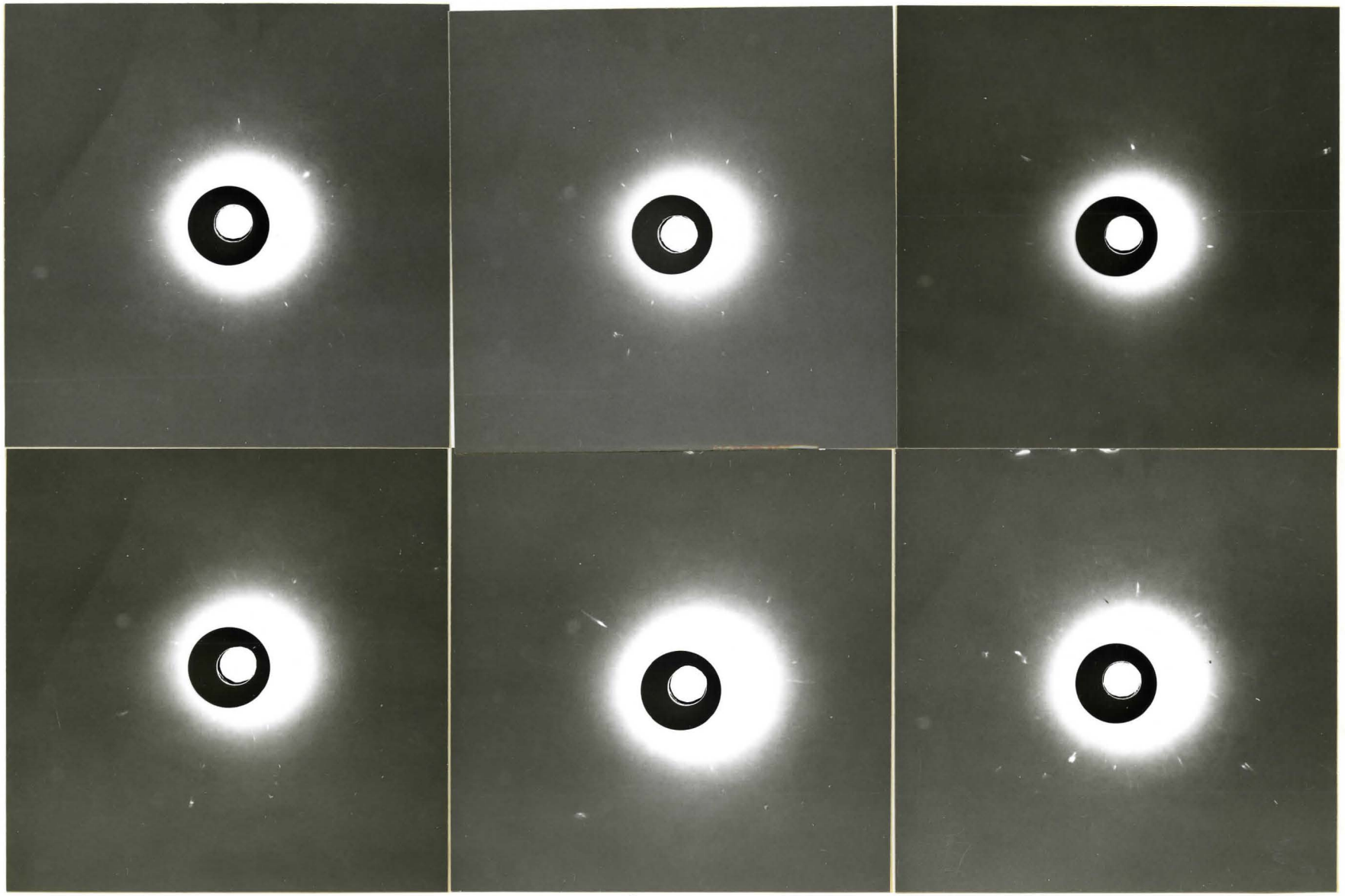

Fig. 4.19 Back reflection Laue patterns from a coarse-grained (G. D. = .16 mm) brass polycrystal (above) and a fine-grained (G. D. = .06 mm) brass polycrystal (below).

TABLE 4.1

Decarburized Iron at 298°K

ε (in/in)	σ_{app} (kg/mm^2)	σ_{int} (kg/mm^2)	σ_{eff} (kg/mm^2)	
Specimen DC-B-2	C.S.A. = .0054 sq. in.		G.S. = .05 mm.	
.005	6.53	3.54	2.98	
.010	7.95	4.92	3.02	
.015	9.21	6.20	3.01	
.020	10.26	7.24	3.02	
.025	11.15	8.21	2.95	
.030	11.95	9.05	2.91	$\pm$ 0.3 kg/mm^2
.040	13.25	10.34	2.91	
.050	14.35	11.61	2.74	
.060	15.16	12.41	2.75	
.080	16.83	14.08	2.75	
.100	17.96	15.21	2.75	
Specimen DC-B-2	C.S.A. = .0054 sq. in.		G.S. = .087 mm.	
.005	6.14	3.53	2.61	
.010	7.76	5.02	2.48	
.015	9.07	6.18	2.89	
.020	10.08	7.12	3.08	
.025	10.99	8.04	3.08	
.030	11.79	8.86	2.93	$\pm$ 0.3 kg/mm^2
.040	13.07	10.19	2.87	
.050	14.22	11.38	2.84	
.060	15.01	12.17	2.85	
.080	16.75	13.90	2.85	
.100	17.89	15.04	2.85	
Specimen DC-B-3	C.S.A. = .0056 sq. in.		G.S. = .18 mm.	
.005	5.73	3.18	2.55	
.010	7.23	4.70	2.53	
.015	8.38	5.68	2.69	
.020	9.30	6.53	2.77	
.025	10.12	7.29	2.83	
.030	10.87	7.98	2.89	

ε (in/in)	σ_{app} (kg/mm^2)	σ_{int} (kg/mm^2)	σ_{eff} (kg/mm^2)
(Cont.)			
Specimen DC-B-3	C.S.A. = .0056 sq. in.		G.S. = .038 mm.
.040	12.14	9.27	2.87
.050	13.18	10.40	2.78
.060	13.90	11.16	2.74 $\pm$ 0.3 $\frac{kg}{mm}$2
.080	15.58	12.84	2.74
.100	16.69	13.95	2.74
Specimen DC-C-1	C.S.A. = .0057 sq. in.		G.S. = .038 mm.
.005	7.03	3.76	3.27
.010	8.63	5.33	3.31
.015	9.93	6.78	3.14
.020	11.06	7.91	3.16
.025	11.91	8.86	3.06
.030	12.73	9.69	3.03 $\pm$ 0.3 $\frac{kg}{mm}$2
.040	14.10	11.14	2.96
.050	15.23	12.38	2.66
.060	16.05	13.38	2.66
.080	17.59	14.86	2.73
.100	18.59	15.97	2.61
Specimen DC-C-2	C.S.A. = .0057 sq. in.		G.S. = .038 mm.
.005	6.97	3.79	3.18
.010	8.47	5.38	3.09
.015	9.72	6.57	3.15
.020	10.82	7.76	3.06
.025	11.81	8.78	3.03
.030	12.65	9.66	3.00 $\pm$ 0.3 $\frac{kg}{mm}$2
.040	14.00	11.10	2.90
.050	15.11	12.23	2.89
.060	16.02	13.28	2.75
.080	17.48	14.73	2.75
.100	18.52	15.81	2.71
Specimen DC-C-3	C.S.A. = .0057 sq. in.		G.S. = .13 mm.
.005	6.18	3.49	2.68
.010	7.62	4.83	2.79
.015	8.76	5.91	2.85
.020	9.76	6.88	2.87
.025	10.61	7.71	2.90 $\pm$ 0.3 $\frac{kg}{mm}$2
.030	11.36	8.47	2.89
.040	12.70	9.79	2.91

ε (in/in)	σ_{app} (kg/mm^2)	σ_{int} (kg/mm^2)	σ_{eff} (kg/mm^2)
(Cont.)			
Specimen DC-C-3	C.S.A. = .0057 sq. in.		G.S. = .13 mm.
.050	13.86	10.98	2.89
.060	14.81	11.96	2.85
.080	16.34	13.51	2.84 $\pm$ 0.3 $\frac{kg}{mm^2}$
.100	17.42	14.43	2.98
Specimen DC-C-4	C.S.A. = .0057 sq. in.		G.S. = .074 mm.
.005	6.60	3.65	2.95
.010	8.14	5.18	2.96
.015	9.37	6.35	3.02
.020	10.42	7.45	2.97
.025	11.32	8.37	2.95
.030	12.12	9.19	2.94 $\pm$ 0.3 $\frac{kg}{mm^2}$
.040	13.53	10.64	2.89
.050	14.74	11.88	2.86
.060	15.79	12.95	2.84
.080	17.37	14.55	2.81
.100	18.50	15.54	2.96

Decarburized Iron at 195°K

Strain	σ_{app} (kg/mm^2)	σ_{int} (kg/mm^2)
Specimen DC-B-6	C.S.A. = .0055 sq. in.	G.S. = .087 mm.
.015	24.65	10.55
.020	26.85	12.75
.030	28.80	14.70
.040	30.13	16.03 ± 2.0 kg/mm^2
.050	30.83	16.73
.060	31.64	17.54
.080	32.58	18.48
.100	32.90	18.80
Specimen DC-B-7	C.S.A. = .0055 sq. in.	G.S. = .18 mm.
.015	23.72	9.95
.020	25.13	11.36
.030	27.21	13.43
.040	28.71	14.93 ± 2.0 kg/mm^2
.050	29.53	15.76
.060	30.41	16.63
.080	31.53	17.75
.100	31.97	18.20
Specimen DC-B-9	C.S.A. = .0054 sq. in.	G.S. = .05 mm.
.015		
.020	27.09	12.45
.030	29.60	14.96
.040	31.10	16.47
.050	32.15	17.51 ± 2.0 kg/mm^2
.060	32.77	18.14
.080	33.61	18.97
.100	33.98	19.34
Specimen DC-C-6	C.S.A. = .0056 sq. in.	G.S. = .13 mm.
.015	24.39	10.25
.020	25.80	11.66
.030	27.50	13.36
.040	29.19	14.98 ± 2.0 kg/mm^2
.050	30.11	15.98
.060	30.98	16.85
.080	31.92	17.78
.100	32.39	18.25

Strain	σ_{app} (kg/mm^2)	σ_{int} (kg/mm^2)
Specimen DC-C-7	C.S.A. = .0058 sq. in.	G.S. = .074 mm.
.015	26.14	11.72
.020	27.57	13.15
.030	29.10	14.68
.040	30.53	16.12 $\pm$ 2.0 kg/mm^2
.050	31.46	17.04
.060	32.41	17.99
.080	33.26	18.85
.100	33.69	19.27
Specimen DC-C-8	C.S.A. = .0056 sq. in.	G.S. = .038 mm.
.015		
.020	27.81	13.45
.030	29.75	15.40
.040	31.01	16.65 $\pm$ 2.0 kg/mm^2
.050	32.14	17.78
.060	32.77	18.41
.080	33.62	19.27
.100	33.96	19.61

70/30 Alpha Brass at 195°K

ε (in/in)	σ_{app} (kg/mm^2)	σ_{int} (kg/mm^2)	σ_{eff} (kg/mm^2)	
Specimen α-brass -2	C.S.A. = .0054 sq. in.		G.S. = .031 mm.	
.012	12.00	11.09	.91	
.025	13.88	12.84	1.04	$\pm$ 0.2 kg/mm^2
.050	16.34	14.98	1.36	
.075	18.48	16.93	1.56	
.100	20.37	18.68	1.69	
.125	22.16	20.43	1.72	
.150	23.76	21.79	1.97	$\pm$ 0.5 kg/mm^2
.200	26.59	24.52	2.07	
.250	28.86	26.66	2.20	
.300	30.65	28.41	2.24	
Specimen α-brass -3	C.S.A. = .0055 sq. in.		G.S. = .091 mm.	
.012	8.46	7.53	0.93	
.025	9.68	8.63	1.05	$\pm$ 0.2 kg/mm^2
.050	11.50	10.16	1.34	
.075	13.06	11.70	1.37	
.100	14.46	13.04	1.52	
.125	15.95	14.38	1.57	
.150	17.38	15.59	1.79	$\pm$ 0.5 kg/mm^2
.200	20.07	18.33	1.74	
.250	22.50	20.64	1.85	
.300	24.49	22.56	1.93	
Specimen α-brass -4	C.S.A. = .0058 sq. in.		G.S. = .075 mm.	
.012	9.04	7.98	1.06	
.025	10.52	9.26	1.22	$\pm$ 0.2 kg/mm^2
.050	12.77	11.43	1.34	
.075	14.43	12.83	1.60	
.100	16.02	14.44	1.58	
.125	17.55	15.80	1.74	
.150	19.04	17.06	1.99	$\pm$ 0.5 kg/mm^2
.200	21.75	19.82	1.92	
.250	24.09	22.12	1.97	
.300	26.08	24.09	1.99	

ε (in/in)	σ_{app} (kg/mm^2)	σ_{int} (kg/mm^2)	σ_{eff} (kg/mm^2)
Specimen α-brass -5	C.S.A. = .0056 sq. in.		G.S. = .19 mm.
.012	7.02	6.05	.96
.025	8.05	6.99	1.06 ± 0.2 kg/mm^2
.050	9.53	8.38	1.15
.075	10.98	9.72	1.26
.100	12.42	11.06	1.36
.125	13.82	12.37	1.45
.150	15.15	13.63	1.51 ± 0.5 kg/mm^2
.200	17.68	16.06	1.63
.250	20.03	18.35	1.68
.300	22.03	20.26	1.77
Specimen α-brass -6	C.S.A. = .0056 sq. in.		G.S. = .16 mm.
.012	7.41	6.40	1.00
.025	8.29	7.23	1.05 ± 0.2 kg/mm^2
.050	9.86	8.66	1.19
.075	11.30	9.99	1.31
.100	12.74	11.36	1.38
.125	14.12	12.81	1.32
.150	15.57	14.17	1.39 ± 0.5 kg/mm^2
.200	18.14	16.57	1.57
.250	20.46	18.77	1.69
.300	22.60	20.84	1.76
Specimen α-brass -7	C.S.A. = .0054 sq. in.		G.S. = .068 mm.
.013	9.45	8.45	1.00
.025	10.91	9.70	1.21 ± 0.2 kg/mm^2
.050	13.02	11.52	1.50
.075	14.88	13.36	1.52
.100	16.47	14.89	1.57
.125	18.01	16.34	1.67
.150	19.54	17.72	1.82 ± 0.5 kg/mm^2
.200	22.26	20.44	1.82
.250	24.67	22.65	2.02
.300	26.86	24.61	2.25

ε (in/in)	σ_{app} (kg/mm^2)	σ_{int} (kg/mm^2)	σ_{eff} (kg/mm^2)	
Specimen α-brass -8	C.S.A. = .0057 sq. in.		G.S. = .057 mm.	
.012	9.92	8.82	1.10	± 0.2 kg/mm^2
.025	11.51	10.23	1.29	
.050	13.91	12.44	1.47	
.075	15.86	14.33	1.53	
.100	17.64	15.98	1.65	± 0.5 kg/mm^2
.125	19.41	17.67	1.74	
.150	20.98	19.21	1.78	
.200	23.74	21.78	1.96	
.250	26.13	24.13	2.00	
.300	28.12	26.04	2.08	
Specimen α-brass -9	C.S.A. = .0055 sq. in.		G.S. = .025 mm.	
.012	13.14	12.14	1.00	± 0.2 kg/mm^2
.025	15.13	13.87	1.27	
.050	17.77	16.23	1.53	
.075	19.98	18.32	1.66	
.100	21.93	20.07	1.79	± 0.5 kg/mm^2
.125	23.65	21.79	1.85	
.150	25.31	23.33	1.98	
.200	28.06	25.89	2.17	
.250	30.42	28.12	2.30	
.300	32.40	29.96	2.44	

Copper at 298°K

ε (in/in)	σ_{app} (kg/mm^2)	σ_{int} (kg/mm^2)	σ_{eff} (kg/mm^2)
Specimen Cu-1	C.S.A. = .0058 sq. in.		G.S. = .018 mm.
.002	4.35	4.07	.28
.005	5.11	4.62	.49
.010	6.24	5.41	.83
.015	7.20	6.32	.88
.020	8.08	7.19	.89
.025	8.88	7.72	1.16
.030	9.61	8.39	1.22
.035	10.27	8.96	1.30
.040	10.89	9.58	1.30 $\pm$ 0.5 kg/mm^2
.045	11.51	10.22	1.29
.050	12.04	10.59	1.45
.060	12.91	11.32	1.58
.070	13.89	12.08	1.81
.080	14.73	12.71	2.02
.090	15.46	13.43	2.03
.100	16.18	13.93	2.25
Specimen Cu-2	C.S.A. = .0056 sq. in.		G.S. = .029 mm.
.002	3.26	3.10	.16
.005	3.89	3.68	.21
.010	5.05	4.51	.54
.015	6.00	5.30	.70
.020	6.90	6.10	.80
.025	7.75	6.82	.93
.030	8.51	7.41	1.10
.035	9.21	8.08	1.13 $\pm$ 0.5 kg/mm^2
.040	9.89	8.69	1.20
.045	10.52	9.26	1.25
.050	11.15	9.86	1.29
.060	12.24	10.62	1.62
.070	13.21	11.44	1.77
.080	14.10	12.24	1.86
.090	14.90	12.99	1.91
.100	15.63	13.55	2.08

ε(in/in)	σ_{app}(kg/mm^2)	σ_{int}(kg/mm^2)	σ_{eff}(kg/mm^2)
Specimen Cu -3	C.S.A. = .0056 sq. in.		G.S. = .043 mm.
.002	2.58	2.45	.12
.005	3.32	3.12	.20
.010	4.45	4.07	.39
.015	5.50	4.91	.58
.020	6.41	5.75	.66
.025	7.28	6.47	.81
.030	8.05	7.17	.88
.035	8.81	7.84	.97
.040	9.48	8.46	1.02 $\pm$ 0.5 kg/mm^2
.045	10.12	9.02	1.09
.050	10.71	9.52	1.19
.060	11.82	10.48	1.34
.070	12.87	11.32	1.54
.080	13.74	12.12	1.63
.090	14.56	12.90	1.65
.100	15.29	13.54	1.75
Specimen Cu -4	C.S.A. = .0055 sq. in.		G.S. = .055 mm.
.002	2.50	2.41	.09
.005	3.17	2.95	.22
.010	4.32	3.86	.46
.015	5.31	4.75	.56
.020	6.18	5.52	.67
.025	7.02	6.36	.65
.030	7.81	7.05	.76
.035	8.57	7.70	.87 $\pm$ 0.5 kg/mm^2
.040	9.24	8.33	1.04
.045	9.88	8.85	1.03
.050	10.48	9.37	1.12
.060	11.65	10.43	1.22
.070	12.65	11.29	1.36
.080	13.57	12.19	1.39
.090	14.37	12.70	1.67
.100	15.11	13.38	1.73

CHAPTER V

THERMAL RECOVERY OF INTERNAL STRESS IN DECARBURIZED IRON

5.1 Introduction

From the results in Chapter 4 it is apparent that work hardening in iron is strongly dependent on the temperature of deformation. The disappearance of the grain size dependence of work hardening in iron deformed at 195°K suggests that the dislocation accumulation process at 195°K is quite different than that occurring during deformation at 298°K.

Since recovery is a process whereby the density of dislocations accumulated during plastic flow is gradually reduced, a knowledge of the rate and temperature dependence of this process for various prestrain conditions might be helpful in formulating a model of the work hardened state. Also the recovery process can be used to examine the stability of the dislocation structure developed during cold working.

Stress relaxation techniques have been employed to measure separately the effects of recovery on the magnitude of the internal stress and effective stress. This type of information is lacking in previous investigations concerning the recovery of flow stress in iron. (Michalak and Paxton, 1961).

A limited part of the investigation was devoted to the direct observation of the dislocation substructure before and after recovery by transmission electron microscopy.

5.2 Experimental Procedure

5.2.1 Materials and Apparatus

The specimen fabrication and decarburization treatment for the

specimens used in the recovery studies are described in section 3.2. All the specimens used for recovery had an average grain diameter of about 0.3 to 0.5 mm.

Recovery anneals were performed on decarburized iron specimens prestrained in tension at both 298°K and 195°K. The testing and recording of stress and strain before and after recovery treatments was accomplished by using the table model Instron tensile testing machine as described in section 3.3.1. All the tensile tests were conducted at a strain rate of 6.66×10^{-4}/sec. and both the prestrain and strain after anneal were carried out at the same temperature.

A range of recovery anneals from 350°C to 500°C were performed in a molten lead bath. The strained specimens were wrapped in steel foil and annealed for increasing intervals of time up to 24 hours. For all the recovery tests, the bath temperature was controlled to within $\pm$ 2°C.

5.2.2 Method of Evaluating Recovery

The degree of recovery after prestraining at both 298°K and 195°K was evaluated in terms of the internal stress measured after various recovery treatments. The magnitudes of internal stress have been determined by the indirect method of dislocation dynamics (D.D.). The effect of a recovery treatment on the determination of internal stress by stress relaxation is shown schematically in Fig. 5.1. The degree of recovery was evaluated in terms of fractional recovery f_R, where f_R is defined as the decrease in the internal stress due to the recovery treatment divided by the decrease experienced if the material recovered completely to the fully annealed state. Thus as illustrated in Fig. 5.1

$$f_R = \frac{\sigma_{int_{(1)}} - \sigma_{int\,(2)}}{\sigma_{int_{(1)}} - \sigma_{int_{(y)}}} \qquad 5.1$$

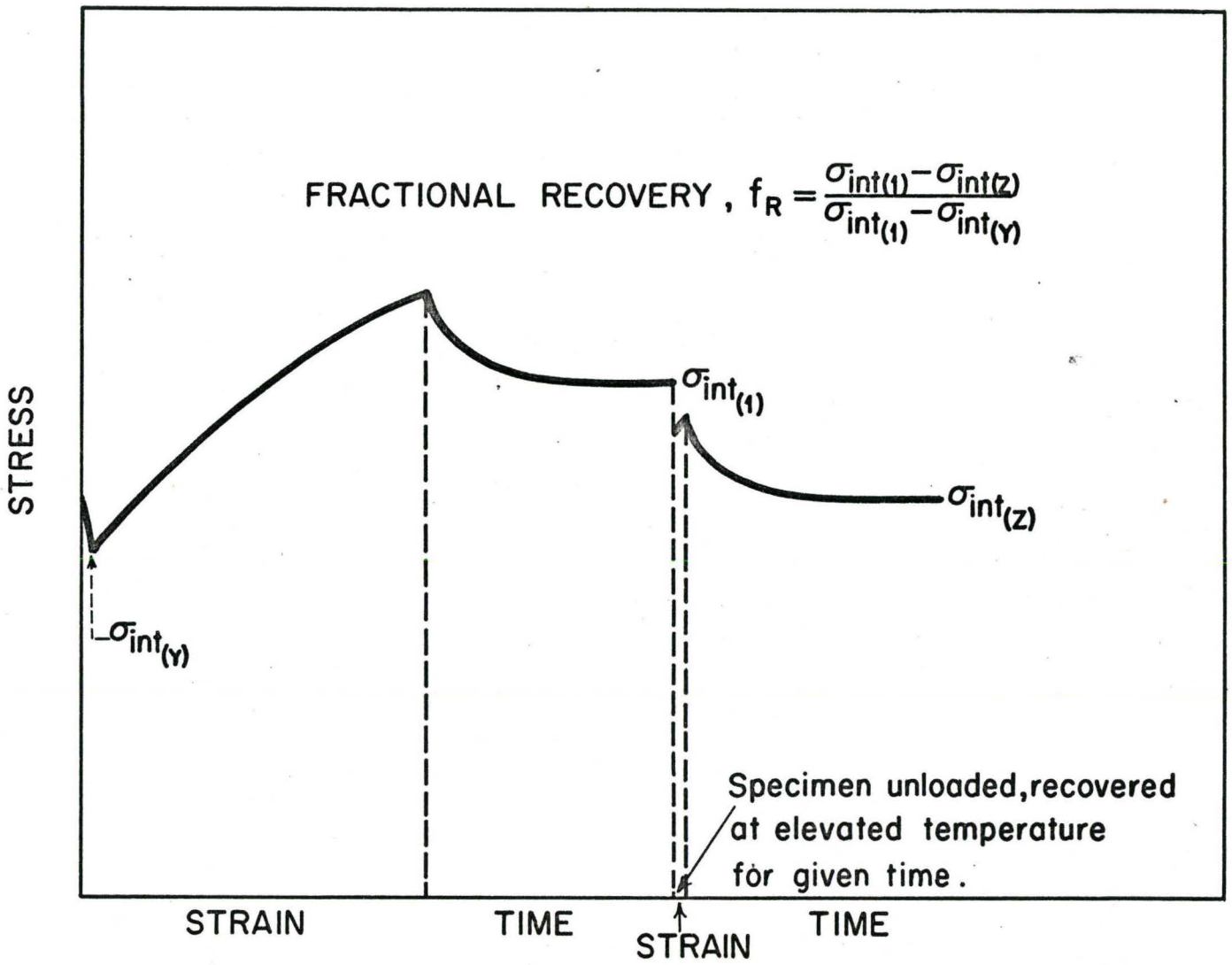

Fig. 5.1 Schematic diagram showing the effect of recovery on σ_{int} and the method used to evaluate the degree of recovery.

where $\sigma_{int_{(1)}}$ = internal stress of strained material at a predetermined constant strain.

$\sigma_{int_{(2)}}$ = internal stress after a recovery anneal.

$\sigma_{int_{(y)}}$ = internal stress of fully annealed material.

An approximate value of $\sigma_{int_{(y)}}$ was obtained by subtracting the value of σ_{eff} from the lower yield stress. This method neglects the effect of the Luder's strain which was less than 0.5% for the specimens strained at 298°K. It introduces a larger error for the specimens prestrained at 195°K since the Luder's strain is ~ 1%. However, it was felt that this method provided a more representative value than would be obtained by trying to extrapolate the internal stress back to zero plastic strain.

The complete recovery curve for each temperature was determined by subjecting one specimen to all the recovery anneals. No significant additional strain was introduced ($< 0.2\%$) during the measurement of the recovered internal stress.

5.2.3 Electron Microscope Study

In order to facilitate preparation of thin foils suitable for transmission electron microscopy, decarburized iron sheet .010 inches thick was rolled 5% at both 298°K and 195°K. Specimens prestrained at both temperatures were recovered at 500°C. for 300 min. to achieve the fully recovered state.

A conventional electropolishing technique was used to obtain thin foils suitable for transmission microscopy. The specimens were first thinned chemically in a solution of 80% H_2O_2, 15% H_2O, and 5% H.F. to about .004" - .005 inches in thickness. Electropolishing was done in a solution of 5% perchloric acid and 95% acetic acid with stainless steel

as a cathode. The electrolyte was at R. T. and an open circuit voltage of 25 - 30 volts was used.

The foils were examined in a Siemens Elmiskop I electron microscope operated at 100 kV.

5.3 Experimental Results

5.3.1 Recovery of Internal Stress

Prestrain 5% at 298°K and 195°K

The effect of recovery treatment at 500°C for 250 min. on the stress relaxation of decarburized iron strained 5% at 298°K is presented in Fig. 5.2. The upper curve represents the stress relaxation just after 5% prestrain at 298°K. Fig. 5.3 presents similar stress relaxation curves for decarburized iron strained 5% at 195°K. The stress relaxation curves were analyzed by the method of dislocation dynamics. For both temperatures of prestrain, σ_{eff} remains constant before and after recovery.

In Fig. 5.4 the residual internal stress $1- f_R$ following prestrain at 298°K is compared with the similar fraction following 5% prestrain at 195°K. Approximate values of internal stress between no recovery and full recovery were obtained by subtracting the value of σ_{eff} from the initial flow stress after each recovery anneal. After about 1 hour annealing a discontinuous yield reappeared on the stress-strain curves obtained at both temperatures. This discontinuous yield was slight and no Luder's region was observed. From the data presented in Fig. 5.4, it can be seen that there is an increased fraction of recovery and an increased rate of recovery due to straining at the lower temperature.

Prestrain 10% at 298°K

The progress of recovery, represented by the residual fraction of internal stress $(1- f_R)$ is shown in Fig. 5.5 as a function of annealing time at temperatures of 350°, 400°, 450° and 500°C. At the higher

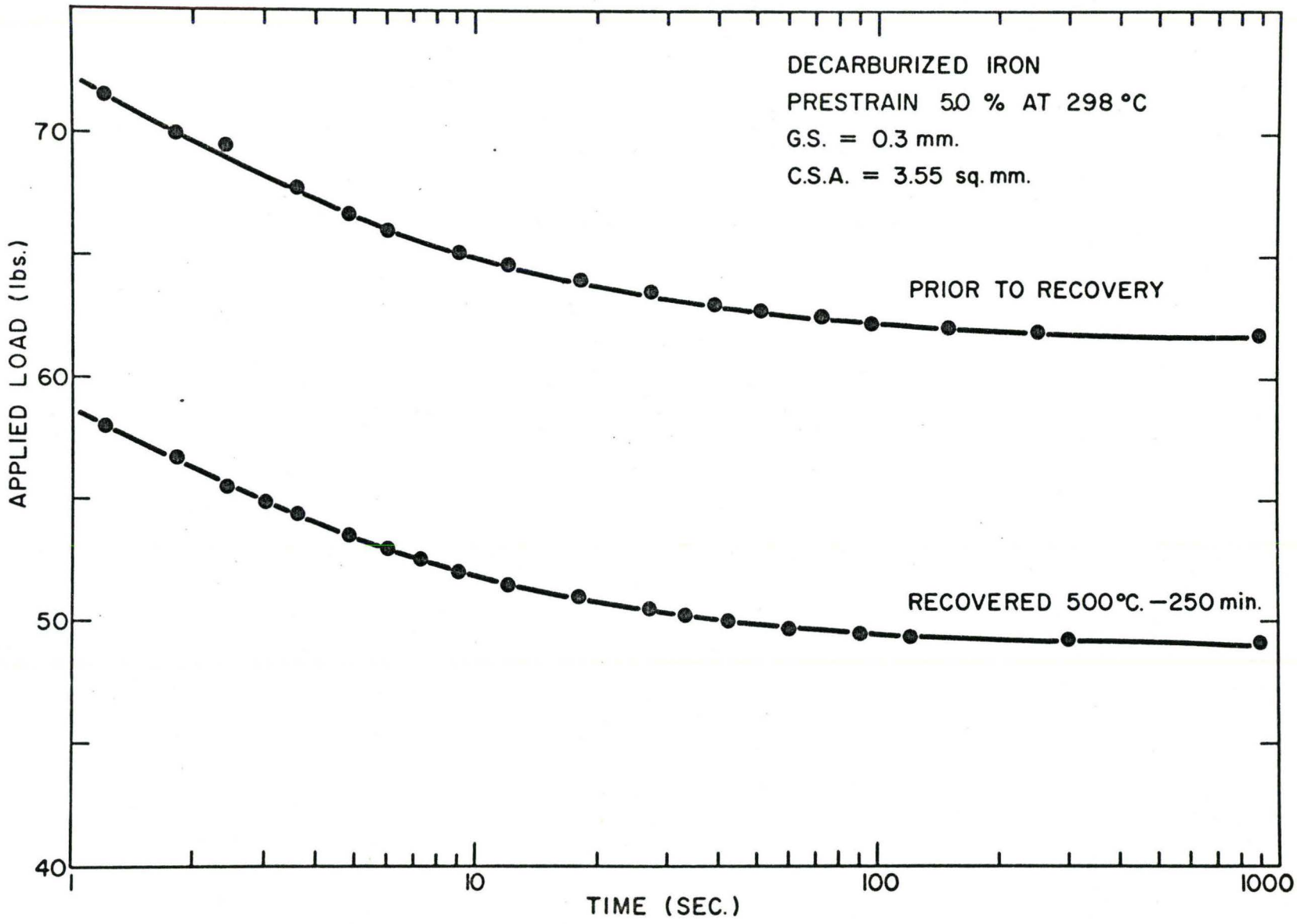

Fig. 5.2 Effect of recovery treatment on stress relaxation.

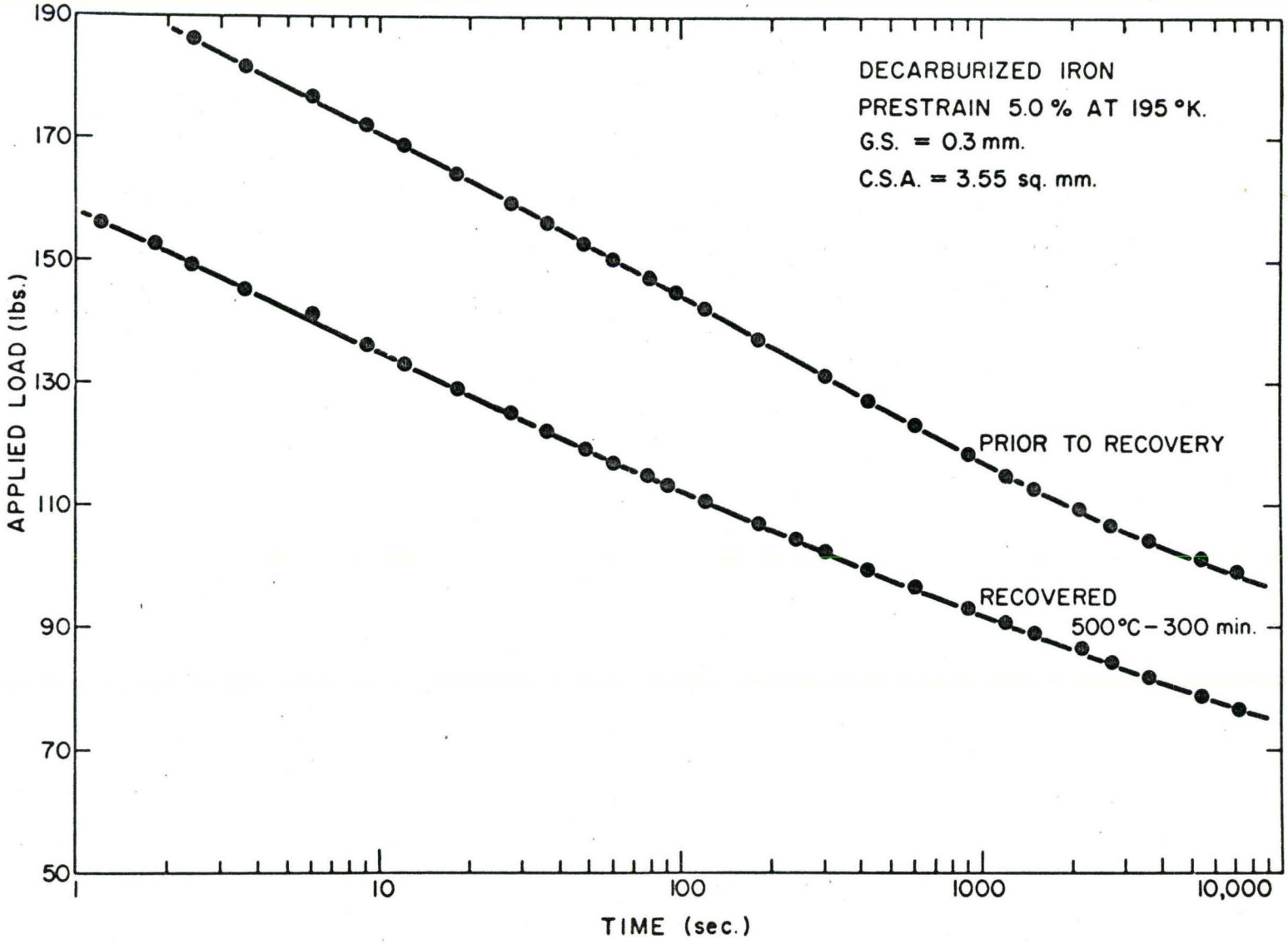

Fig. 5.3 Effect of recovery treatment on stress relaxation.

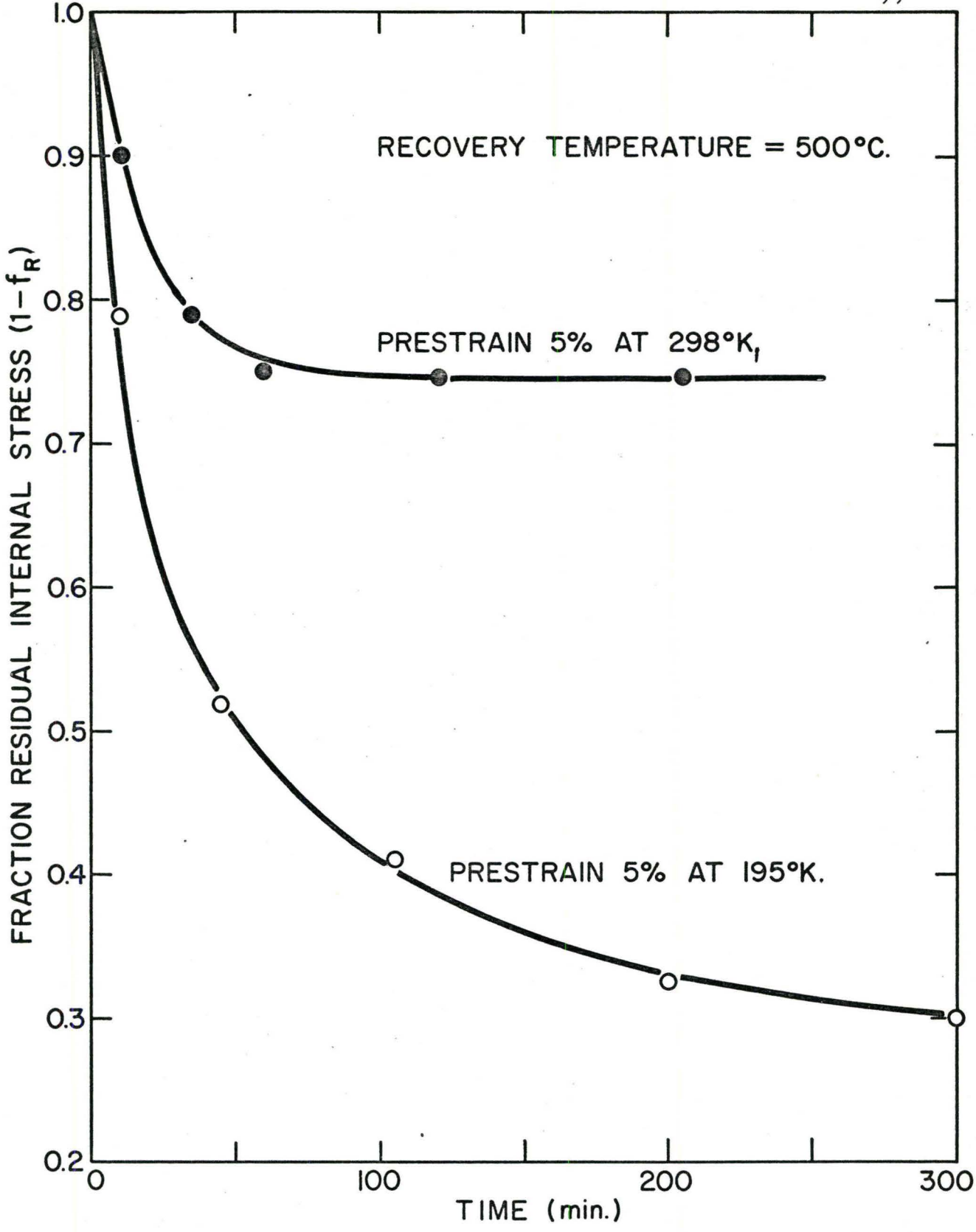

Fig. 5.4 Progress of recovery in decarburized iron prestrained at 298°K and 195°K.

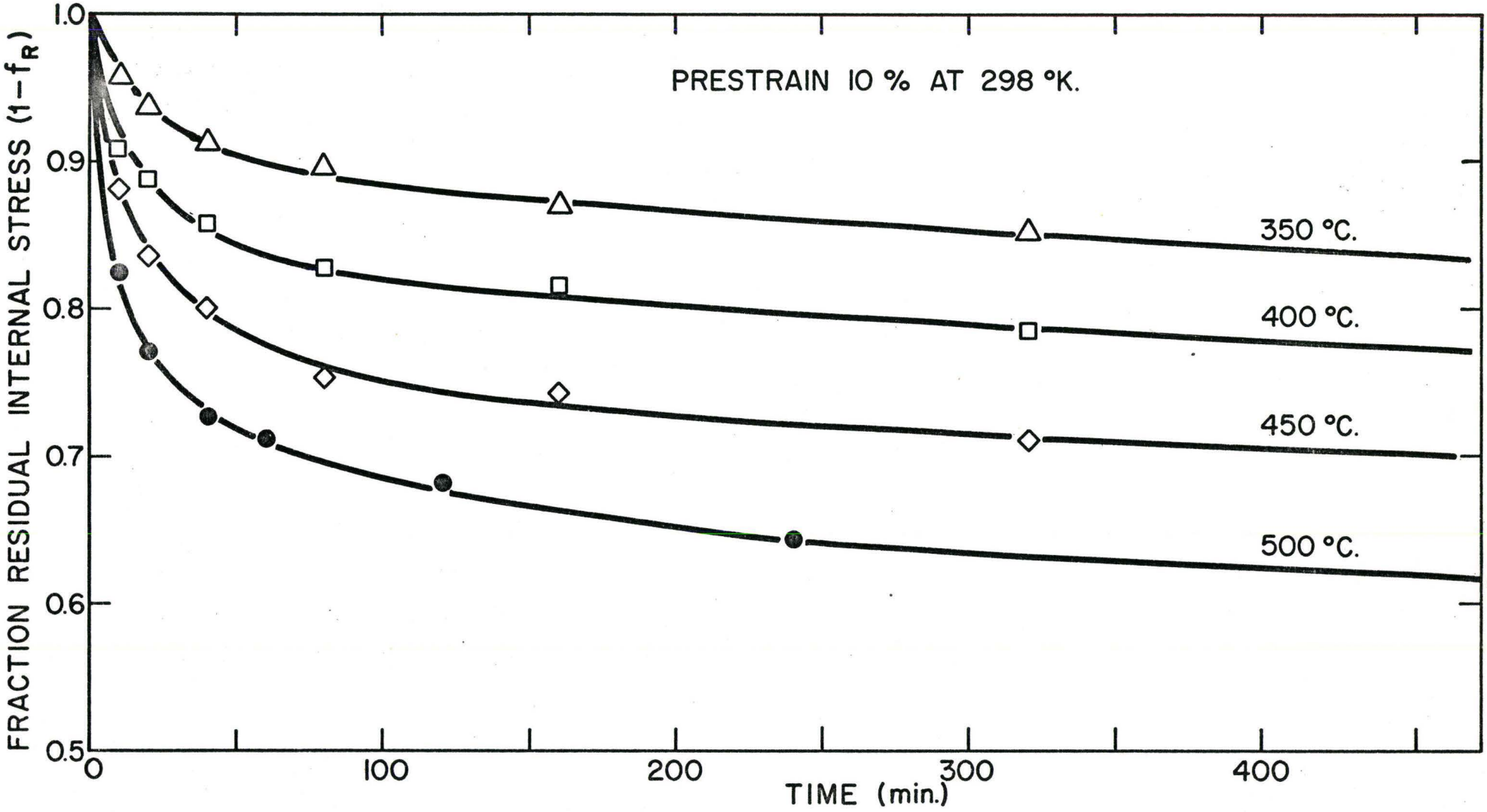

Fig. 5.5 Progress of recovery in decarburized iron.

temperatures, there appears to be a saturation value of recovery, characteristic of the temperature, beyond which the internal stress does not change significantly with time. This recovery behavior is very similar to that reported by Michalak and Paxton (1961) for the measurements of the recovery of flow stress in zone refined iron. A discontinuous yield did not reappear after long periods of recovery for the specimens prestrained 10% at 298°K.

5.3.2 Electron Microscopy Results

(a) Effect of Deformation Temperature on the Dislocation Distribution

Figures 5.6 and 5.7 shows the dislocation arrangement in a specimen strained 5% by rolling at 298°K. The important feature of these micrographs is that the dislocation distribution is non uniform with a large fraction of the total dislocation density residing in tangled arrangements of dislocations. The tangles have no large misorientations across them, thus are not simple accumulation of dislocations of one sign. The remaining small fraction is distributed randomly throughout the grains. A greater density of small dislocation loops is formed during deformation at room temperature. The tangles show the broad outlines of a dislocation cell structure that is just beginning to form in selected regions. Keh and Weissmann (1963) have clearly shown that these tangles eventually join together as the amount of deformation is increased and form a cell structure.

When decarburized iron is rolled at 195°K the tendency for tangling and cell formation is less pronounced and the dislocation distribution is more uniform as shown in the micrographs of Figs. 5.8 and 5.9. Although there is some evidence of dislocation clustering, when compared to a specimen strained to an equivalent amount at 298°K, the distribution of dislocations is characterized by greater uniformity and by a higher density of long and straight dislocation segments. These observations are in accord

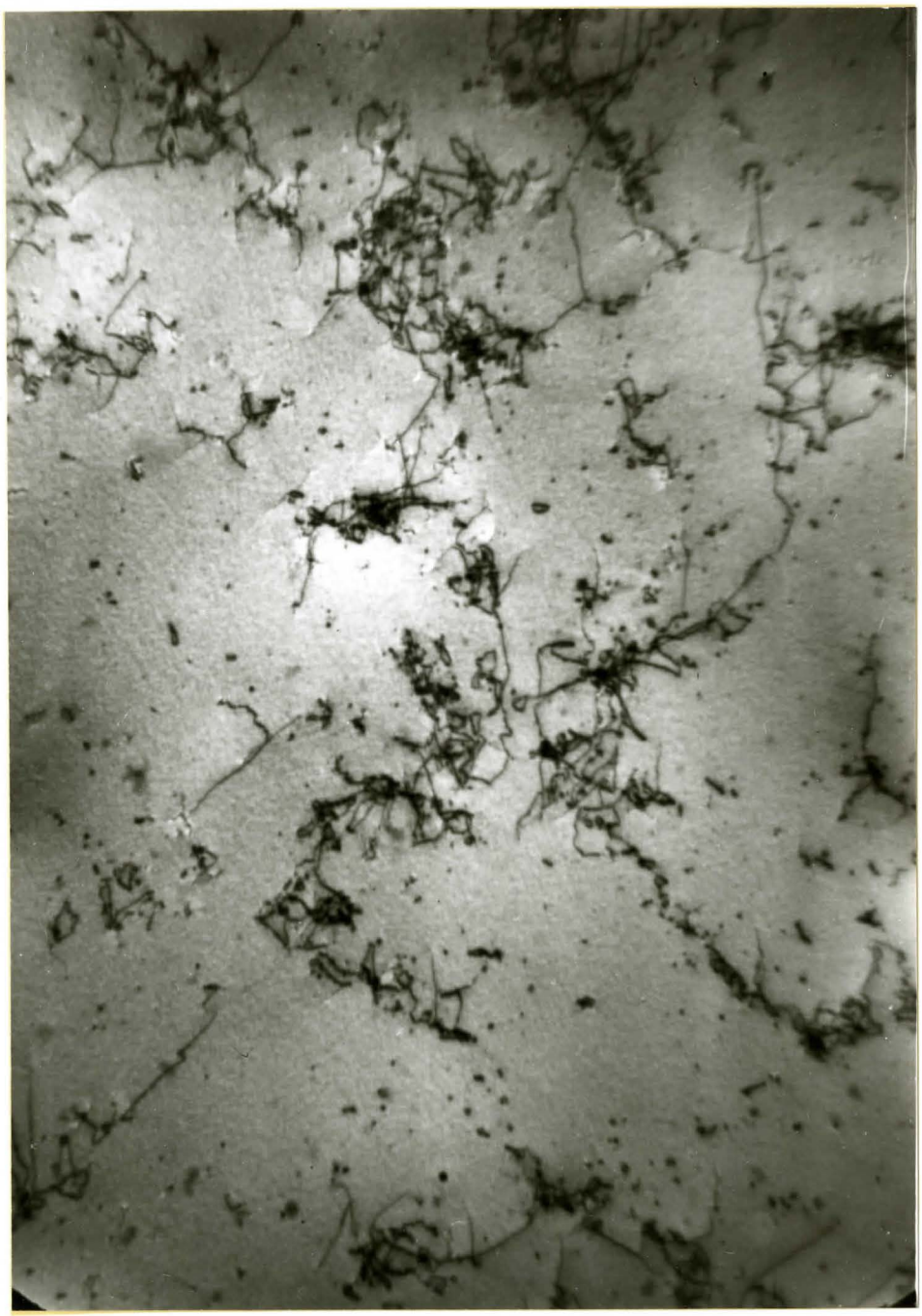

Fig. 5.6 Dislocation structure in iron strained 5% by rolling at 298°K.

Fig. 5.7 Dislocation structure in iron strained 5% by rolling at 298°K.

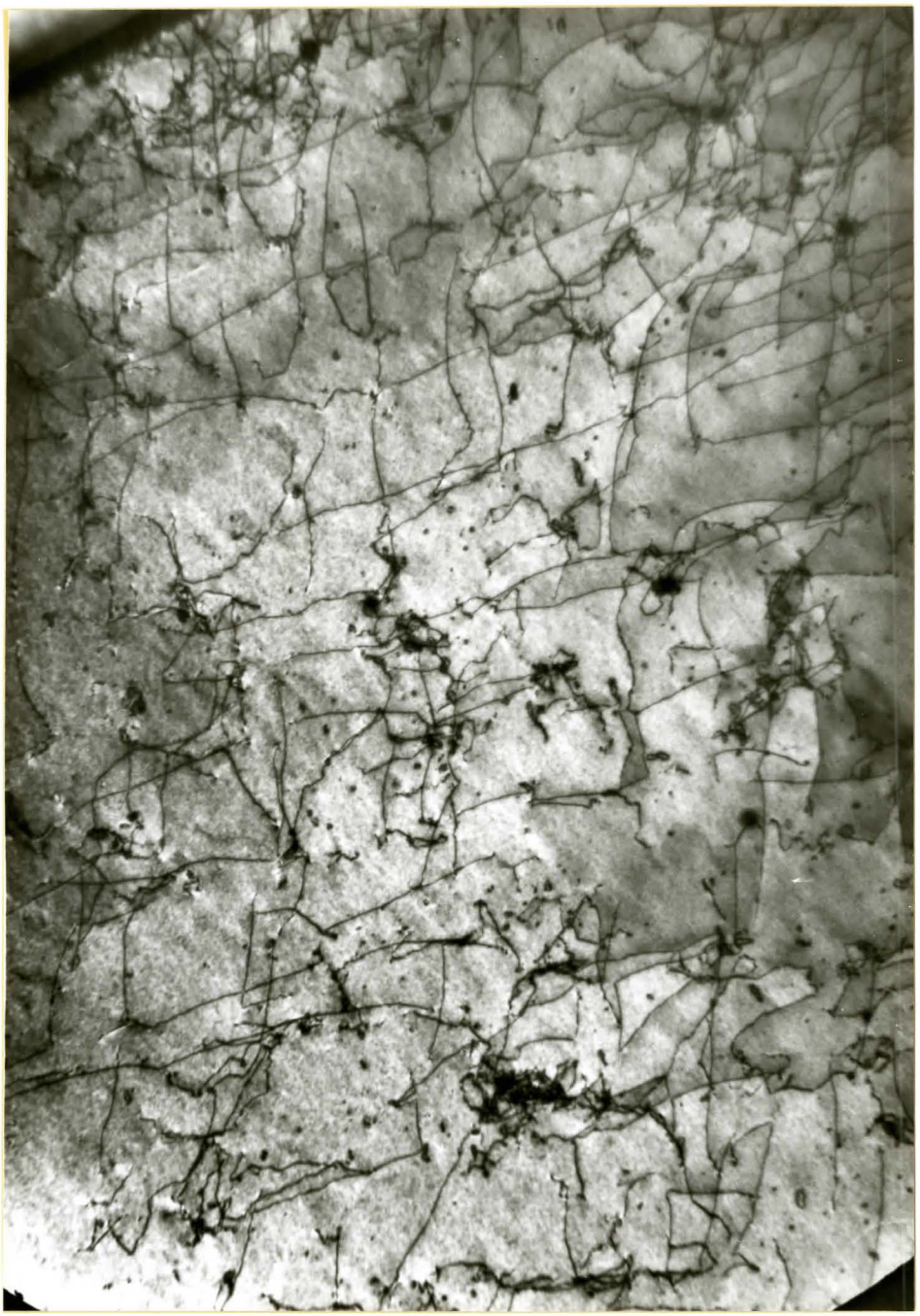

Fig. 5.8 Dislocation structure in iron strained 5% by rolling at 195°K.

Fig. 5.9 Dislocation structure in iron strained 5% by rolling at 195°K.

Fig. 5.10 Dislocation structure of fully recovered iron prestrained 5% at 298°K.

Fig. 5.11 Dislocation structure of fully recovered iron prestrained 5% at 298°K.

Fig. 5.12 Dislocation structure of fully recovered iron prestrained 5% at 195°K.

Fig. 5.13 Dislocation structure of fully recovered iron prestrained 5% at 195°K.

with previous studies (Keh and Weissmann, 1963; Solomon and McMahon, 1966).

(b) Effect of Recovery on the Dislocation Distribution

The dislocation structure of fully recovered iron prestrained 5% at 298°K is shown in Figures 5.10 and 5.11. The tangled dislocations have arranged themselves into regular subboundaries. Similar observations have been made by Keh (1962) and by Carrington et al (1960). All of these findings are consistent with the view that the tangles of dislocations will arrange themselves into more stable configurations during recovery.

Similar networks were observed for iron full recovered after a prestrain of 5% at 195°K as shown in Figures 5.12 and 5.13. The structures observed after recovery were similar for specimens prestrained at 195°K with those prestrained at 298°K.

5.4 Discussion of Results

5.4.1 Effect of Temperature on Work Hardening

The results of section 4.3 show that the work hardening behavior of iron varies a great deal with deformation temperature. The rate of work hardening at 195°K is lower than at 298°K. Similar observations of this type were reported by Keh and Weissmann (1963) for polycrystals and Keh and Nakada (1967) for single crystals. In addition, transmission electron microscopy results indicate that the change in the rate of work hardening with deformation temperature is accompanied by a change in the distribution of dislocations.

Deformation at room temperature is characterized by the formation of tangles and eventually a cell structure. This type of deformation structure has been discussed by Li (1963). He concludes that the formation of tangles must involve the interaction of two slip systems acting in such a way as to reduce the internal stress in the material. In

simple terms the long range stress fields of dislocation arrays on the primary system can attract dislocations of the secondary system to form tangles and cells. Keh and Nakada (1967) have shown that the work hardening rate in both Stage I and Stage II for iron single crystals of different orientation at room temperature was related to the density of secondary dislocations present, relative to the primary density. In both the first and second stages, from 10 to 40% of the dislocations present in the crystal have Burgers vectors other than the primary Burgers vector.

When the deformation temperature is lowered to 195^{o}K the dislocation density in the tangled regions is decreased and the distribution of dislocations is more uniform. A large increase in σ_{eff} is also observed at the lower temperature.

In general then, a decrease in deformation temperature results in a large effective stress, a more uniform dislocation distribution, and a lower work hardening rate. The influence of temperature on the dislocation distribution can be rationalized on the basis of an increasing effective stress. The obstacles controlling the magnitude of σ_{eff} can be the Peierls stress, impurity atoms, or even jog drag on screw dislocations. If the amplitude of the stress needed to overcome these obstacles is large, it will prevent the dislocations from grouping together to form tangles and the probability of dislocations becoming immobilized in the region between the tangles is increased. Thus on the average a much greater number of dislocations become distributed randomly in the lattice rather than grouped together in tangles and cell walls. The change in the distribution of dislocations (and thus the magnitude of σ_{int}) is illustrated by the work of Keh and Weissmann (1963) who found that in iron deformed 8% at room temperature a cell structure was formed. Upon restraining at -135^{o}C the distribution of dislocations became more uniform due to the increase in the magnitude of the stress needed to overcome lattice

obstacles. Similar results were reported by Solomon and McMahon (1966).

Since the tendency for tangle formation is reduced when the deformation temperature is lowered, the rate of internal stress development is decreased. This results in a lower rate of work hardening at low temperatures.

5.4.2 Recovery of Internal Stress

In discussing the recovery of internal stress due to work hardening it is important to examine two salient features of the results. Firstly the extent of recovery is markedly dependent on the temperature of prestrain and secondly the kinetics of recovery for specimens prestrained 10% at 298°K should be discussed.

1) Effect of Temperature of Prestrain

In regard to the influence of the temperature of prestrain it is apparent from Fig. 5.4 that the rate and extent of recovery is much greater after 5% deformation at 195°K than at 298°K. In view of the differences in dislocation distribution produced at these temperatures, the observations can be rationalized as follows. After deformation at 298°K the accumulated dislocations are predominantly in the form of complex tangles together with some randomly distributed dislocations between the tangles. Thus during recovery at elevated temperatures, closely spaced dislocations of opposite sign within the tangles and random dislocations between the tangles can annihilate. This would result in the partial reduction in internal stress observed during the initial portion of recovery. However, the internal stress associated with the tangles themselves is not removed by this process. The tangles can only be removed by a large scale coarsening of the existing structure or by recrystallization. Thus softening which occurs by this process is expected to occur at an appreciable rate only at high temperatures and probably only during recrystallization.

Deformation at 195°K produces a uniform distribution of dislocations however, and a substantial fraction of the internal stress is associated with these uniformly distributed dislocations. Thus during recovery at an elevated temperature, the annihilation of these randomly dispersed dislocations would proceed more quickly and to a greater extent and complete recovery could be achieved by this process alone.

Leslie et al (1961) have shown that vacancies will migrate in body-centered cubic metals in the temperature range of 10-15% of their melting point. The temperature of prestrain (195°K) used in this work is in the range where vacancies might be expected to be considerably less mobile than at 298°K. By a formula due to Mott (1953) the excess vacancy concentration produced at a strain of .05 due to dislocation cutting would be about 5×10^{-6} compared to the equilibrium vacancy concentration at 500°C of 5×10^{-13}. Thus recovery would also be expected to proceed more rapidly and to a greater extent due to the excess of vacancies and the more random distribution of vacancies.

2) Activation Energy for Recovery

If the initial portion of the recovery of internal stress is ascribed to the annihilation and rearrangement of closely spaced dislocations of opposite sign, an activation energy for recovery may be determined as follows.

The rate of recovery of the density of dislocations which are annealing out by thermally activated motion is often expected to follow a rate equation of the form,

$$- \frac{d\rho}{dt} = f(\rho) \exp\left(-\frac{Q}{RT}\right) \qquad 5.2$$

where ρ represents the dislocation density; t, the time; T, the temperature; R, the gas constant and Q, the activation energy. The kinetics of recovery can be measured by measuring the change in σ_{int} which is

connected to ρ by some functional equation,

$$\sigma_{int} = g(\rho) \qquad 5.3$$

independent of t, and T. Then Eq. (5.2) can be written as

$$-\frac{d\sigma_{int}}{dt} = F(\sigma_{int}) \exp(-\frac{Q}{RT}) \qquad 5.4$$

Eq. (5.4) can be integrated with respect to time to give,

$$-\int_{int_{(o)}}^{int_{(t)}} \frac{\sigma_{int}}{F(\sigma_{int})} = \exp(-\frac{Q}{RT})\ t = u \qquad 5.5$$

If the times required to reach a given value of σ_{int} during isothermal annealing are measured at different temperatures, the value of u in Eq. (5.5) is a constant. Thus,

$$\log t = \log \text{constant} + \frac{Q}{2.303\ RT} \qquad 5.6$$

From Eq. (5.6) the activation energy, Q, is immediately calculable.

An activation energy for recovery has been determined for the specimens prestrained 10% at 298°K by plotting the temperature dependence of the times required to reach a given fraction of recovery as shown in Fig. 5.14. The values of Q, determined by a least squares analysis, indicate that the activation energy, Q, increases systematically as the fraction of recovery increases in the manner shown in Fig. 5.15. A similar result was found for the recovery of flow stress in zone refined iron (Michalak and Paxton, 1961). This is qualitatively in agreement with the suggestion that there is a linear increase of activation energy with the

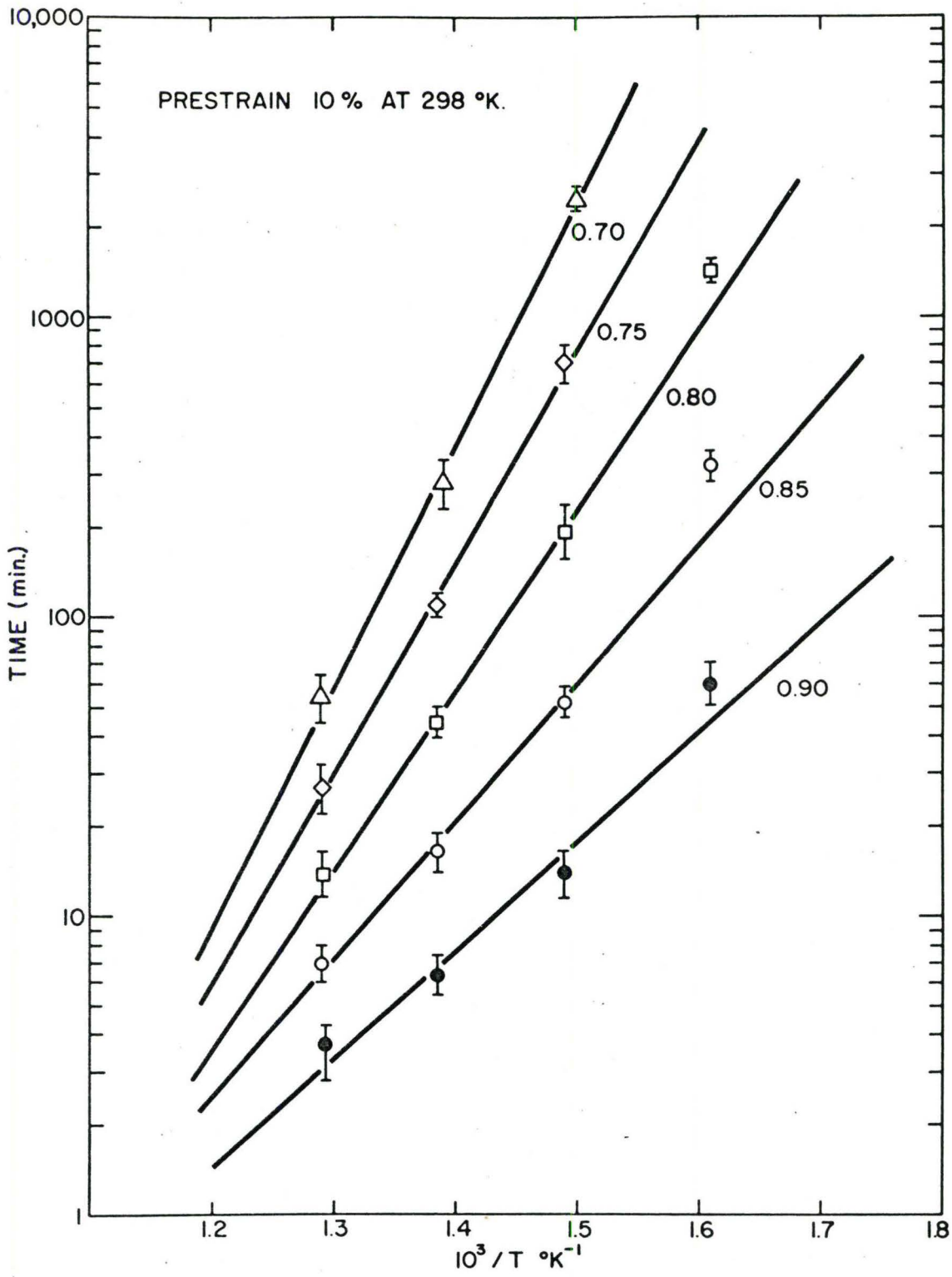

Fig. 5.14 Temperature dependence of the time required for various amounts of recovery.

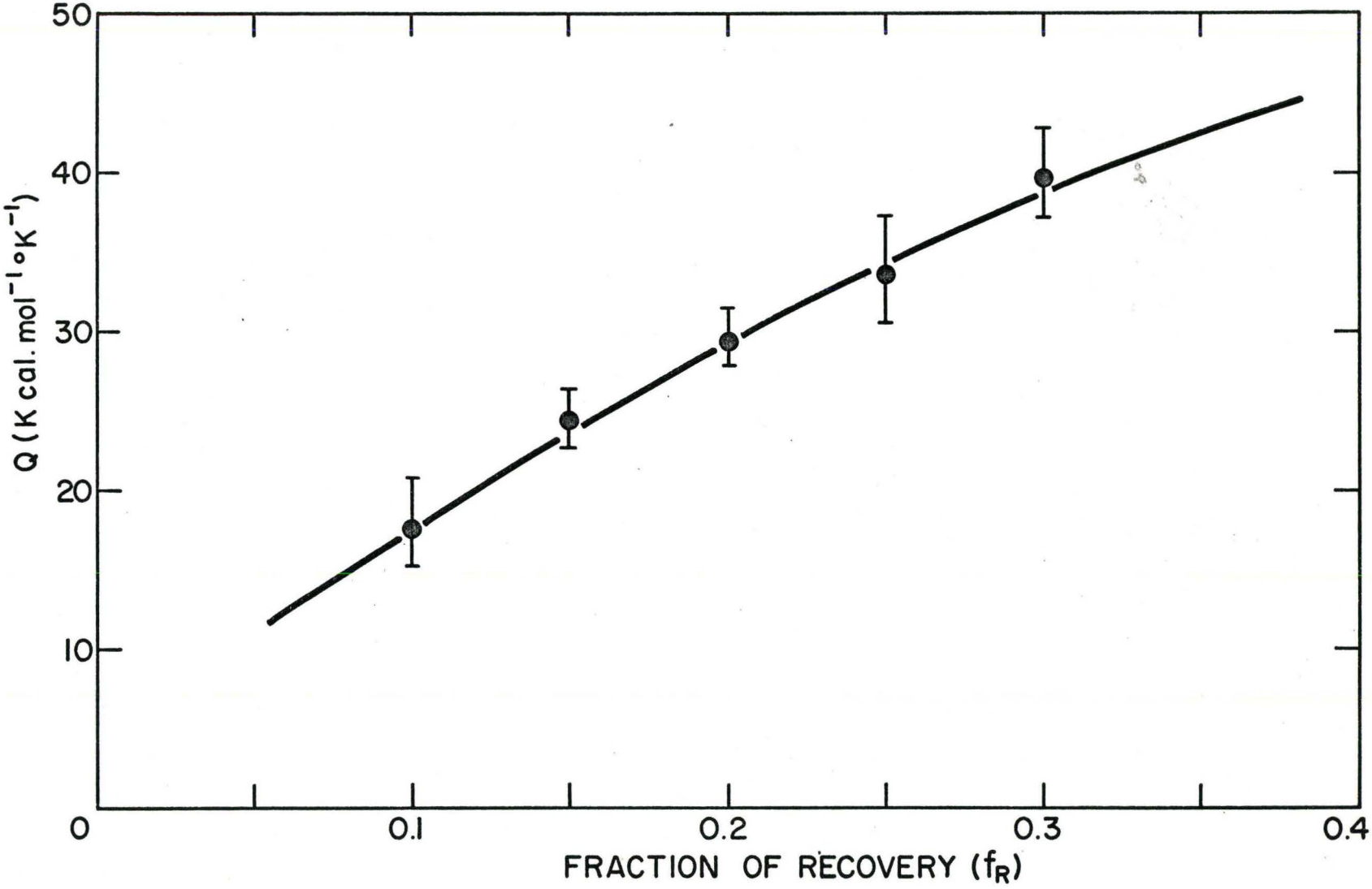

Fig. 5.15 Dependence of activation energy for recovery on the fraction of recovery.

fraction of recovery (Kuhlmann, 1947; Dorn et al, 1949). This is based on the rationale that as recovery progresses the annihilation of dislocations is made increasingly more difficult because of less assistance to the fluctuations of local free energy from the decreasing internal stress, (i.e. recovery occurs most rapidly in regions of highest σ_{int}). It is of interest to note that the activation energy at the start of recovery is not inconsistent with the activation energy for migration of vacancies in iron (18 kcal $^{o}K^{-1}mol^{-1}$, Leslie et al (1961). It is not unreasonable to assume that vacancy migration alone would play a role in the very earliest stages of recovery. An extrapolation to 100% recovery is not really possible on the basis of these results, but they do suggest that the activation energy is approaching that for self diffusion in iron (67 kcal $^{o}K^{-1}$ mol^{-1}). This too is reasonable in that the last stage of recovery would involve dislocation climb and would rely upon the formation and migration of vacancies.

The analysis presented here is purely phenomenological. It allows a determination of the activation energy, Q, without any but the most general assumptions concerning the recovery process. Within the limits of experimental error it has been shown that at any fixed fraction of recovery, the slope of the log t vs. 1/T plot is linear just as in the simple case of constant activation energy, but manifests itself in a systematic change of slope with the fraction of recovery at which Q is being determined. Before the mechanism of the recovery process can be fully elucidated, the exact relation between the unspecified function $F(\sigma_{(int)})$ in Eq. (5.4) and the dislocation density, ρ, must be determined independently. By a purely phenomenological analysis, only the activation energy can be calculated.

The aim of this chapter was to examine the relationship between the work hardened state of a crystal and its subsequent recovery behavior. By examining the recovery of internal stress a fair qualitative description

of the state of imperfections causing work hardening has been made. The role of σ_{eff} in producing a uniform distribution of dislocations at low temperatures is consistent with the recovery behavior observed.

CHAPTER VI

DISCUSSION OF RESULTS

6.1 Introduction

In this research a variety of experimental techniques have been employed to investigate the effect of grain size on the plastic deformation of metal polycrystals. Measurement of the magnitudes of the components of the flow stress have been achieved through the use of stress relaxation tests. These measurements have proved very useful in evaluating the effect of grain size on both the effective stress and the internal stress. Recovery tests have also proven very valuable in investigating the work hardened state in iron. In relating the structure of the material to the mechanical state, X-ray micro-beam and transmission electron microscopy have been employed. Before going on to a discussion of the experimental results it is worth noting the following,

(a) The effective stress in decarburized iron remains constant with strain and is independent of grain size at both 298°K and 195°K.

(b) The effective stress can vary with strain in 70/30 alpha brass in a manner dependent on the grain size.

(c) The effective stress varies with strain in copper and this variation is almost independent of grain size.

(d) The internal stress or athermal component dominates the work hardening behavior in all the materials tested. In iron at 195°K the entire increase in flow stress with decrease in temperature is due to the increase in effective stress.

(e) A grain size dependent contribution to internal stress determines the work hardening behavior in 70/30 alpha-brass and to a lesser degree in iron at 298°K. Additional evidence in support of this conclusion is

offered by the observation of X-ray asterism.

(f) The Hall-Petch slope k_f increases with strain in 70/30 alpha brass and in iron at 298°K. Any model used to describe the flow stress-grain size relation must be able to predict quantitatively the variation of k_f with strain.

(g) Work hardening in copper is independent of grain size. The major contribution to the internal stress comes from $\sigma_{stat.}$. The work hardening behavior of iron at 195°K also shows no dependence on grain size.

(h) The thermal recovery of internal stress in iron is very dependent on the distribution of dislocations in the work hardened state. The rate of recovery and fraction of recovery are much larger in iron deformed at 195°K compared to iron deformed at 298°K.

It is apparent from the above experimental results that grain size exerts a strong influence on the work hardening behavior of certain polycrystalline metals. This dependence is strongly influenced by the inherent properties of the metal and the temperature of deformation. A model used to rationalize these results must certainly consider how these factors determine the rate of accumulation of dislocations in metal polycrystals. These factors are important in determining the distribution of dislocations and the subsequent stability of the work hardened structure.

6.2 Effect of Grain Size on Internal Stress

Present experimental results suggest that the grain size dependence of the internal stress is due to differences in work hardening behavior rather than dislocation pile-ups as envisaged by Armstrong et al. (1962). Their hypothesis is that grain boundary strengthening arises from the critical stress needed to produce new slip bands from the ends of old ones at the grain boundaries. On the basis of this model it is difficult to

explain the changes in k_f with strain observed in the experiments. In their model k_f is written as,

$$k_f = \bar{m}^2 \tau_d r^{1/2} \qquad 6.1$$

where $\bar{m}$ is an orientation factor, τ_d is the stress required to activate new dislocation sources and r is the distance between the end of the pile-up and the sources of dislocations in neighboring grains. It is difficult to understand why k_f should increase with strain in 70/30 alpha brass and iron when it appears unlikely that τ_d should be greatly affected by plastic strain, and r most likely will decrease.

If on the other hand the effect of grain size on internal stress is explained in terms of a work hardening model, the problem arises concerning the mechanism of production of higher dislocation densities in fine-grained materials. In the work hardening models discussed in section 2.1.3 (c) it is assumed that the average distance a dislocation moves is proportional to the grain size. From this assumption the relation between dislocation density and grain size is derived. But the physical reasons for assuming that the slip distance be proportional to the grain size are not made clear in this model.

The calculation of the number of dislocations stored during deformation is not an easy problem. Consider for example a single crystal which deforms by simple shear. The overall geometry of the deformation does not require any of these dislocations to remain in the crystal. In spite of this, dislocations do remain in the crystal as a result of chance encounters and there is no simple way to predict the density of these dislocations.

The tensile deformation of a polycrystal is even more complex since it deforms plastically in a non-uniform way. One of the reasons for this non-uniform deformation is the requirement that contiguity of the

grains must be maintained during plastic flow. In regions on either side of the grain boundaries lattice planes will be bent and twisted setting up gradients of plastic strain in the specimen. Thus in the tensile deformation of a polycrystal, dislocations will be accumulated in two ways. First, dislocations will be stored in the grains as a result of mutual random trapping. This has been termed the statistical storage of dislocations and their density is identified as $\rho_{stat.}$ (Ashby, 1970). The dislocation density $\rho_{stat.}$ and the state of work hardening within each grain must be the same as a single crystal so oriented that it deforms on the same slip system or slip systems as the grain under consideration. This type of work hardening behavior can be explained reasonably by the averaging model of Taylor (1938) and more recently Kocks (1970). Superimposed on the statistical storage is the storage of geometrically necessary dislocations, (ρ_{geom}), needed to accommodate the non-uniform lattice deformation. In section 2.1.3 (d) it was shown that the minimum density of dislocations necessary to produce any arbitrary non-uniform lattice deformation can be calculated. This theory forms the basis of a model proposed by Ashby (1970) to account for the way in which the work hardening behavior is influenced by the scale of the microstructure (hard particles in two-phase alloys, grain size in polycrystals). A comparison of this theory with experiment is described below.

6.2.1 Dislocation Storage Model for the Internal Stress-Grain Size Relation

The existence of a grain size dependent internal stress, in addition to that due to statistical storage of dislocations during plastic flow, implies that the process of dislocation accumulation is dependent on the scale of the microstructure, i.e. the grain size. Let us consider a simple model in which the boundaries are considered as obstacles to the spread of plastic flow. Dislocations are assumed to spread across

the grains without hinderance and impinge on the boundaries. For these conditions the model proposed by Ashby (1970) to describe the non-homogeneous deformation of two-phase materials containing rigid inclusions can be used to relate the density of stored dislocations to the scale of the microstructure.

If each grain in a polycrystal deformed independently of its neighbours, voids and overlap would occur in the region of the boundaries. As a result of maintaining contiguity of the grains, deformation gradients will form when the polycrystal is deformed.

In the simplest case consider slip occurring on a single system in each individual grain of the polycrystal strained in uniaxial tension as shown in Fig. 6.1. Consider a section of grain of diameter D and impose a shear of magnitude γ on the slip planes with normal NN' as shown in Fig. 6.2. Due to the restrictions imposed by neighbouring grains this shear cannot propagate freely from one grain to the next. Hence the central part of each slip plane shears by an amount γ, but the ends of the slip planes are bonded to the neighbouring grain and are prevented from shearing. Therefore the shear in an element of grain immediately adjacent to the grain boundary is zero. It follows then that the material immediately adjacent to the grain boundary is rotated through an angle $\phi = \tan^{-1}\gamma$ relative to the original slip plane normal NN', and that the slip planes themselves are bent from ϕ through zero to ϕ again as shown in Fig. 6.2. The grain acquires a curvature whose mean magnitude is $2\phi/D$. The rapid development of asterism in fine-grained brass polycrystals indicates that deformation gradients are present. The additional density of dislocations, ρ_{geom}, required to accommodate this lattice rotation can be calculated as follows.

Construct a Burgers' circuit BB'NN' in the grain as shown in Fig. 6.3. This Burgers' circuit which would close in an undeformed grain, fails to close in the deformed one. The closure failure is ϕ L, and the

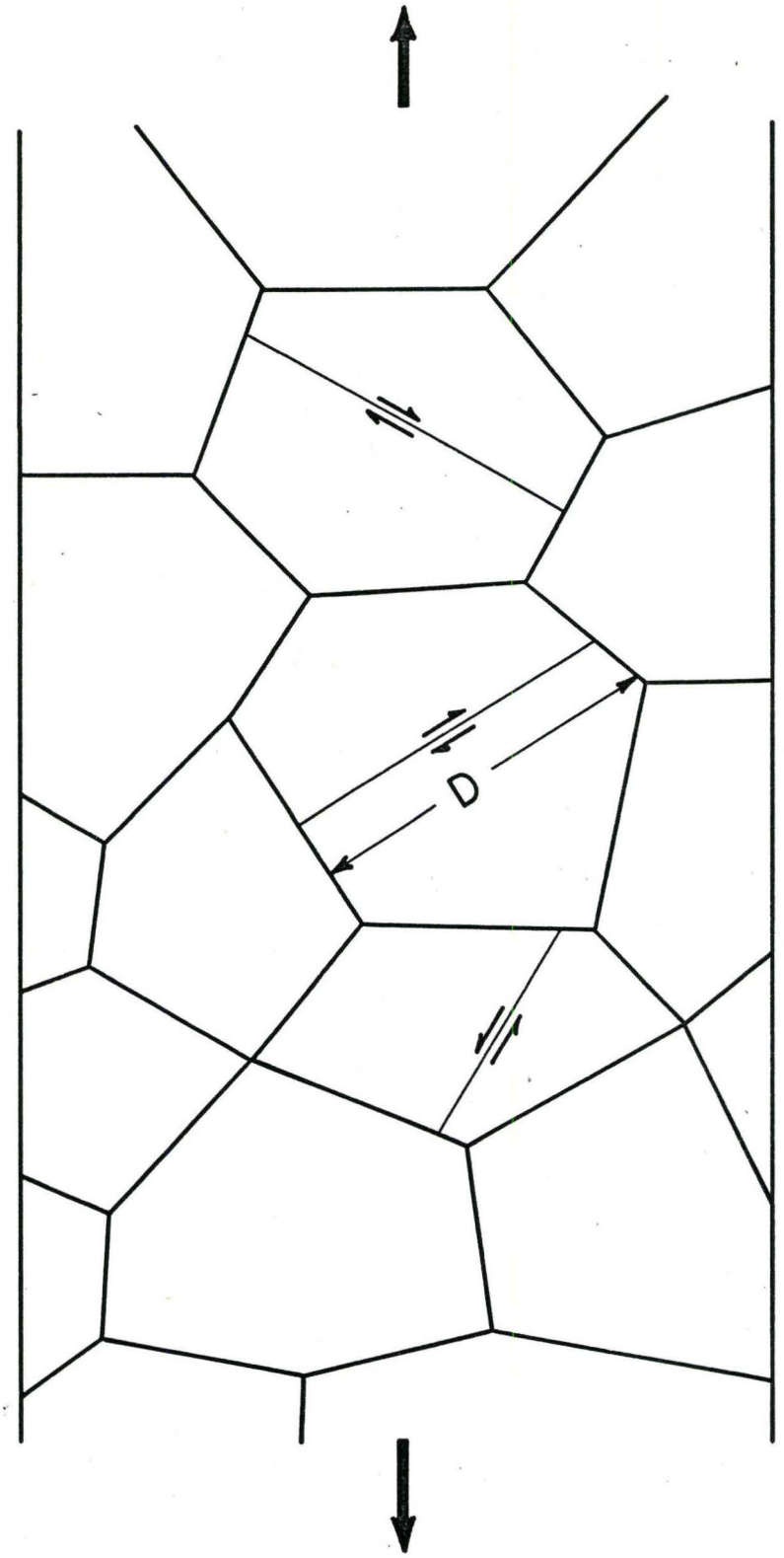

Fig. 6.1 Schematic diagram of a polycrystal strained in uniaxial tension.

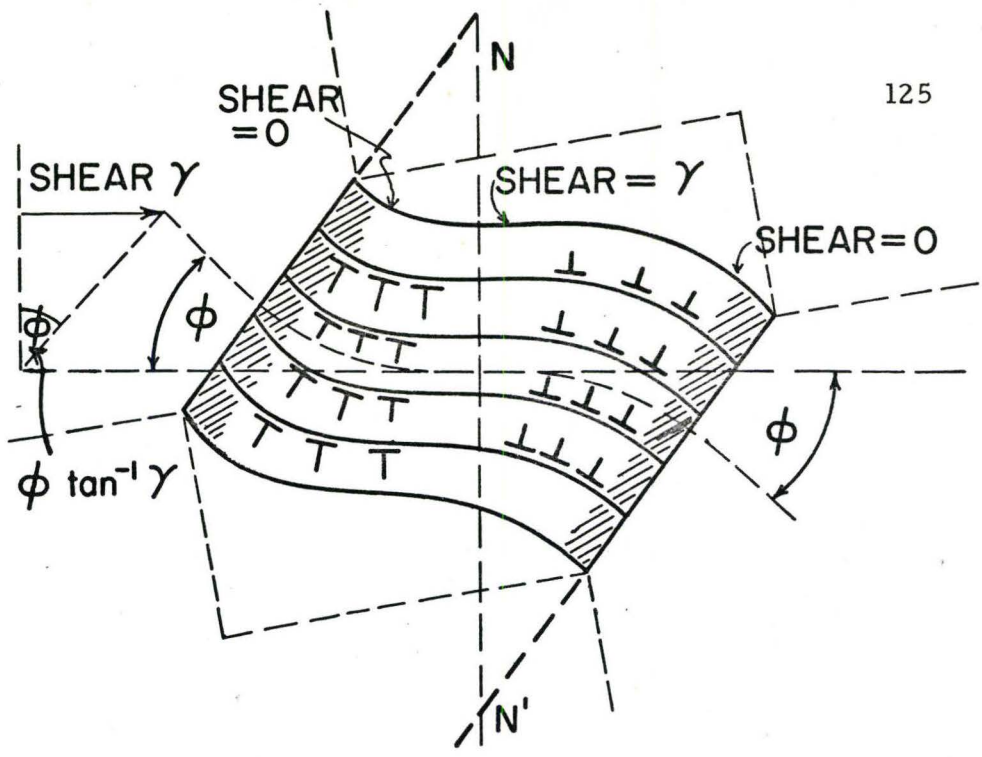

Fig. 6.2 Schematic diagram showing lattice rotation in a deformed grain.

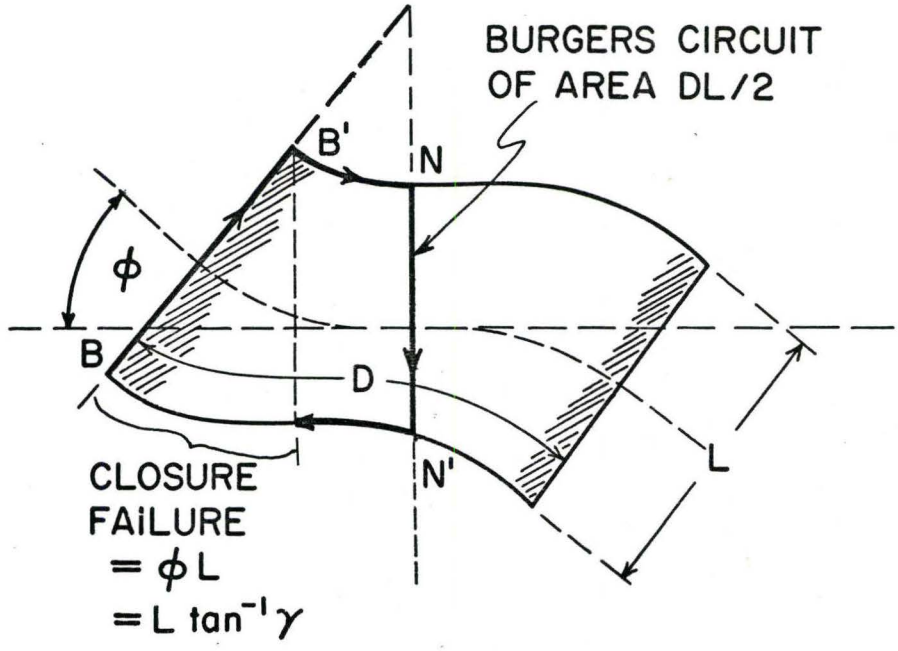

Fig. 6.3 Burgers circuit construction used to calculate ρ_{geom}.

circuit encloses a number of dislocations of Burgers' vector b equal to $\phi L/b$. Since this Burgers' circuit has an area equal to one-half the area DL of that part of the grain shown in Fig. 6.3, the volume average dislocation density in that part of the grain enclosed by the circuit is therefore

$$\rho_{geom} = \frac{2}{DL} \cdot \frac{\phi L}{b} \qquad 6.2$$

The angle ϕ can be replaced by γ to within 5% error even at strains as high as 0.4, giving,

$$\rho_{geom} = \frac{2\gamma}{Db} \qquad 6.3$$

Here D, is the grain size, γ, the engineering shear, and b, the Burgers' vector.

Of course, the grains in a real polycrystal are bounded on all sides and the grain will acquire additional components of curvature. The problem of calculating the density of geometrically necessary dislocations is best handled by the tensor methods suggested by Nye (1953), since the closure failure of a Burgers' circuit now depends on the details of the lattice curvature. However, the important results of the model can still be demonstrated by the simple Burgers' construction shown in Fig. 6.3.

The value of ρ_{geom} given in Eq. 6.3 measures the dislocation density over and above that found in an equivalent single crystal, and thus in this simple model is the origin of the grain-size dependent part of the work hardening in polycrystals. In a deformed polycrystal the total dislocation density is the sum of the geometrically necessary dislocations ($\rho_{geom.}$) and the statistically-stored dislocations ($\rho_{stat.}$). For a first approximation assume that the two dislocation storing mechanisms do not interact, then qualitatively the internal stress, ρ_{int}, which depends on

dislocation density will reflect the presence of the geometrically necessary dislocations when their density $\rho_{geom.}$ dominates the total density ρ_{total}.

The relation between internal stress and dislocation density is a familiar one. All estimates of the stress required to move a dislocation through a region having a density of dislocations ρ_{total} are of the form,

$$\tau_{int} = a\mu b\sqrt{\rho_{total}} \qquad 6.4$$

where μ is the shear modulus, b the Burgers' vector and a is a dimensionless constant whose magnitude can vary between 0.15 and 0.4 depending on the detailed calculation of the interaction between dislocations. The actual mechanism which determines the magnitude of the internal stress will depend not only on the density, but also on the type and arrangement of stored dislocations. However, the general validity of Eq. (6.4) is almost independent of this arrangement as has been shown by general dimensional arguments (Nabarro, Basinski and Holt, 1964).

Thus in order to retain simplicity, it is convenient to describe the array of stored dislocations by its average density only. The total dislocation density, ρ_{total}, is simply $(\rho_{geom} + \rho_{stat})$. Under certain conditions depending primarily on the nature of slip, ρ_{geom} will dominate and the total dislocation density is given by Eq. 6.3. Inserting this value into Eq. 6.4 gives,

$$\frac{\tau_{int}}{\mu} = (0.35 \pm .15)\sqrt{\frac{\gamma b}{D}} \qquad 6.5$$

Thus Eq. (6.5) provides an explanation for the way in which work hardening behavior of a polycrystal is influenced by the grain size.

The model as outlined above neglects the interaction of the two

components of dislocation density and in general this interaction will alter the rate of work hardening. It also assumes that no attrition of the stored dislocations occurs by dynamic recovery during deformation. In the present context we can consider the dynamic recovery process to include both dislocation annihilation during deformation and dislocation interactions which result in a decrease in the internal energy associated with the stored dislocations, such as the formation of a cell structure. With these restrictions in mind, let us consider the application of the above model to the results of the present study. The model predicts that in addition to the grain size dependence of the initial internal stress at yield, an increment of internal stress should develop during work hardening which is also proportional to the inverse square root of the grain size. The grain size dependent portion of the internal stress is obtained by subtracting σ_{stat} from the total internal stress σ_{int}. This term is plotted as a function of the extent of plastic strain in Fig. 6.4 for 70/30 alpha brass at 195°K and in Fig. 6.5 for iron at 298°K. These curves can be converted to shear stress and shear strain by dividing the stress and multiplying the strain by Taylor's average orientation factor $\bar{m} = 3.06$. The results can then be replotted and compared with Eq. 6.5.

The data for 70/30 alpha brass shown in Fig. 6.6 are in good quantitative agreement with the theory for strains up to 15% as determined by a linear regression analysis. The data for iron, shown in Fig. 6.7 also shows an additional increment of internal stress which is proportional to the inverse square root of grain size, but only up to strains of 5%. Also, from the data presented in section 4.4 the model is obviously not applicable to copper at 298°K or to decarburized iron at 195°K. Thus the results indicate that the temperature and mode of slip are important parameters controlling the influence of grain size on the work hardening process.

In order to elucidate the influence of these factors let us consider the basic premise of the model that the slip distance be equivalent to the

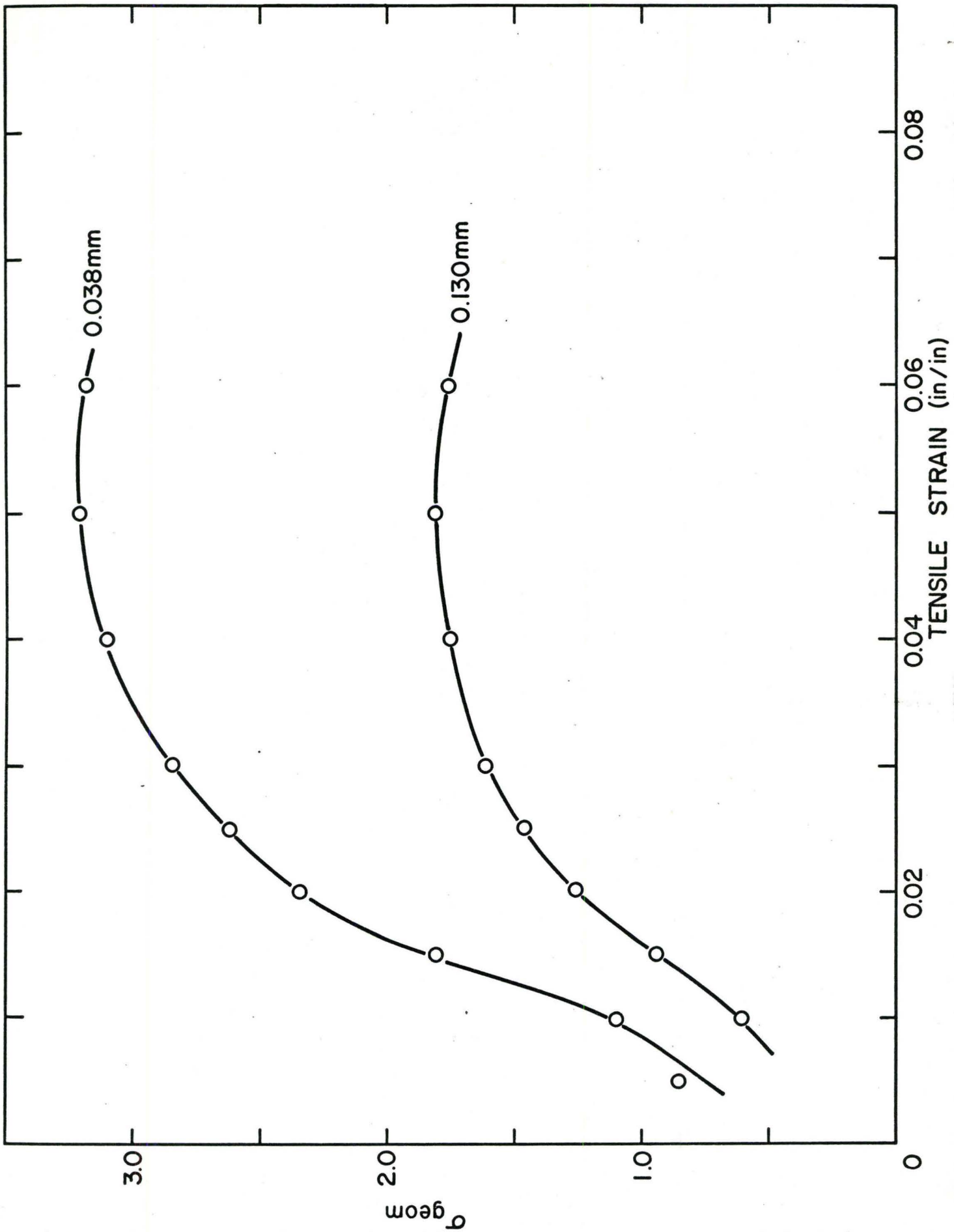

Fig. 6.4 Grain size dependent portion of internal stress as a function of strain for decarburized iron at 298°K.

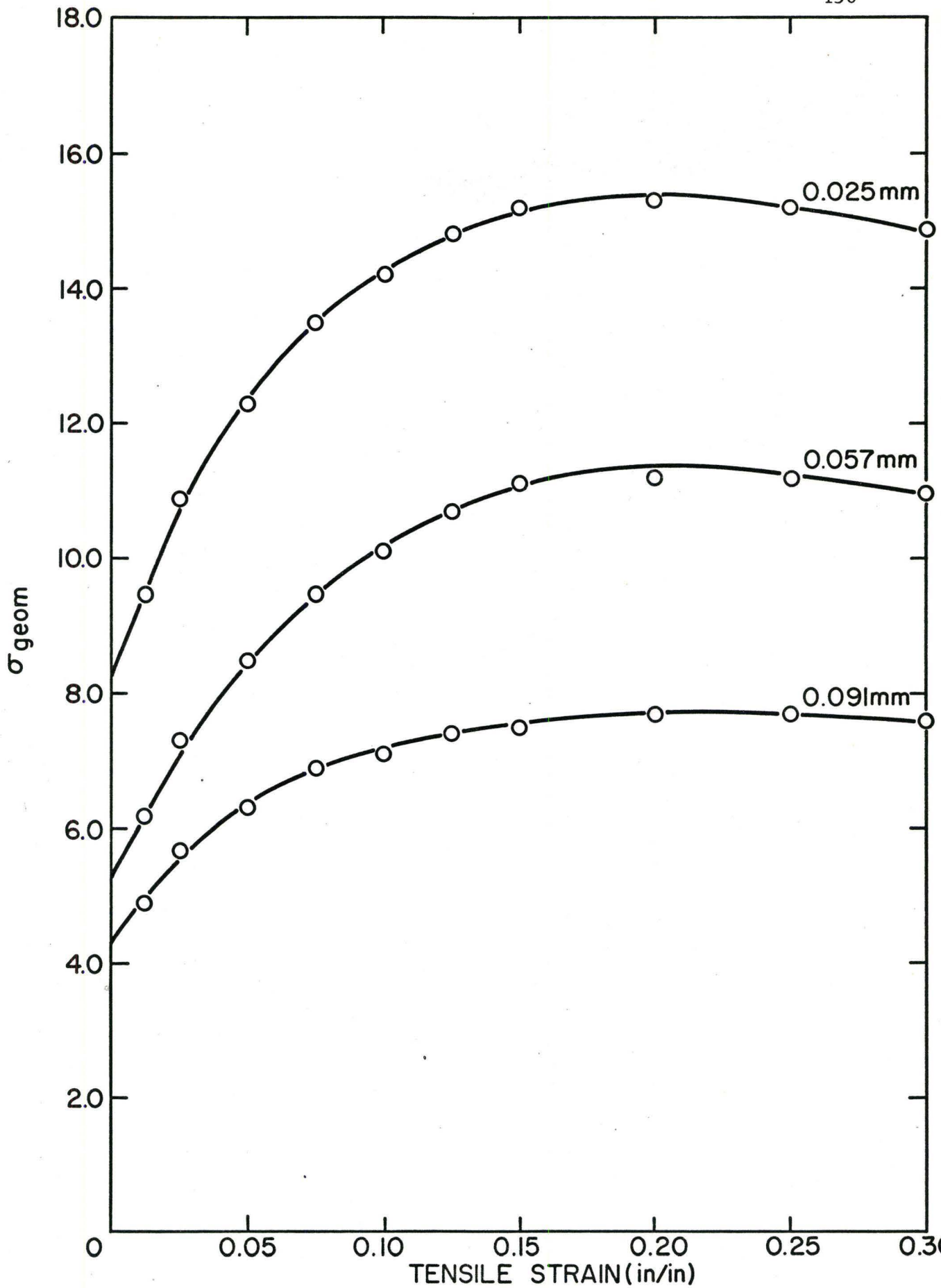

Fig. 6.5 Grain size dependent portion of internal stress as a function of strain for 70/30 alpha brass at 195°K.

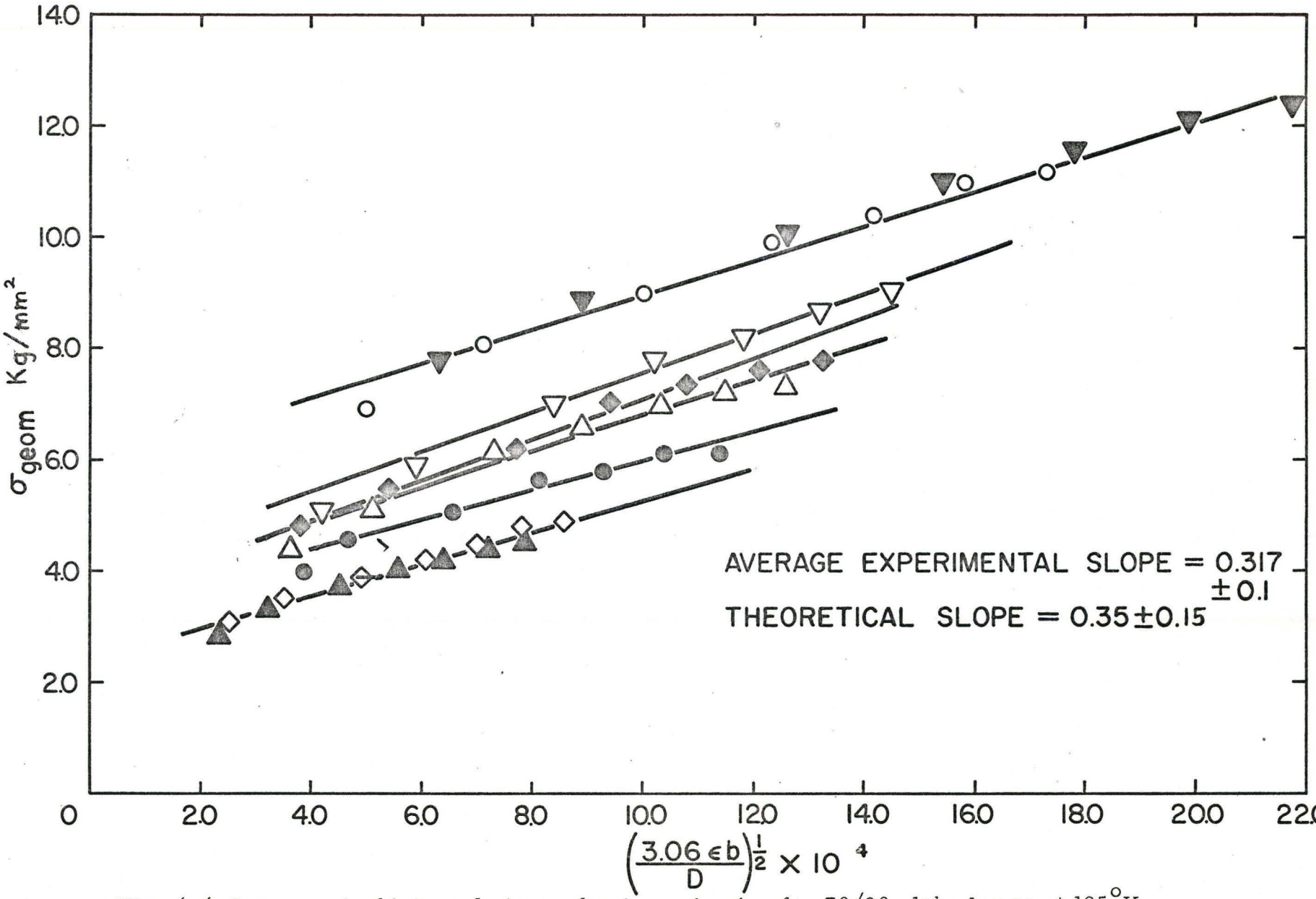

Fig. 6.6 Increment of internal stress due to grain size for 70/30 alpha brass at 195°K.

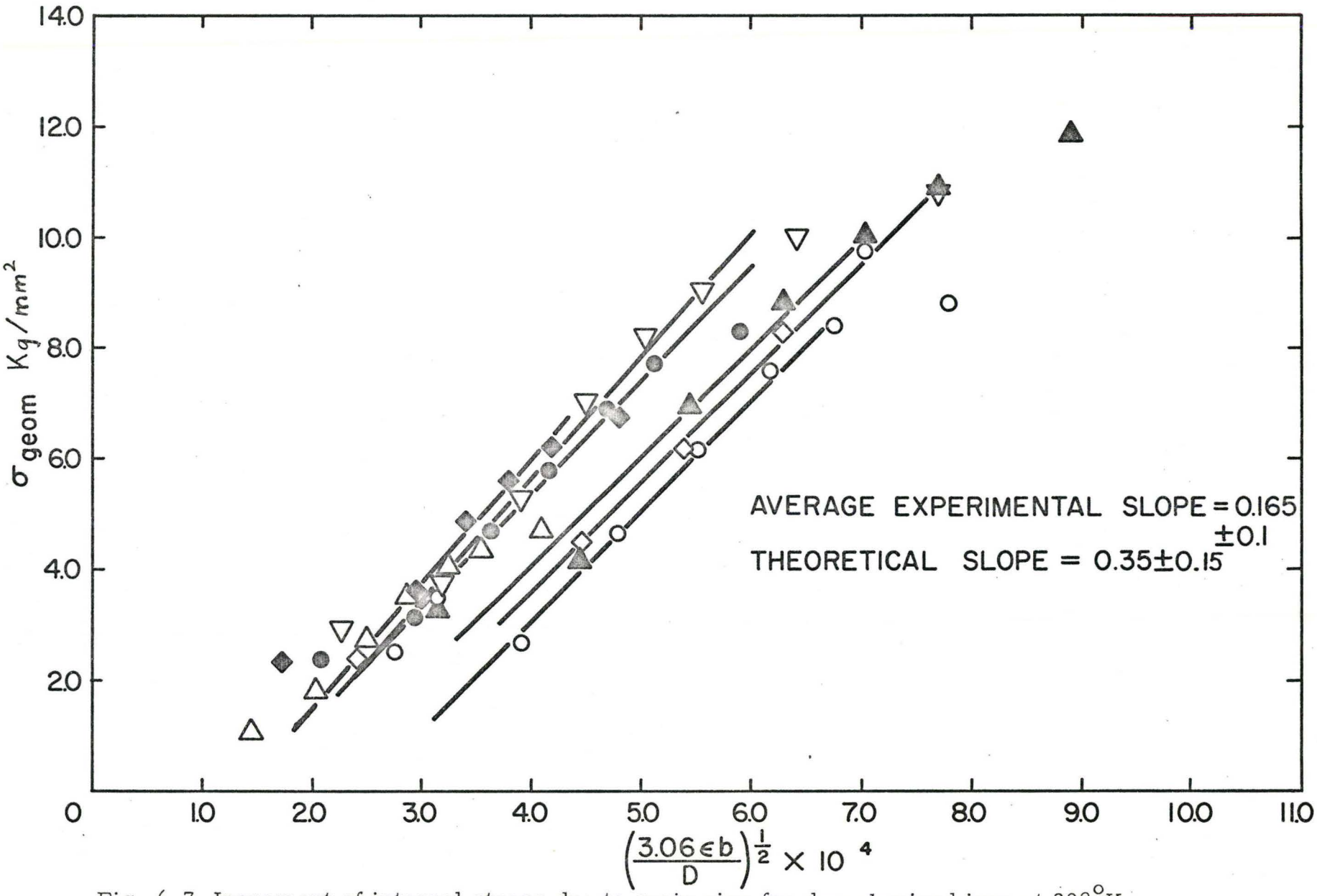

Fig. 6.7 Increment of internal stress due to grain size for decarburized iron at 298°K.

grain diameter. According to Ashby (1970) the effectiveness of particles, or plates, or grain boundaries in causing dislocations to be stored is conveniently described by the geometric slip distance. The geometric slip distance (λ_{geom}) is analogous to the quantity (λ_{stat}), the slip distance for statistical storage. (λ_{stat} is often regarded as the diameter, in a pure crystal, to which a dislocation ring, generated by a source, expands before it stops permanently). The geometric slip distance, λ_{geom}, is a characteristic of the microstructure and is independent of strain. For the purpose of this discussion, λ_{geom} is set equal to the grain size. λ_{stat}, on the other hand, does vary with strain and can be measured from the length of slip lines (λ_{geom} cannot). We can expect little effect of the grain size on the work hardening behavior of polycrystals when the grain size imposes a geometric slip distance which is larger than λ_{stat}. But when λ_{geom} is much less than λ_{stat} we can expect the grain size to have a strong effect on dislocation storage, and thus on work hardening.

The work of Kuhlmann-Wilsdorf and Wilsdorf (1953) has definitely shown that λ_{stat} in brass is equivalent to the grain size. They investigated the surface structure of deformed 70/30 alpha brass, aluminum, copper and silver by a replica technique in the electron microscope. They observed that in brass the slip lines on the average were widely spaced and that very few slip bands were formed. From their measurements they concluded that the grain size limited the amount of slip and that the average depth of slip lines agreed with this upper limit for the extent of slip. In addition it is well known that the low stacking fault energy in 70/30 alpha brass results in a planar slip mode. Planar slip inhibits the tendency for tangling and cell formation and in general very little interaction between dislocations on neighbouring slip planes occurs. Thus the basic premise of the model is fulfilled and the grain boundaries exert an important influence on the accumulation of dislocations during deformation in

70/30 alpha brass. The influence of the grain boundaries will decrease at larger strains due to the formation of tangles and eventually a cell structure (Swann, 1963). The tangles and cell walls block dislocation movement within the grains and reduce the slip line length to some fraction of the grain diameter. Thus at large strains σ_{stat} will dominate the work hardening behavior. The formation of tangles and cells is consistent with the view that at large strains dynamic recovery occurs simultaneously with the work hardening process and lowers the apparent rate of work hardening.

In direct contrast to 70/30 alpha brass, the surface structure of deformed polycrystalline copper reveals the formation of numerous slip bands and an elementary structure (Khulmann-Wilsdorf and Wilsdorf, 1953). The elementary structure consists of fine slip lines covering the whole surface between the slip bands. The formation of slip bands is due to the strong interaction between dislocations of neighbouring slip planes by cross slip multiplication, (Koehler, 1952; Li, 1963). In addition evidence obtained by electron microscopy shows the early formation of tangles and cells in deformed copper (Swann, 1963). Hence after small amounts of plastic strain the grain size dependence of the work hardening disappears because the important obstacles to slip are those created by dislocation interactions within the grains. Published results estimate that slip line lengths in pure copper single crystals strained into stage III to be about 10μ (Mader 1963) (much less than the grain size used in this work). In materials which exhibit cell formation at small strains the accumulation of dislocations by statistical storage will dominate and no grain size dependent work hardening is expected.

In decarburized iron at room temperature the initial slip lines extend across the grains. Thus for small strains ($<$ 5% in this study) the grain boundaries present the major obstacles to slip and it follows that we would expect a strong influence of grain size on the accumulation

of dislocations. However, in iron, slip can occur readily on a multiplicity of slip systems, resulting in the formation of tangles and eventually a cell structure. It is expected then that for strains greater than 5%, hardening due to dislocation interactions within the grains dominates.

In chapter 5 it was shown that at low temperatures, obstacles within the grains, either in the form of a Peierls stress or impurity atoms dominate the dislocation accumulation process. At 195°K the distribution of dislocations becomes more uniform due to the increase in magnitude of the stress needed to overcome lattice obstacles. In addition slip lines observed after low temperature deformation in iron tend to be much finer and closely spaced indicating that obstacles within the grains are governing the slip process. (Keh and Weissmann, 1963; Rosenfield and Hahn, 1970). Hence grain size is not expected to influence the work hardening rate in iron deformed at low temperatures as was observed. It should also be emphasized that the type of grain size dependent work hardening discussed in Ashby's model will be obscured by an extensive Luders strain. The Luders strain at 195°K in iron went from 1.0% in the coarse-grained specimens to 1.5% in the finest-grained specimen. This is compared to only 0.2% Luders strain at 298°K.

The results can be used to formulate a general strain dependence of the Hall-Petch equation. From Eq. (6.5) the effect of strain on the Hall-Petch slope can be expressed as

$$k_\varepsilon = \alpha\mu\,(3.06\,\varepsilon b)^{1/2} \qquad 6.6$$

where $3.06\,\varepsilon = \gamma$ and 3.06 is Taylor's average orientation factor. The data from Fig. 4.14 can then be replotted according to Eq. (6.6) as shown in Fig. 6.8 for 70/30 alpha brass and iron at room temperature. It can be seen from this plot that Hall-Petch slope increases parabolically with strain until some value where the obstacles within the grains become

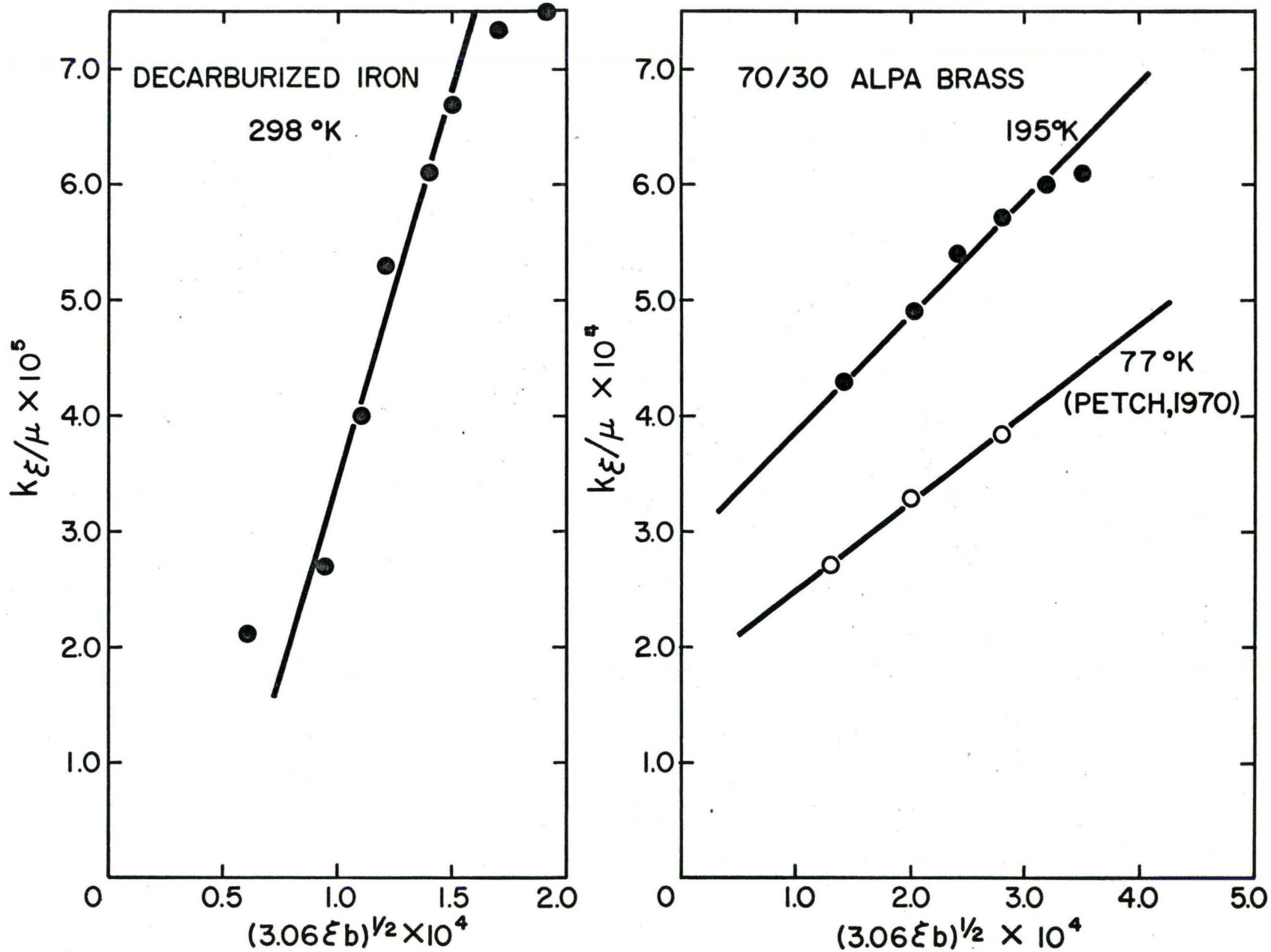

Fig. 6.8 Variation of Hall-Petch slope with strain.

dominant. This is supported by the results of Petch (1969) on Cu-Zn solid solutions which indicate that as the stacking fault energy and testing temperature of the material is lowered the Hall-Petch slope increases with plastic strain. His result for 70/30 alpha brass tested at 77°K is also shown in Fig. 6.8. The data of Fisher and Marcinkowski (1965) for Fe-Co shows that on ordering, the more planar character of slip results in a marked increase of the Hall-Petch slope with plastic strain compared with that in the disordered condition. However, Fisher and Marcinkowski did not observe a linear relation between the Hall-Petch slope and the square root of strain as required by Eq. (6.6). In hexagonal materials such as zinc (Armstrong et al; 1962), the Hall-Petch slope also increases with strain as expected from the model.

An interesting feature of the results is the marked variation with temperature exhibited by k_y (Hall-Petch slope at yield) in iron. Cottrell (1963) has suggested that under certain conditions iron will show a temperature dependent k_y. The conditions being that unpinning of dislocations from carbon atoms is easier than creation of fresh dislocations at yield. The annealing history of this iron excludes any possibility that yielding occurs by the unpinning of dislocations from carbon atoms. However, it might be possible to resolve the problem of a temperature dependent k_y in iron by comparing the extent of the Luder's strain at the two temperatures. The Luder's strain at 195°K is about 5 times as large as the Luder's strain at 298°K. (1.0% ε compared .2% ε). On the basis of the "dislocation storage model", this represents an additional internal stress which is developed during the Luder's strain at 195°K. This would make a difference in the determination of k_y at the end of the Luder's strain. It is not possible to calulate this magnitude from the experimental results because the rate of work hardening during the discontinuous yield is unknown. The above suggestion receives some support from the recent findings of Bailon and Dorlot (1970) who reported

a change in the Hall-Petch slope with the onset of Luder's strain in Armco iron.

6.3 Summary and Conclusions

The objective of this thesis was to examine, with the aid of a variety of experimental techniques the factors which determine the work hardening behavior of metal polycrystals and the subsequent stability of the work hardened structure. Using stress relaxation tests, the magnitudes of the components of the flow stress, namely σ_{eff} and σ_{int}, have been measured as a function of strain for various metal polycrystals with different grain sizes.

As in Ashby's model (1970) the total density of dislocations stored in a deformed polycrystal was divided into two parts. The extra density of dislocations which allow the grains of a polycrystal to deform in a compatible way were called "geometrically necessary dislocations" to distinguish them from the "statistically stored dislocations" which accumulate by random mutual trapping within each grain.

It was found that for certain polycrystalline metals, the density of geometrically-necessary dislocations exceeds that of the statistically-stored ones during deformation. When this happens the work hardening behavior is grain size dependent. In order for a material to show a grain size dependent work hardening it must satisfy the requirement that the major obstacles to slip are the grain boundaries. This was demonstrated in the case of 70/30 alpha brass and iron at room temperature. However, when local obstacles within the grains limit the amount of slip the density of statistically stored dislocations dominates and no grain size dependent work hardening is observed. (e.g. copper and iron at 195^{o}K.)

On the basis of Ashby's model it was shown that for materials which show grain size dependent work hardening behavior the Hall-Petch slope depends on strain in a predictable way.

The application of this model has led to a better understanding of the effect of temperature on work hardening behavior in iron. The disappearance of grain size dependent work hardening at low temperatures in iron has been attributed to an increase in the effectiveness of local obstacles within the grains (either in the form of a Peierls stress or impurity atoms) to control the accumulation of dislocations. The dislocations accumulated during low temperature deformation are distributed more uniformly and with fewer tangles. This type of distribution leads to an increased instability of the work hardened structure when subjected to a recovery anneal at elevated temperatures.

APPENDIX A

STRESS RELAXATION IN THE INSTRON

An Instron tensile testing machine is essentially a hard machine, i.e. the deformation of the machine itself is small, and it imposes a nearly constant strain rate on the specimen. One end of the specimen is maintained in a fixed position and constant strain rate is achieved by pulling the other end at a constant speed.

The purpose of this appendix is to investigate the characteristics of the testing machine and explain how it affects stress relaxation. In an Instron the crosshead moves at the speed V under zero load. When a specimen is in the machine, as shown in Fig. A-1, the crosshead moves a distance $L-L_o$ in the time dt, and the load increases by an amount dP. If we represent the machine stiffness by a spring constant k_m, then

$$L - L_o = Vdt - \frac{dP}{k_m} \qquad \text{A-1}$$

where $\frac{dP}{k_m} = \Delta_m$ is the machine extension. This distance is taken up by the extension of the specimen, load cell and couplings as

$$L - L_o = \Delta_s + \frac{dP}{k_\ell} + \frac{dP}{k_c} \qquad \text{A-2}$$

where Δ_s is the extension of the specimen, $\frac{dP}{k_\ell} = \Delta_\ell$ and $\frac{dP}{k_c} = \Delta_c$ are the extensions of the load cell and couplings respectively. The extension in the specimen is composed of an elastic plus a plastic extension and by equating Eq. (A-1) and Eq. (A-2) we obtain,

$$Vdt = \Delta_{s_p} + \frac{dP}{k_s} + \frac{dP}{k_\ell} + \frac{dP}{k_c} + \frac{dP}{k_m} \qquad \text{A-3}$$

where Δ_{s_p} is the plastic part of the specimen extension and $\frac{dP}{k_s} = \Delta_{s_e}$ is the elastic part. The stiffness constants can be combined as

$$\frac{1}{k_t} = \frac{1}{k_s} + \frac{1}{k_\ell} + \frac{1}{k_c} + \frac{1}{k_m}$$

and Eq. (A-3) can be written as

$$Vdt = \Delta s_p + \frac{dP}{k_t} \qquad \text{A-4}$$

Dividing Eq. (A-4) through by dt gives

$$V = \frac{\Delta_{s_p}}{dt} + \frac{1}{k_t} \frac{dP}{dt} \qquad \text{A-5}$$

When the crosshead is stopped, V = 0 so that now,

$$\frac{\Delta_{s_p}}{dt} = - \frac{1}{k_t} \frac{dP}{dt} \qquad \text{A-6}$$

Equation (A-6) is a phenomenological equation describing stress (load) relaxation in the Instron. During stress relaxation the specimen undergoes a permanent plastic extension at the expense of elastic displacements, thereby decreasing the total elastic energy of the system.

Eq. (A-6) may be rewritten in terms of strain rates and stress rates giving,

$$\dot{\varepsilon}_p = - \frac{1}{K} \dot{\sigma} \qquad \text{A-7}$$

where $\frac{1}{K} = \frac{A_o}{k_t L_o}$, A_o and L_o being the nominal cross-sectional area and gauge length of the specimen respectively. In most treatments of stress relaxation K is usually regarded as the combined modulus of specimen and machine.

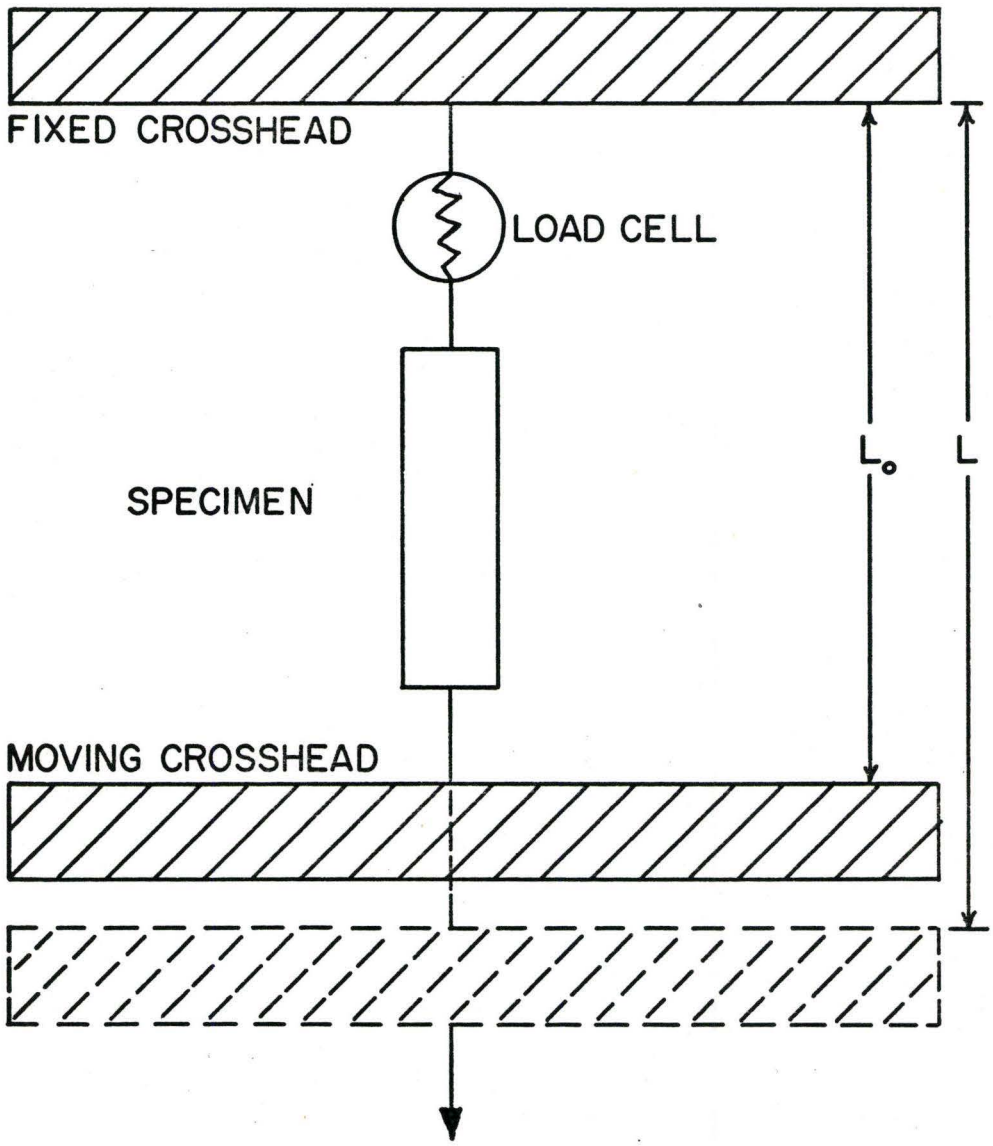

Fig. A-I Schematic of tensile testing machine.

REFERENCES

Armstrong, R., Codd, I., Douthwaite, R.M., and Petch, N.J., 1962, Phil. Mag., 7, 45.

Ashby, M.F., 1970, Phil. Mag., 21, 399.

Bailon, J.P. and Dorlot, J.M., 1970, Paper intended for publication in Acta Met.

Balasubramanian, N., Gensamer, M., and Li, J.C.M., 1969, Thermally Activated Deformation in Alpha-Brass, Paper presented at T.M.S. Fall Meeting, October 1969.

Barrett, C.S. and Massalski, T.B., 1966, Structure of Metals, (McGraw-Hill, N.Y.).

Beck, P.A., 1954, Adv. Phys., 3, 245.

Bilby, B.A., Gardner, L.R.T., and Smith, E., 1958, Acta Met. 6, 29.

Bishop, J.F.W. and Hill, R., 1951, Phil. Mag., 42, 414; 1951, Phil. Mag., 42, 1298.

Boas, W. and Hargreaves, M.E., 1948, Proc. Roy. Soc., A193, 89.

Carreker, R.P. and Hibbard, W.R., 1953, 1, 654.

Carreker, R.P., 1957, Trans. Metall. Soc. AIME, 209, 112.

Carrington, W., Hale, K.F., and McLean, D., 1960, Proc. Roy. Soc., A259, 203.

Conrad, H., 1963(a), Electron Microscopy and Strength of Crystals, edited by G. Thomas and J. Washburn (New York, Interscience), p.299; 1963 (b), Acta Met., 11, 75.

Conrad, H., 1965, High Strength Materials, (Wiley-New York), p.436.

Conrad, H., Feuerstein, S., and Rice, L., 1967, Mater. Sci. Eng. 2, 157.

Conrad, H., Feuerstein, S. and Rice, L., 1968, Suppl. Trans. Japan Inst. Metals, 9, 481.

Cottrell, A.H., 1953, Dislocations and Plastic Flow in Crystals, (Oxford at the Clarendon Press).

Cottrell, A.H., 1963, Symp. Relation between Structure and Strength in Metals and Alloys, HMSO, p.455.

Cottrell, A.H., 1964, The Mechanical Properties of Matter (New York: Wiley) p.277.

Crussard, C., 1963(a), N.P.L. Symp., Relation Structure and Strength Metals and Alloys, HMSO, 548; 1963(b) J. Austr. Inst., 8, 317.

Dorn, J.E., Cherian, T.V., and Pietrokowsky, P., 1949, Trans. AIME 185, 948.

Eshelby, J.E., Frank, F.C., and Nabarro, F.R.N., 1951, Phil. Mag., 42, 351.

Feltham, P., 1961, J. Inst. Met., 89, 210.

Gibbs, G.B., 1966, Phil. Mag., 13, 317.

Guiu, F., 1969, Scripta Met., 3, 753.

Gupta, I and Li, J.C.M., 1970, Paper Intended for Publication in Met. Trans.

Hall, E.O., 1951, Proc. Phys. Soc., London, B64, 747.

Johnston, W.G. and Gilman, J.J., 1959, J. Appl. Phys., 30, 129.

Karnop, R. and Sachs, G., 1927, Z. Phys., 41, 161.

Keeler, J.H., 1955, Trans. A.S.M., 47, 157.

Keh, A.S., 1962, Direct Observation of Imperfections in Crystals, (Interscience- New York), p.213.

Keh, A.S., and Weissmann, S., 1963, Electron Microscopy and Strength of Crystals, edited by G. Thomas and J. Washburn (New York: Interscience), p.231.

Keh, A.S. and Nakada, Y., 1967, Can. J. Phys., 45, 1101.

Kochs, U.F., 1958, Acta Met., 6, 85.

Kocks, U.F., 1970, Met. Trans.

Keohler, J.S., 1952, Phys. Rev., 86, 52.

Kroner, E., 1962, Appl. Mech. Rev., 15, 599.

Kulhlmann, D., 1947, Z. Phys., 124, 468.

Kuhlmann-Wilsdorf, D. and Wilsdorf, H., 1953, Acta Met., 1, 394.

Leslie, W.C., Michalak, J.T., and Aul, F.W., 1963, Iron and Its Dilute Solutions (Interscience-New York), p.119.

Li, J.C.M., 1963, J. Aust. Inst. Metals, 8, 206.

Li, J.C.M., 1963, Trans. Met. Soc., A.I.M.E., 227, 247.

Li, J.C.M., 1966, Recrystallization, Grain Growth and Textures, A.S.M., p.45.

Li, J.C.M., 1967, Can. J. Phys., 45, 493.

Li, J.C.M. and Chou, Y.T., 1970, Met. Trans. 1.

Lloyd, D.J. and Embury, J.D., 1970, Met. Sc. J., 4, 6.

Lucke, K. and Lange H., 1952, Z. Metallk., 43, 55.

MacEwan, S.R., Kupeis, O.A. and Ramaswami, B., 1969, Scripta Met., 3, 441.

Mader, S., 1963, Electron Microscopy and Strength of Crystals, edited by G. Thomas and J. Washburn (New York-Interscience), p.183.

Marcinkowski, M.J. and Fisher, R.M., 1965, Trans. Met. Soc. A.I.M.E., 233, 293.

Meakin, J.D. and Petch, N.J., 1963, Symp. Role of Substructure in Mech. Behavior of Metals, ASD-TDR-63-324, Orlando, Florida, p.243.

Michalak, J. T., and Paxton, H. W., 1961, Trans. A. I. M. E., 221, 850.

Mott, N. F., 1953, Phil. Mag., 44, 187.

Nabarro, F. R. N., 1950, Some Recent Developments in Rheology, (The British Reology Club, London).

Nabarro, F. R. N., Basinski, Z. S. and Holt, D. B., 1964, Adv. Phys., 13, 193.

Nix, W. D. and Barrett, C. R., 1968, Trans. A. S. M., 61, 695.

Nye, J. F., 1953, Acta Met., 1, 153.

Orowan, E., 1940, Proc. Roy. Soc., (London) 52, 8.

Otte, H. M., and Cahn, R. W., 1959, J. Sci. Instr., 36, 463.

Perryman, E. C. W., 1957, Creep and Recovery, A. S. M., p. 111.

Petch, N. J., 1953, J. Iron St. Inst., 174, 25.

Petch, N. J., 1969, Met. Jour., University of Strathclyde, p. 9.

Rodriguez, P., 1968, J. Materials Sci., 3, 98.

Rosenfield, A. R., and Hahn, G. T., 1970, Met. Trans., 1, 1080.

Russell, K., and Ashby, M. F., 1968, Harvard University Technical Report, No. 581, December.

Sachs, G., 1928, Z. d. Ver. deut. Ing., 72, 734.

Schmid, E., 1924, Proc. Int. Cong. App. Mech. Delft, p. 342.

Schoek, G., 1965, Phys. Stat. Sol., 8, 499.

Seeger, A., 1957, Dislocations and Mechanical Properties of Crystals, (Wiley-New York), p. 243.

Smith, C. S., and Guttman, L., 1953, Journal of Metals, 81.

Solomon, H. D., and McMahon, C. J., 1966, Work Hardening, edited by J. P. Hirth and J. Weertman, (Gordon and Breach: New York), p. 309.

Swann, P.R., 1963, Electron Microscopy and Strength of Crystals, edited by G. Thomas and J. Washburn, (New York-Interscience), p.131.

Taylor, G.I., 1938, J. Inst. Metals, 62, 307.

Taylor, G.I., 1955, IUTAM Colloq., Madrid; 1956, Springer Verlag, Berlin.

Tegart, W.J. McG., 1966, Elements of Mechanical Metallurgy, (Collier-MacMillan, Limited, Toronto).

Worthington, P.J. and Smith, E., 1964, Phil. Mag. 9, 211.